A Study on Impedance Measurement of Small-Capacitance Circuit using Transient Waveforms

by

Diah Permata

A Thesis Submitted to Doshisha University, Kyoto, Japan

For the Degree of Doctor of Engineering

December 2014

ACKNOWLEDGEMENTS

First of all, I would like to express my sincere gratitude to my supervisor Professor Dr. Naoto Nagaoka for his valuable advice, guidance and encouragement during my research work. Without his support and persistent help this thesis would not have been possible. It has been a pleasure and an honor to work with you and learn many things from you.

I wish to thank Professor Dr. Akihiro Ametani for the great opportunity to let me pursue my doctoral degree in Power System Analysis Laboratory, Doshisha University and provided a valuable guidance during my first semester of research.
I would like to thank Professor Dr. Yoshihiro Baba for his advice throughout the study period and for agreeing to review on my thesis. I would also like to thank Professor Dr. Koji Fujiwara for serving as my reviewer.

I thank to my colleagues at the Power System Analysis Laboratory for their help and support.
I also want to thank to The Directorate General of Higher Education, Ministry of Education, Republic of Indonesia for providing the scholarship and Lampung University for providing me to study leave.

Finally, my deepest gratitude goes to my parents, especially for my mother, whose pray during her life, brought me to the highest level of education. Many thanks to my husband and all of my children, without their supports and loves it is impossible to complete this study. Special thanks to my aunt, my brothers and sister for their supports throughout this time.

Kyoto, December 2014.
Diah Permata

ABSTRACT

Predictive calculations of overvoltages generated due to lightning are most essential for a reasonable insulation design of power system. For an accurate lightning surge analysis, power system apparatus should be represented with its stray capacitors even if its capacitance is some picofarads, because the surge includes high frequency components. An accurate measurement of the small capacitance becomes indispensable. A measurement method of small-capacitance using transient waveforms is proposed in this thesis. A pi-circuit is used to express the stray capacitors between terminals and those from each terminal to ground. Two measuring modes, differential and common modes, are required to obtain the parameters of the circuit. The parameters are determined by transient current waveforms of the modes with an applied voltage, i.e., the open circuited voltage at the end of the current injection cable.

At first, a measurement using an impedance measuring instrument, which is categorized as a steady state method, is investigated. Although the method is applicable in a laboratory test, it is difficult to apply to practical systems due to instability by radio interference.

On the other hand, the transient measuring method, which gives the impedance as a ratio between the voltage and current frequency responses transformed from time domain, can be easily applied to the power system apparatus. However, the measurement of the small stray capacitance is difficult due to the low impedance of the voltage probe, which is indispensable to the transient voltage measurement. The parasitic capacitance of the voltage probe obscures the small capacitance.

A current injection cable is indispensable to the transient measurement. Investigation of the effect of the sheath surge impedance clarifies that stray capacitor grounding from a terminal is short-circuited by the low impedance of the sheath surge impedance in the differential mode. A correcting method of the effect of the sheath surge impedance is proposed in this thesis.

The parameters of the pi-type circuit are obtained from a slope of the transient current waveforms or a waveform fitting by a nonlinear method. These methods enable the derivation without a voltage measurement by a probe connecting across the small capacitance. The first

method has high resistance to extraneous noise, because the numerical time to frequency transformation, which is sensitive to noise, is not required. The parameter estimation can be carried without any numerical simulation. In the nonlinear fitting method, the time to frequency transformation is simply done in the form of analytical equations. Since the analytic method is a closed form solution, it is insensitive to noise in comparison with numerical transformation. Although the nonlinear method requires numerical calculations, the accuracy is higher than that of the former method. The former method is useful to determine the initial values for the nonlinear fitting calculation.

The transient measuring methods are applied to define the circuit parameter of the equivalent pi-circuit of the following elements: (1) impedance between electrodes implanted into a piece of wood, (2) a gas arrester (GA) and (3) a miniature circuit breaker (MCB).

The contact and leakage resistances between the electrode and the wood and the capacitance between the electrodes are simultaneously obtained with the stray capacitances to ground by the proposed methods. The methods are applicable to measure not only the small stray capacitances but also the resistances. The transient methods can be applied to a measurement of a high impedance circuit. The wood model is useful for an insulation design of wooden insulators such as a wooden pole.

The GA is a basic device for protecting a circuit from a lightning surge. It can be used as a voltage sensor to evaluate the voltage across a small-capacitance circuit, because its internal capacitance is smaller than that of the conventional voltage probe. The breakdown voltage of GA can be known from a current measurement.

Characteristic of MCB can be simply expressed by a switch at a power frequency. However, the transient characteristic of MCB has to be expressed by some capacitors. For example, even if the MCB is turned off, some voltage is induced from a surge-entering terminal on the other terminal via the stray capacitor between its contacts. The contact capacitance with the stray capacitances determines the penetrating surge.

The accuracies of the models are confirmed by numerical simulations using the Electromagnetic Transients Program. Good agreements between the measured and calculated results show the high reliability of the proposed methods.

To illustrate the usefulness of the proposed method and the equivalent circuit, an MCB is used as an example. Because the induced voltage across a small stray capacitance cannot be directly measured, the induced voltage is indirectly measured by a flashover of a GA connected to the terminal. In addition, the circuit of the MCB with the GA enables a prediction of the applied voltage from the flashover. If the stray capacitances of the MCB as well as the GA are accurately known, the ratio between input and output voltage can be theoretically obtained. The voltage dividing ratio is useful to estimate and design the insulation level of distribution power system. The ratio obtained by a theoretical calculation agrees well with that between the voltage across the incoming-terminal of the MCB and that of the GA just before the flashover obtained by EMTP simulation.

A circuit-parameter derivation method of the models of a wood as an insulator, a switch (MCB) and a gas-arrester for a fast transient simulation have been developed in this thesis. These components are basic elements not only for power system but also electronic and/or communication system. In addition to this, the proposed method is applicable to the other elements, whose capacitance cannot be accurately measured by conventional methods. This thesis will open up a new field in a transient simulation.

TABLE OF CONTENTS

1 INTRODUCTION

1.1 General

Electrical transients are generated by sudden change in circuit such as lightning and switching. All electrical and electronic devices connected to a power system can be damaged by transient overvoltages. Transient assessment is required in the field of power engineering to verify the immunity of electrical and/or electronic equipment connected to the power system. Protection against such hazards is a necessity. Lightning is one of the key phenomena for an insulation design of power systems. For estimating an accurate lightning surge, power system apparatus should be represented with their stray capacitors. Even if the stray capacitance is some picofarads it has to be taken into account because the surge includes high frequency components. An accurate measurement of the small-capacitance is indispensable [1].

This thesis deals with a measurement method to assess a small-capacitance. The method is firstly developed by a steady-state measurement using an impedance-measuring instrument. Although the method is applicable in a laboratory test, it is difficult to apply to the field of power systems. For example, instability due to radio interference is a problem when the method is applied to a practical system. The capacitance measurement is generally difficult by the impedance-measuring instrument for its small signal source and low immunity to noise [2].

The capacitance can be obtained from a set of transient voltage and current responses with a time-to-frequency transformation, such as numerical Fourier transformation. The transformation is, however, sensitive to noise and its truncation error is unavoidable. The parasitic capacitance of a voltage probe, which is indispensable to the measurement, is also a fatal disadvantage for an estimation of the small-capacitance of a specimen [3].

A method to measure a small-capacitance with a loss is proposed in this thesis. Parameters are determined using transient current waveforms with the applied voltage, i.e., the open circuited voltage of a voltage source. The capacitance and loss are obtained from the slope of the current waveform at its wave-tail or by a nonlinear fitting method. The methods have a high resistance to extraneous noise, because the numerical time-to-frequency transformation, which is sensitive to noise, is not required. In these methods, the time-to-

frequency transformation is simply performed in the form of analytical equations. Since the analytic method is a closed form solution, it is insensitive to noise in comparison with the numerical transformation. Furthermore, these methods enable a measurement without a voltage across the small-capacitance. The effect of parasitic capacitance of the voltage probe is removed [1, 3].

However, a current injection cable is indispensable to the transient measurement. The effect of the low sheath surge impedance, which reduces the reliability of the measured result, is investigated and a correction method is proposed [1].

The proposed methods have advantages in a modeling of power apparatus for a fast transient comparing with the steady-state measurement using an impedance-measuring instrument.

The predictive calculations of overvoltages generated due to lightning are most essential for a reasonable insulation design. The accuracy of a miniature circuit breaker (MCB) model, whose parameters are evaluated by the proposed method, is confirmed by breakdown voltages of a gas-filled arrester (GA). The models of the MCB and the GA for a fast transient are useful to evaluate the overvoltage. These models can be applicable to communication systems such as telephone system as well as to low-voltage distribution system [4].

1.2 Overview of Modeling of Fast Transient for Digital Simulation

Power systems are subjected to many forms of transient phenomena brought by sudden changes in the systems. Transient phenomena are important to analyze especially for systems during times of the electrical stress. The sources of the stress can be divided into four: (1) lightning overvoltages (LOV) produced by lightning flashes, (2) switching overvoltages produced by switching breakers or disconnecting switches, (3) temporary overvoltages produced by faults, generator overspeed, ferro-resonance, etc., and (4) normal power frequency voltage in the presence of contamination [5].

The applicability of the small-capacitance measurement method is intended to the power apparatus in a low voltage system. For the system, lightning overvoltage is a dominant factor to determine the insulation level. Withstanding voltage of insulator depends on the shape of

the lightning surge waveform and its duration. In general, the lightning overvoltages are represented by fast front transient. These are characterized by a time-to-crest (front-time T_1) in the range $0.1<T_1<20$ μs. In the laboratory, these are simulated with a standard lightning impulse of 1.2/50 μs [6].

There have been representative methods to evaluate lightning overvoltage as follows: (1) experimental approaches, (2) observations of real lightning phenomena, (3) theoretical or analytical approaches, and (4) numerical approaches [7]. Among the four methods, the numerical approaches have many advantages from an economic and accuracy point of view. Accurate computation of the electromagnetic transient can be done using simulation tools based on a circuit theory and on an electromagnetic theory. Simulation based on a circuit theory, such as Electro-Magnetic Transients Program (EMTP), is widely used to estimate the overvoltage in overhead lines and substations. Whereas the electromagnetic theory based simulation, such as Virtual Surge Test Lab (VSTL) based on the Finite Difference Time Domain (FDTD) method, is used to solve the transient overvoltage in a three-dimensional structure. Recently, the numerical electromagnetic analysis method is becoming popular to solve transient phenomena. However, EMTP has been widely used as a powerful tool to analyze power system transients in view of their straightforward implementation and use in relation to the modeling of power system components [8].

In simulation based on a circuit theory, such as EMTP, all apparatuses are modeled by their equivalent circuit. A prior knowledge of circuit parameters is indispensable. Many researchers have reported a guideline to model the apparatus in a power system for fast transient such as tower, circuit breaker, power transformer, instrument transformer CT/VT, surge arrester, and so on [9-13]. A modeling of power system apparatus can be carried out by theoretical analysis, measurement or numerical simulation. The measurement method for the modeling can be classified as follows: (1) steady-state measurement using an impedance-measuring instrument (impedance/network analyzer), (2) transient measurement using a transient-generating equipment (impulse generator/pulse generator or switch) and a transient-measuring equipment (digital storage oscilloscope) [14]. The both measurement methods are investigated in this thesis. The advantages and disadvantages of the methods are discussed.

The transient measurement method has an advantage allowing to model a fast transient of power apparatus compared with a steady-state measurement.

Transient characteristics of power system apparatus in a high frequency region should be modeled by stray capacitors [15-21]. In general, the capacitances are difficult to assess by the measurement approaches. The numerical calculation, such as finite element method, is widely used to estimate the stray capacitances [15-18].

A circuit model of the fast transient simulation can be a lumped-parameter circuit or a distributed-parameter circuit. Substation equipment, such as circuit breaker, transformer, current transformer, voltage transformer, and disconnector switch is basically represented by a lumped circuit. Another apparatus modeled by a lumped circuit is a line insulator. Busbars and interconnections between the equipment in a substation are also represented by lumped parameter inductors, when their lengths do not exceed 10-15 m. Otherwise, they are represented by three-phase distributed parameter lines [10,22]. Of course, a distributed parameter line is used to model an overhead line and cable.

1.3 Project Objectives and Organization of Thesis

This thesis proposes a measurement method of small-capacitance for fast transient. The method is used to estimate the stray capacitance of the apparatus, which is normally in a few picofarads. The objectives of the thesis are listed below:

(1) To investigate the effect of measuring system in the small-capacitance circuit.

(2) To measure the stray capacitance of the apparatus.

(3) To define the circuit parameters by analyzing the transient waveforms.

(4) To investigate the applicability of the method in the calculation of transient overvoltages.

This thesis contains six chapters as follows:

Chapter 1 introduces transient overvoltages in a power system and the modeling method for fast transient.

Chapter 2 summarizes the study to date on lightning overvoltages, as well as the transient measurement and the fast transient simulation of power system through a comprehensive literature review.

Chapter 3 proposes a measuring method of a high impedance circuit using steady-state measurements. The impedance between electrodes implanted into a piece of wood is presented.

In Chapter 4, a modeling method of the fast transient using transient waveforms is described. The effect of probe capacitance, which has a fatal disadvantage for the transient measurement in small-capacitance circuit, is discussed. The effect of the sheath surge impedance is investigated and a correcting method is proposed. Two methods to obtain the circuit parameters by analyzing the transient waveforms are proposed.

In Chapter 5, applications of the proposed method to assess the stray capacitances are explained. Following are the applications: parallel electrodes implanted into a piece of wood, a miniature circuit breaker, and a gas-filled arrester. The reliability of the proposed method to define an equivalent circuit is discussed.

Chapter 6 is dedicated to the conclusions of this research and presents suggestions for further studies.

1.4 References

[1] D. Permata and N. Nagaoka, "An impedance measurement of a small-capacitance circuit using transient responses for lightning surge analysis," *IEEJ Trans. Electrical and Electronic Engineering*, vol.9, no.S1, pp.S37-S43, Oct. 2014.

[2] D. Permata, N. Nagaoka and A. Ametani, "A modeling method of impedance between the electrodes implanted into a wood," *The Papers of Technical Meeting on High Voltage Engineering IEEJ*, Kyoto, HV-13-035, pp.59-63, Jan. 2013.

[3] D. Permata and N. Nagaoka, "Effect of Measuring System on Small-Capacitance Measurement using Transient Waveforms," *The Science and Engineering Review of Doshisha University*, vol.55, no.4, pp.55-60, Jan. 2015.

[4] D. Permata and N. Nagaoka, "Modeling Method of fast transient for Unsymmetrical Stray Capacitance to Ground," *IEEJ Trans. Electrical Electronic Engineering*, vol.10, Supplement, Oct. 2015 (accepted for publication).

[5] A. R. Hileman, *Insulation Coordination for Power Systems*, Marcel Dekker Inc., NewYork, 1999.

[6] A. M. Farouk, and G. N. Trinh, *High voltage engineering*, CRC Press, p. 649-650, 2014.

[7] P. Yutthagowith, "Development of the PEEC method and its application to a lightning surge study," P.hD thesis, Dept. Electrical and Electronic Engineering, Doshisha Univ., Japan, 2010.

[8] WG C4.501,"Guideline for numerical electromagnetic analysis method and its application to surge phenomena," *CIGRE*, June 2013.

[9] A. Ametani and T. Kawamura, "A method of lightning surge analysis recommended in Japan using EMTP," *IEEE Trans. on Power Del*., vol.20, no.2, pp.867- 875, April 2005

[10] IEEE Modeling and Analysis of System Transients Working Group, "Modeling guidelines for fast front transients," *IEEE Trans. on Power Del.*, vol.11, no.1, pp.493-506, Jan. 1996.

[11] S. Okabe, M. Koto, G. Ueta, "Development of high frequency circuit model for oil-immersed power transformers and its application for lightning surge analysis," *IEEE. Trans. Dielectr. and Electr. Insul.*, vol.18, no.2, pp.541-552, April 2011

[12] M. Ishii, T. Kawamura, T. Kouna, E. Ohsaki, K. Shiokawa, K. Murotani, and T. Higuchi, "Multistory transmission tower model for lightning surge analysis," *IEEE Trans. on Power Del*., vol.6, no.3, pp.1327-1335, July 1991.

[13] R. B. Anderson and A. J. Eriksson, "Lightning parameters for engineering application," *Electra*, no.69, pp.65, 1980.

[14] Francois D. Martzloff, "Surge testing," Surge Protection Anthology-Part6, GE, 2004.

[15] P. Valsalal, S. Usa, and K. Udayakumar, "Modelling of metal oxide arrester for very fast transients," *IET Sci. Meas. Technol*., vol.5, no.4, pp.140-146, Feb. 2011.

[16] Qin Yu and Thomas W. Holmes, "A study on stray capacitance modeling of inductor by using the Finite Element Method," *IEEE Trans. on Electromagn. Compat.*, vol.43, no.1, pp.88-93, Feb. 2001.

[17] M.J. Hole and L.C. Appel, “Stray capacitance of a two-layer air-cored inductor,” *IEE Circuits, Devices and Systems*, pp.565-572, 2005.

[18] Z.J. Csendes and J.R. Hamann, “Surge arrester voltage distribution analysis by the finite element method,” *IEEE Trans. Power App. Syst*., vol. PAS-100, no.4, pp.1806-1813, April 1981.

[19] Z. Zhongyuan, L. Fangcheng, and L. Guishu, “A high-frequency Circuit Model of a Potential Transformer for the Very Fast Transient Simulation in GIS,” *IEEE Trans. Power Del.*, vol.23, no.4, pp.1995-1999, Oct. 2008.

[20] G. Grandi, M. K. Kazimierczuk, A. Massarini, and U. Reggiani, “Stray capacitances of single-layer solenoid air-core inductors,” *IEEE Trans. Ind. Appl.*, vol.35, no.5, pp.1162-1168, Sept./Oct.1999.

[21] S. R. Naidu and A. F. C. Neto, “The stray-capacitance equivalent circuit for resistive voltage dividers,” *IEEE Trans. Instrum. Meas*., vol.IM-34, no.3, pp.393-398, Sept. 1985.

[22] W. Nowak, and R. Tarko, “Computer modelling and analysis of lightning surges in HV substations due to shielding failure,” *IEEE Trans. Power Del.*, vol.25, no.2, pp.1138-1145, April 2010.

2 SUMMARY OF LIGHTNING OVERVOLTAGES

2.1 Introduction to Lightning Overvoltages

Transient overvoltages in a power system are due to injection a bulk of energy. The source can be from a lightning discharge or switching. Lightning discharge may not necessarily mean direct termination of a lightning stroke onto the power system [1]. An indirect stroke, i.e., a lightning hit on an object nearby a power line, will induce voltages into the loop formed by the conductors of the power system. Lightning overvoltages are an impulse, for which the prospective magnitudes of overvoltages closely depend on the insulation level, i.e., system voltage. A typical impulse transient occurring on a normal voltage waveform caused by a lightning surge is shown in Fig. 2.1. The magnitude can be many times larger than the peak value of the normal voltage waveform. Impulse transients are usually characterized by their rise (T_1) and decay (T_2) times and peak value. The most common waveforms of impulsive transient overvoltage are double exponential-type waveform [2].

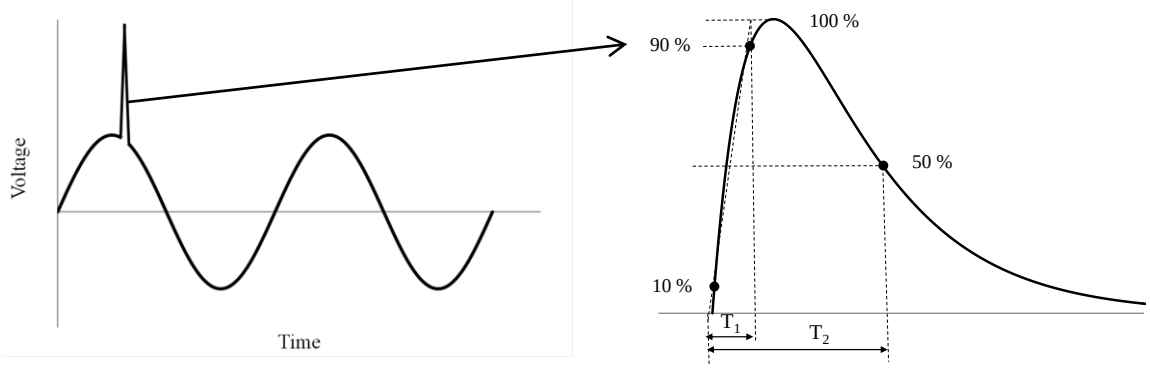

Fig. 2.1. A typical impulse transient.

Transient overvoltage can be classified into slow front, fast front, and very fast front characterized by the following shape [3]:

Slow front: These are characterized by a time-to crest (front-time T_1) in the range $20<T_1<5000\mu s$ and a time to half value (decay time T_2) $T_2 \leq 20$ ms. In the laboratory, these are simulated by a standard switching impulse with 250/2500 μs.

Fast front: These are characterized by a time-to crest (front-time T_1) in the range $0.1<T_1<20\mu s$. In the laboratory, these are simulated with a standard lightning impulse of 1.2/50 μs.

Very fast front: These are characterized by a time-to crest (front-time T_1) in the range $3<T_1<10ns$. So far, no test has been standardized for laboratory works.

The typical lightning transient overvoltage is a fast front-type. While very fast front transient is caused by switching operations within the gas insulated substation (GIS).

Transient overvoltages are a common cause of damage to power systems and electrical and/or electronic equipment, which is connected to the systems. The transient assessment becomes essential since it is required to verify the immunities of the equipment. The laboratory that works to test the equipment requires a standard waveform of the applied voltage or injected current. Standard publications describe several test waveforms that are representative of transient overvoltage. There are five of the most common transient overvoltage test waveforms: the ring wave specified in ANSI C62.41-1980, the fast transient specified in IEC 61000-4-4, the 8/20 μs, 1.2/50 μs, and the 10/1000 μs as shown in Figs. 2.2 to 2.4 [4].

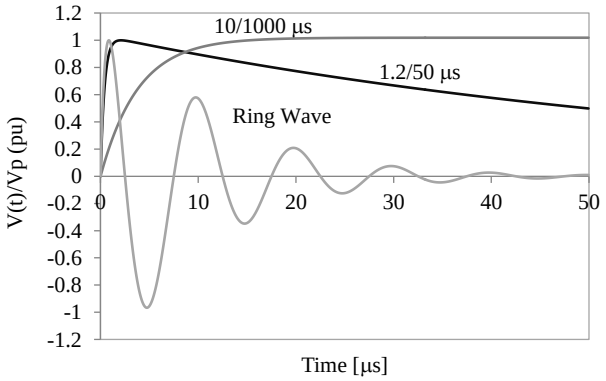

Fig. 2.2. Various overvoltage test waveforms.

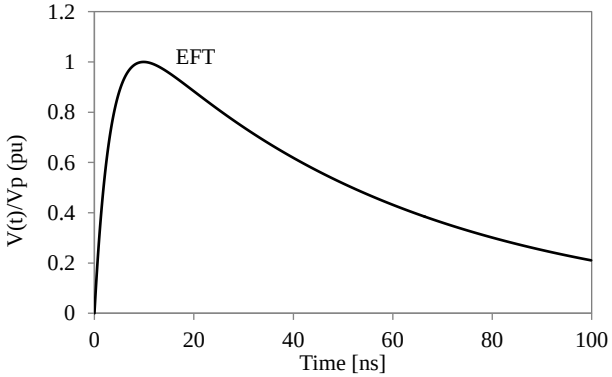

Fig. 2.3. EFT test waveform (5/50 ns).

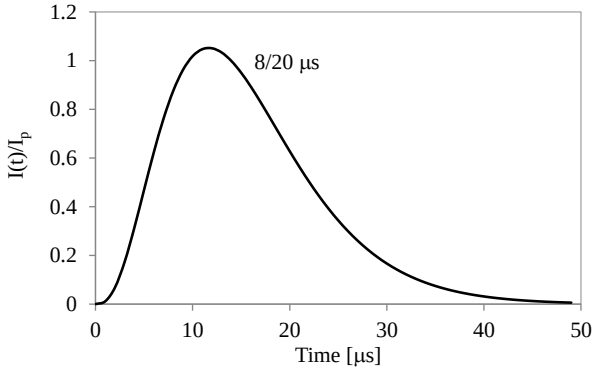

Fig. 2.4. Current test waveform (8/20 μs).

Originally, the standard waveforms were used during experiments in a laboratory. Since transient analysis by digital simulation has enough accuracy in comparison with that by

experiment, many engineers have also performed computer simulations to obtain the response of equipment to transient overvoltage. Therefore, the representation of the waveforms in the mathematical equations is required. The 1/50 μs, 10/1000, and electrical fast transient (EFT) waveforms, represented in (2.1), while the ring wave expressed in (2.2). The four waveforms are a voltage waveform. The current waveform is only represented by 8/20 μs in (2.3). The constants of those equations are listed in Table 2.1 [4].

$$V(t) = AVp\{1 - \exp(-t/\tau_1)\}\exp(-t/\tau_2) \tag{2.1}$$

$$V(t) = AVp\{1 - \exp(-t/\tau_1)\}\exp(-t/\tau_2)\cos(\omega t) \tag{2.2}$$

where V_p = the peak value of V(t)

$$I(t) = AI_p t^k \exp(-t/\tau) \tag{2.3}$$

where I_p = the peak value of I(t), t = time in μs, k = 2.93

Table 2.1 List of constants of waveform [4].

Waveforms	A	τ_1 [μs]	τ_2 [μs]	ω
Ring Wave	1.590	0.5334	9.788	$2\pi 10^5$
1/50 μs	1.037	0.4074	68.22	NA
10/1000 μs	1.019	3.827	1404	
EFT	1.270	$3.5 \cdot 10^{-3}$	$55.6 \cdot 10^{-3}$	
8/20 μs	0.01405	3.977		

2.2 Transient Measurement

A surge testing is very essential in transient analysis studies. For the testing, transient source as well as transient measuring equipment is required [1].

(1) Surge generator

The basic surge generator is a charged capacitor, and it is discharged through a wave-shaping circuit into the test object [1]. Impulse generator (IG) is composed of capacitors, and

pulse generator (PG) is composed of a coaxial cable, which is a kind of a capacitor [5]. For an experimental work, the IG or PG is commonly used to inject a current or to apply a voltage to the test object either in a laboratory or in real systems. The IG has been widely used especially when an insulation test of a power apparatus is carried out because the IG inherently produces the exponential waveform [5]. The PG is widely used for a surge testing. A limitation of the PG compared to the IG is that the PG cannot apply a high voltage like IG. However, the PG has very fast rise time. For an example, PGs with its rise time less than 1 ns is not rare. The PG has been used for a surge testing to verify the immunity of the equipment to noise. In this research, a PG is used to apply a voltage to a test object. The transient responses of the test object to the pulse waveform from a PG are used to model the object for a fast transient simulation.

(2) Transient-measuring equipment

The cutting-edge tool for measuring transient response is a digital storage oscilloscope. It can store the data for a further analysis. However, it normally contains noise of the digitizer. At a fast transient measurement, the user should be aware of whether the oscillation is generated by the impulse or induced from measuring system. Following are some simple checks that should be done prior the measurement: freedom from noise, proper compensation of probes, and avoidance of ground loops [1].

2.3 Fast Transient Simulation

Recently, many engineers use a digital simulation to carry out transient overvoltage studies. Although the circuit based simulation tools like EMTP has many limitations, they have been widely used as powerful tools to analyze power system transients. EMTP-type simulation tools can give reasonable results with a satisfactory accuracy in comparison with experimental test results [7-8].

Formerly, lightning overvoltage studies by simulation tools are performed to design transmission lines and substations, and for the protection of power system equipment. The objectives of the studies are to characterize the magnitude of the lightning overvoltage for

insulation requirements, and/or to find the critical lightning stroke current that causes insulation flashovers [9]. Therefore, the modeling of the apparatus used in overhead transmission lines and substations has been vastly developed. Many researchers also contribute to modeling of apparatuses for fast transient analysis [8-10].

The circuit theory based simulation such as EMTP, SPICE and PSCAD requires the circuit parameters of their models. For a fast transient simulation, the equipment should be represented with their stray capacitance because the transient overvoltage contains high frequency components. Substation equipment such as circuit breaker, disconnector switch, bus support insulator, power transformer and instrument transformer are basically represented by a lumped circuit of capacitance as shown in Table 2.2. These data are based on supplier information, and only the lowest values are reported as a pessimistic assumption [9]

Table 2.2. List of capacitance-to-ground [in pF] of substation equipment [9].

Equipment	Rated Voltage		
	115 kV	400 kV	765 kV
Circuit Breaker (Dead Tank)	100	150	600
Disconnector Switch	100	200	160
Bus Support Insulator	80	120	150
Capacitive Potential Transformer	8000	5000	4000
Magnetic Potential Transformer	500	550	600
Current Transformer	250	680	800
Auto Transformer	3500	2700	5000

For overhead line, busbars and interconnections are represented by three phases distributed parameter lines. If the length of these lines is less than 10-15 m, it can be represented by a lumped parameter inductor with its unit inductance of 1μH/m [11].

Transient overvoltage studies in distribution lines have been reported in Ref. [12] and [13]. Both papers used EMTP simulation to study the transient overvoltage. The circuit models and their parameters used in the simulation are presented.

Table 2.2 shows that the equipment in high voltage substation has a larger stray capacitance with increase of its rated voltage. For the equipment connected to the low voltage systems, i.e., distribution line, the stray capacitances become smaller than those shown in Table 2.2. The smaller size of equipment result in the decreasing of the stray capacitance. The stray capacitance of equipment in distribution line is not more than some tens pF.

In general, valid information of the stray capacitances for numerical simulations is not available from a manufacturer [7]. Therefore, the researchers have to obtain the stray capacitances themselves. The stray capacitance cannot be obtained by a theoretical equation, and its measurement is difficult, especially if the equipment has a small stray capacitance.

2.4 References

[1] Francois D. Martzloff, "Surge testing," Surge Protection Anthology-Part6, GE, 2004.

[2] V. Smith, V. Ilango, S. Perera, V. Gosbell, and D. Robinson, "Transient overvoltages on the electricity supply network-classification, causes and propagation," *Integral Energy Tech. Note* , no. 8, University of Wollongong, April 2005.

[3] A. M. Farouk, and G. N. Trinh, *High voltage engineering*, CRC Press, p. 649-650, 2014.

[4] R. B. Standler, "Equations for some transients overvoltage test waveforms," *IEEE Trans. Electromagn. Compat.*, vol. 30, no. 1, pp.69-71, February 1988.

[5] A. Ametani, N. Nagaoka, Y. Baba and T. Ohno, *Power system transients theory and applications*, CRC Press, pp. 2013.

[6] *Noiseken Technical Note*, 2009.

[7] WG C4.501, "Guideline for numerical electromagnetic analysis method and its application to surge phenomena," *CIGRE*, June 2013.

[8] A. Ametani, "The history of transient analysis and the recent trend," *IEEJ Trans. Electrical Electronic Engineering*, vol. 2, pp. 497-505, 2007.

[9] IEEE Modeling and Analysis of System Transients Working Group, "Modeling guidelines for fast front transients," *IEEE Trans. Power Del.*, vol.11, no.1, Jan. 1996.

[10] Rioual M., "Measurement and computer simulation of fast transients through indoor and outdoor substations," *IEEE Trans. Power Del.*, vol. 5, no. 1, pp. 117-123, Jan 1990.

[11] W. Nowak, and R. Tarko, “Computer modeling and analysis of lightning surges in HV substations due to shielding failure,” *IEEE Trans. Power Del*, vol. 25, no. 2, April 2010.

[12] S. Matsuura, T. Noda, A. Asakawa, and S. Yokoyama, “A distribution line model for lightning overvoltage studies,” *IEEJ Trans. Electrical Electronic Engineering*, vol. 173, no. 1, 2010.

[13] K.Oka, T. Takinami, H. Takei, T. Hirai, K. Murata, and M. Yoshikawa, “Measurement and Analysis of Transient Overvoltages in Full-size 11.4kV Distribution Line.” *Proc. Transmission Distribution Conf. 2012: Asia Pacific*, 2002, pp.1253-1258.

3 MODELING METHOD OF HIGH-IMPEDANCE CIRCUIT BY STEADY-STATE MEASUREMENT

3.1 Introduction

Wooden pole is widely used for a medium voltage line all over the world. The pole is equipped with a wooden cross arm to support conductors and equipment up to its maximum design load, and to maintain conductor clearances. The conductor is supported by an insulator, which is commonly mounted on the cross arm with a bolt. In Japan, many houses are made of wood. A power or telecommunication line is led from a concrete pole into the house and is attached to the wooden wall using a screw.

In both cases, if a lightning strikes a distribution line, a surge voltage will be generated and it travels along the line. If the lightning voltage is high, a flashover will be produced at the insulator strings on a wood and the lines are bridged or grounded through the wood. The characteristic is determined by the impedance of the wood. The impedance between the electrodes implanted into a piece of wood becomes important for a transient calculation of a power system including a lightning surge analysis.

There have been two approaches to determining the electrical properties of a wooden pole, i.e. whole pole evaluations and wood stake studies [1]. The research in this paper employs a wood stake as a specimen and screws as electrodes.

The electrical properties of the wood are influenced by many factors such as: moisture content, species, treatment type, temperature and so on [1]. This study focuses on the effect of distance of the electrodes on the frequency characteristics of the impedance. In this study, a model of the impedance between the electrodes is proposed. The model consists of a branch impedance between the electrodes Z_{el} and branches of grounding impedance from the electrodes to ground Z_g. The branch impedance between the electrodes Z_{el} is modeled by the first and the second Foster-type equivalent circuit.

3.2 Initial Model of Impedance between Electrodes Implanted into a Piece of Wood [2]

The straightforward method to obtain the impedance of the specimen is a measurement by an impedance analyzer instrument. It measures the impedance (*Z*), capacitance (*C*), inductance (*L*), and/or conductance (*G*) in a frequency domain. Nowadays, the frequency range of the instruments covers from mHz to some hundreds MHz. The measurement bandwidth becomes wider year by year. In general, the advantage of the impedance measurement using the impedance analyzer is that an accurate result can be obtained with ease.

It is essential to know the impedance of wood as an insulating material especially in an investigation of the transient overvoltage across the electrodes implanted into a piece of wood. In this paper, the impedance characteristics of several kinds of woods are measured using an impedance analyzer, Agilent 4294A. Its specification is shown in Table 3.1.

Table 3.1. Specification of impedance analyzer Agilent 4294A.

Frequency range	40Hz – 110MHz
Voltage signal	$5mV_{rms}$ to 1 V_{rms}
Current signal	200 μA_{rms} to 20 mA_{rms}

The initial model of the impedance between the electrodes implanted into a piece of wood is not taken account of the stray impedance from the electrodes to ground modeled by an aluminum plate. The impedance measurement is carried out as shown in Fig. 3.1.

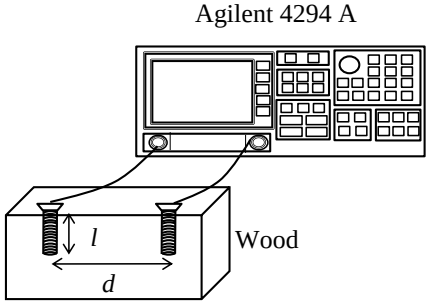

Fig. 3.1. Measurement setup (differential mode).

The initial model of the impedance between the electrodes implanted into a piece of wood is assumed to be a parallel *RC* circuit shown in Fig. 3.2. The impedance $|Z|$ and its angle θ define the resistance *R* and the capacitance *C* by the following equations:

$$R = |Z| / \cos\theta \tag{3.1}$$

$$C = -\sin\theta / |Z| \omega \tag{3.2}$$

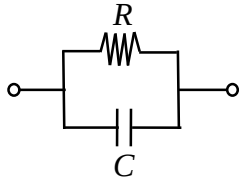

Fig. 3.2. An initial model of impedance between electrodes.

A specimen made of pine is used in the measurement, and its size is 3.6 cm × 3.6 cm × 45 cm. Two screws of 4 mm diameter are used as the electrodes of three lengths *l* (1 cm, 2 cm, and 3 cm) with four distances between the electrodes *d* (5 cm, 7 cm, 9 cm, and 11 cm). The resistance and the capacitance in twelve cases (3 cases in length, 4 cases in distance) at frequency 1 MHz are shown in Figs. 3.3 and 3.4. The parameters at the length of 1 cm with a distance of 9 and 11 cm (cases l_1d_9 and l_1d_{11}) and at the length of 2 cm with a distance of 11 cm (case l_2d_{11}) cannot be obtained. In these cases, the current becomes smaller than the minimum value of the measuring instrument due to the quite high impedances between the electrodes.

Figs. 3.3 and 3.4 show the effects of the length of the electrodes *l* and the distance between the electrodes *d* on the resistance and capacitance. The resistance *R* decreases with the increase of length and it increases with the increase of the distance. On the contrary, the capacitance *C* increases with the increase of the length and it decreases with the increase of the distance.

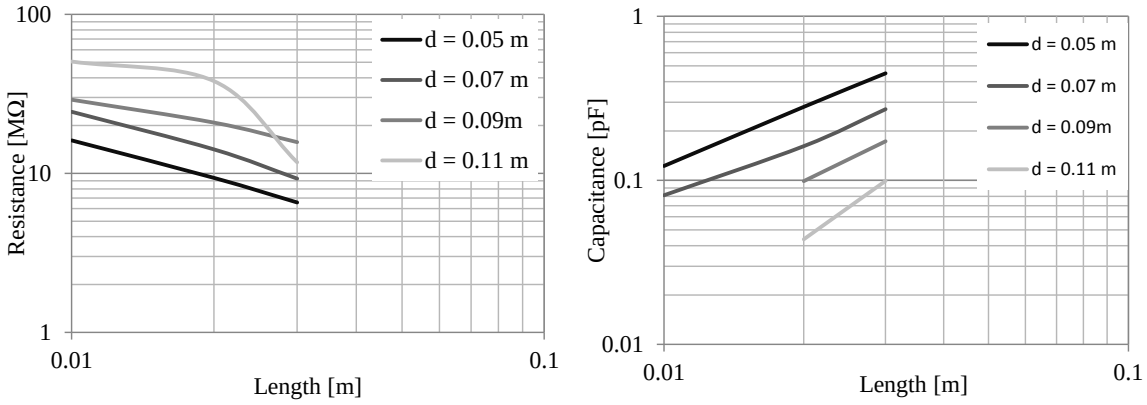

(a) Resistance (b) Capacitance

Fig. 3.3. Measured resistance and capacitance versus length *l*.

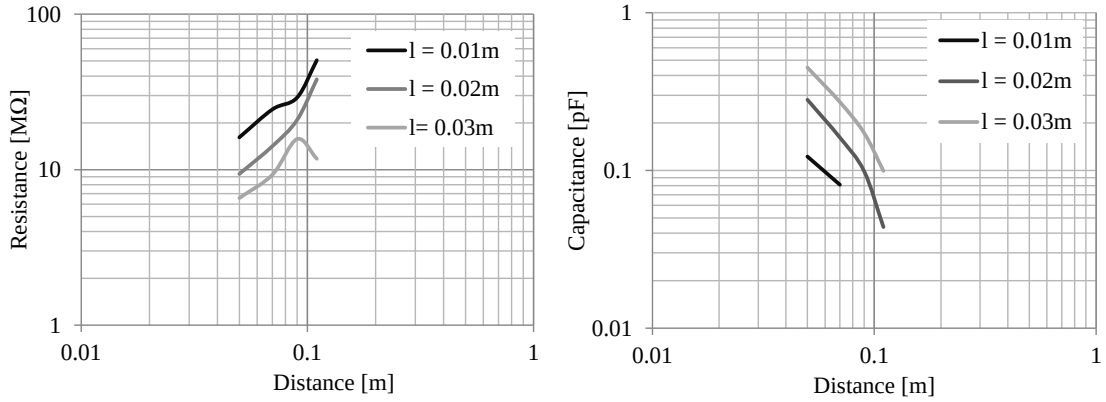

(a) Resistance (b) Capacitance

Fig. 3.4. Measured resistance and capacitance versus distance *d*.

3.3 Modified Model of Impedance between Electrodes Implanted into a Piece of Wood Taking Account of Stray Impedance [3]

The impedances with their angles are measured in two types of measurements, i.e., common- and differential-modes as illustrated in Fig. 3.5 to take into account a stray impedance from each electrode to ground. The first setup is to measure the stray impedance Z_s from the electrodes to ground modeled by an aluminum plate. The low-end terminal of the impedance analyzer is connected to the aluminum plate, and the high-end terminal is

connected to the short-circuited electrodes. The second one is to measure the impedance Z_t between the electrodes by connecting the electrodes to the terminals of the impedance analyzer. The definition of stray impedance to ground Z_s and those between the electrodes Z_t is illustrated in Fig. 3.6.

Two specimens are used in this investigation; (1) Zelkova serrata (keyaki), a rectangular parallelepiped wood of 12 cm × 12 cm × 50 cm; (2) Japanese cedar (sugi), a log wood of 18 cm diameter and 48 cm length. Prior to the measurement, the moisture contents are measured by Timber Master (made by GE Protimeter). They are 11.1-11.5 % for the Zelkova serrata (keyaki) and 10.6 – 10.9 % for the Japanese cedar (sugi) at a temperature of 20 °C. Two screws of 4 mm diameter are used as the electrodes whose length l is 0.075 m and the distance between the electrodes d is 0.05 m or 0.1 m.

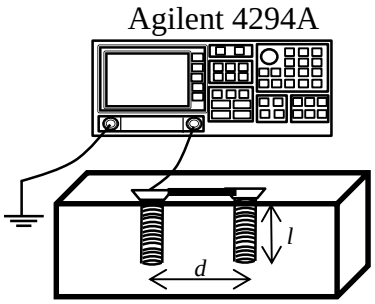

(a) Common-mode

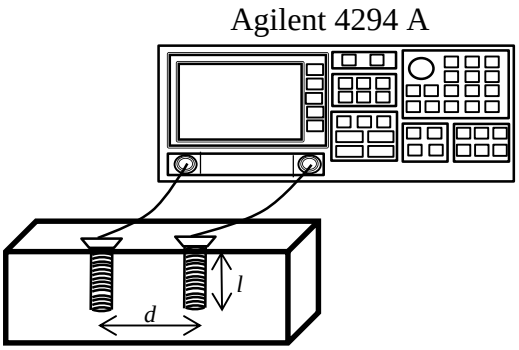

(b) Differential-mode

Fig. 3.5. Setup of steady-state measurement.

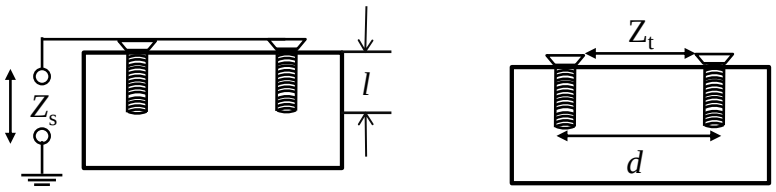

Fig. 3.6. Definition of impedances Z_s and Z_t.

3.3.1 Equivalent circuit composition

An equivalent circuit of the impedance between the electrodes is illustrated in Fig. 3.7. The circuit is a pi-equivalent circuit, which is commonly used to represent the stray impedance between two terminals. The circuit consists of an impedance between the electrodes Z_{el} and two branches to ground Z_g.

The impedance between the electrodes implanted into a piece of wood (Z_t) is determined by the parallel connected branches, which consist of the impedance between the electrodes Z_{el} and the series connected grounding impedance $2Z_g$ (=$4Z_s$). An *RC* network based on the first and the second Foster circuits are used to synthesize the impedance Z_{el}.

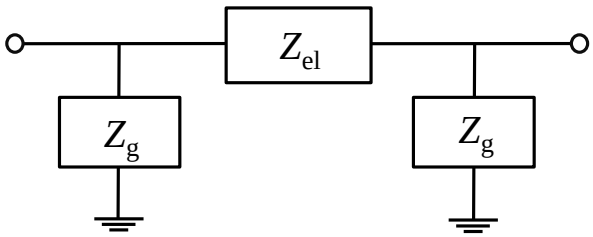

Z_{el} : Branch impedance between electrodes
Z_g : Grounding impedance

(a) Equivalent circuit for total impedance Z_t

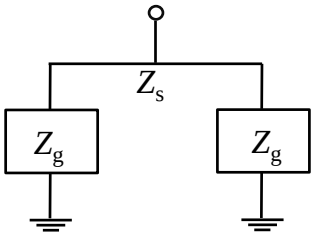

(b) Equivalent circuit for stray impedance Z_s

Fig. 3.7. Circuit model of impedance between electrodes implanted into a piece of wood.

From the measured branch impedance Z_{el}, the branch impedance per unit distance is obtained. The impedance between the electrodes Z_{el} for an arbitrary electrode-distance can be obtained from the characteristic shown in Fig. 3.4.

3.3.1.1 Total impedance between electrodes

For the modeling, the measured results of the impedance between the electrodes Z_t and the stray impedance to ground Z_s are assumed to be a capacitive i.e., the angle of the impedance is ranging $-90° < \theta_t, \theta_s < 0°$. As the definition of the impedance between the electrodes Z_t aforementioned, it is expressed by (3.3).

$$\frac{1}{Z_t} = \frac{1}{Z_{el}} + \frac{1}{2Z_g} \tag{3.3}$$

The stray impedance from the electrode to ground Z_s can be expressed by a parallel connection of the grounding impedances Z_g as shown in Fig. 3.7 (b) and (3.4).

$$Z_g = 2Z_s \tag{3.4}$$

From (3.3) and (3.4), the branch impedance between the electrodes Z_{el} is obtained from the measured impedance Z_t and the stray impedance Z_s.

$$\frac{1}{Z_{el}} = \frac{1}{Z_t} - \frac{1}{4Z_s} \tag{3.5}$$

The impedance Z_{el} obtained from the measured results can be synthesized by a circuit consisting of some resistors and capacitors.

3.3.1.2 Circuit synthesize

There are two measured results, i.e., the stray impedance to ground Z_s obtained by the common mode measurement and the impedance between the electrodes Z_t obtained by the

differential mode measurement. These two impedances are used to define the branch of impedance between the electrodes Z_{el} using (3.5). The impedance Z_{el} consists of a frequency dependent resistance $R_{el}=1/G_{el}(\omega)$ and a capacitance $C_{el}(\omega)$.The Z_{el} is synthesized into the capacitive circuit, i.e., the second Foster circuit as illustrated in Fig. 3.8. The circuit expresses the frequency dependence by a constant-parameter lumped-circuit.

$$Z_{el} = \frac{1}{Y_{el}} = \frac{1}{\dfrac{1}{R_{02}} + \dfrac{1}{R_{12} + 1/j\omega C_{12}} + \dfrac{1}{R_{22} + 1/j\omega C_{22}} + j\omega C_{\inf}} = \frac{1}{G_{el}(\omega) + j\omega C_{el}(\omega)} \tag{3.6}$$

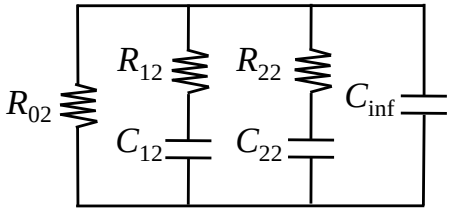

Fig. 3.8. The second Foster circuit model for the branch impedance Z_{el}.

The resistance R_{0k} and the capacitance $C_{\inf}$ determine the impedance of the wood in a low and a high frequency region, respectively. The resistance R_{k2} and capacitance C_{k2} of the second Foster circuit are determined by "Data solver" installed in MS Excel to solve the nonlinear problem. The objective of the solver is the sum of the errors between the measured and calculated results of the conductance G_{el} and the capacitance C_{el} as shown in (3.7). The parameters of the circuit are determined by the characteristics of the impedance in a frequency range of 100 kHz to 100 MHz. The parameters G_{el} and C_{el} are logarithmically compressed to improve the accuracy because the measured results distributed in a wide range.

$$\begin{aligned} SumError = & \sum_{f=100kHz}^{100MHz} \left| log_{10}(G_{el-m}) - log_{10}(G_{el-c}) \right| \\ & + \left| \log_{10}(C_{el-m}) - \log_{10}(C_{el-c}) * C_{weighted} \right| \end{aligned} \tag{3.7}$$

where subscripts *m* and *c* denote the measured and calculated results, respectively.

A weight coefficient C_{weighted} is required for a stable convergence. In this study, the value of C_{weighted} is selected to be 10 as shown in (3.8). The logarithmic of the capacitance, which is the important element, is weighted ten times greater than that of the resistance.

$$SumError = \sum_{f=100kHz}^{100Mhz} \left| log_{10}(G_{el-m}) - log_{10}(G_{el-c}) \right| + \left| log_{10}(C_{el-m}) - log_{10}(C_{el-c}) * 10 \right| \tag{3.8}$$

The convergence calculation is started from their initial values of R_{k2} and C_{k2}, and stopped when the objective reaches the minimum value.

The second Foster circuit is impractical for a further analysis, because the parameters cannot be expressed as a function of distance between the electrodes *d*. The first Foster circuit should be used to compose a generalized equivalent circuit. The parameter R_{k1} and C_{k1} of the first Foster circuit model shown in Fig. 3.9 are synthesized from the second Foster circuit. The total impedance for the first Foster circuit model is obtained by (3.9).

$$Z_{el} = \left[\frac{1}{1/R_{11} + j\omega C_{11}} \right] + \left[\frac{1}{1/R_{21} + j\omega C_{21}} \right] + \left[\frac{1}{1/R_{31} + j\omega C_{31}} \right] \tag{3.9}$$

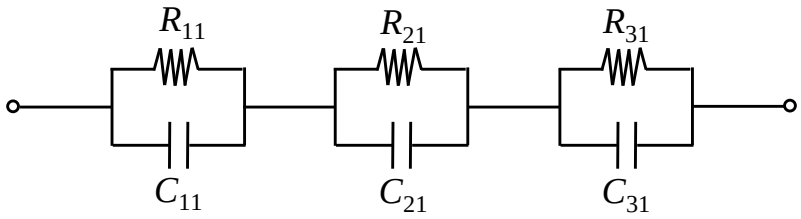

Fig. 3.9. The first Foster circuit model for the branch impedance Z_{el}.

The circuit parameters shown in Fig. 3.10 are represented by a function of the distance between the electrodes *d.* The resistance and the inverse of the capacitance (R_{k1} and $1/C_{k1}$) are proportional to the distance between the electrodes *d*. Once the resistance R_{k1} and the capacitance C_{k1} for a specific value of *d* are determined, their value per unit distance, i.e., R'_{k1} and C'_{k1} can be obtained as shown in (3.10).

$$R_{k1} = R'_{k1} d,$$

$$C_{k1} = C'_{k1} / d \tag{3.10}$$

From the above equations, the impedance Z_{el} for an arbitrary distance can be obtained.

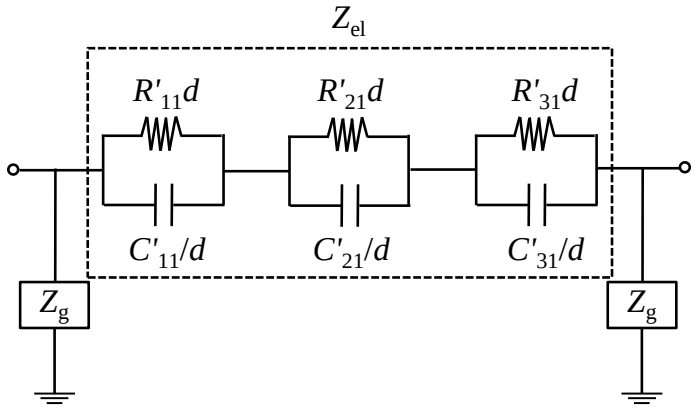

Fig. 3.10. A circuit for calculating the impedance Z_t for an arbitrary distance between the electrodes d.

3.3.1.3 Measured and calculated results of circuit parameters

The measured result of the stray impedance $|Z_s|$ and the impedance between the electrodes $|Z_t|$ and their angles θ_s and θ_t for the two specimens are shown in Figs. 3.11 and 3.12. Fig. 3.11 shows a minor difference in the measured results of $|Z_s|$ and θ_s for both specimens and for the distance between the electrodes d. The oscillations in a region above the frequency of 10 MHz are due to noise. Fig. 3.12 also shows that the impedances between the electrodes $|Z_t|$ and their angles θ_t of Keyaki and Sugi are quite similar. It might be due to the fact that they belong to the same group of woods and there is a minor difference in the moisture content.

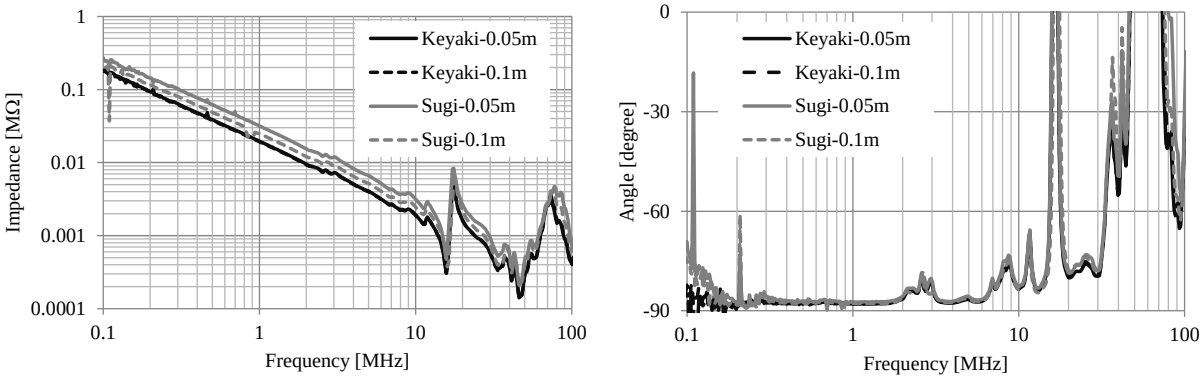

Fig. 3.11. Measured result for the stray impedance $|Z_s|$ and angle θ_s for Keyaki and Sugi.

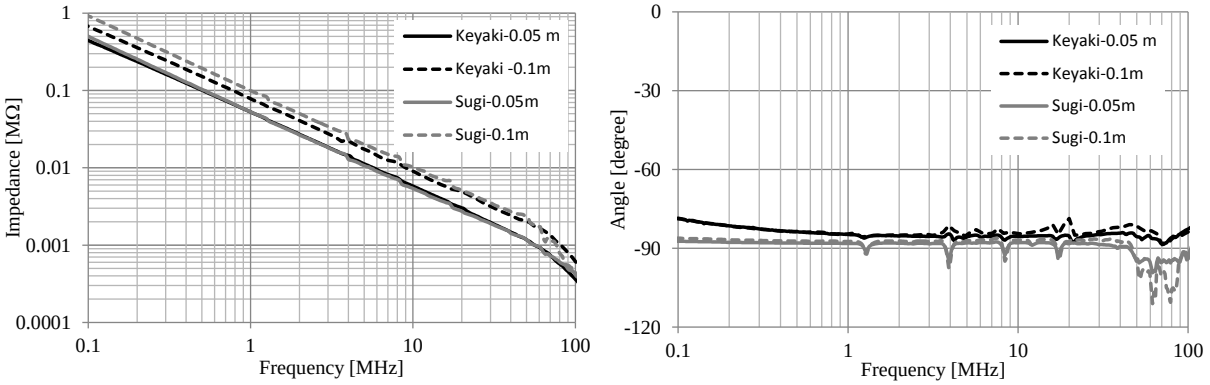

Fig. 3.12. Measured result for the impedance between the electrodes $|Z_t|$ and angle θ_t, Keyaki and Sugi.

The parameters R_k and C_k of the first and the second Foster circuit are determined by "Data solver" using the measured result at the distance d of 0.05 m. Those are listed in Table. 3.2. The circuit parameter of R'_{k1} and C'_{k1} are obtained by (3.10) as shown in Table. 3.3.

Table 3.2. The circuit parameters of R_k and C_k at the distance of 0.05 m, the first and the second Foster circuit parameters.

First Foster			Second Foster		
Element	Keyaki	Sugi	Element	Keyaki	Sugi
R_{11} [MΩ]	540	48900	R_{02} [MΩ]	544	48900
R_{21} [MΩ]	0.55	4.31	R_{12} [MΩ]	0.57	1.70
R_{31} [MΩ]	0.03	0.002	R_{22} [MΩ]	1.90	13.3
C_{11} [pF]	2.43	4.14	C_{12} [pF]	0.25	0.06
C_{21} [pF]	2.13	3.13	C_{22} [pF]	1.33	2.36
C_{31} [pF]	3.34	50.3	C_{inf} [pF]	0. 85	1.72

Table 3.3. The parameter of R'_{k1} and C'_{k1} as a function of distance between the electrodes d.

Element	Keyaki	Sugi
R'_{11} [MΩ/m]	10800	978000
R'_{21} [MΩ/m]	10.9	86.3
R'_{31} [MΩ/m]	0.65	0.04
C'_{11} [pFm]	0.12	0.21
C'_{21} [pFm]	0.11	0.16
C'_{31} [pFm]	0.17	2.52

The impedances between the electrodes Z_{t} versus frequency characteristic are calculated in a frequency range from 100 kHz to 100 MHz. The circuit parameters in Table 3.3, which are derived based on measured results at d = 0.05 m, are used to estimate the impedance between the electrodes Z_{t} at 0.1 m. The comparison between the measured and estimated result for two distances d of 0.05 m and 0.1 m for two specimens are shown in Fig. 3.13.

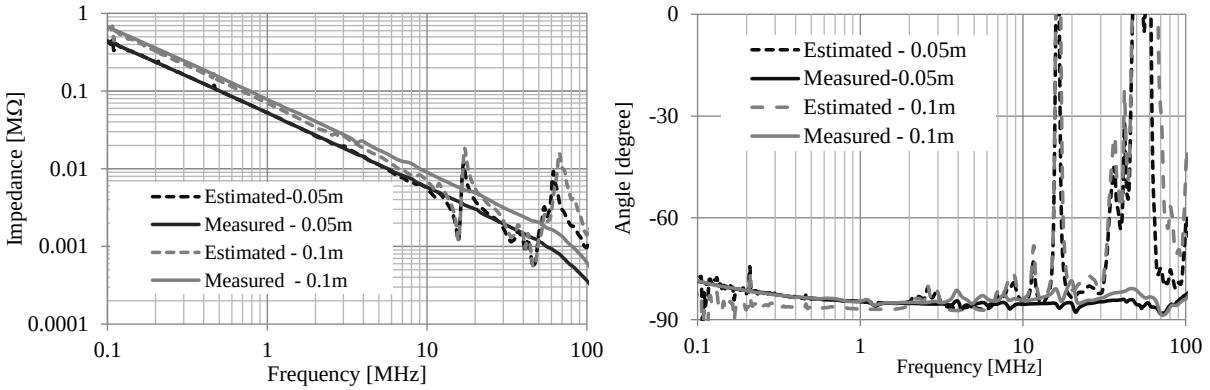

(a) The impedance $|Z_t|$ and its angle θ_t for Keyaki

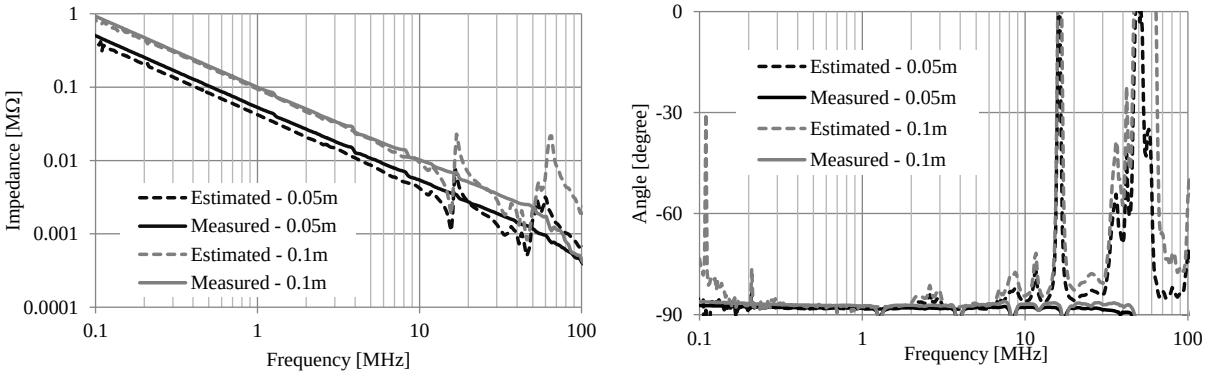

(b) The impedance $|Z_t|$ and its angle θ_t for Sugi

Fig. 3.13. Comparisons between the measured and the estimated result of the impedance between the electrodes Z_t and angle θ_t.

The circuit model (Fig. 3.10) with the circuit parameter of R'_{k1} and C'_{k1} as listed in Table 3.3 expresses the impedance between the electrodes Z_t with satisfactory accuracy as illustrated in Fig. 3.13. The deviation between the estimated result and the measured result of the impedance Z_t in a frequency range higher than 10 MHz is due to noise included in the measured stray impedance. The frequency range lower than 10 MHz is sufficient for a transient calculation of a power system including a lightning surge analysis.

3.3.2 Simplified circuit

The first Foster circuit shown in Fig. 3.10 can be simplified by analyzing the contribution of each branch to the impedance between the electrodes Z_{el}. The time constant of each branch is calculated as shown in Table. 3.4.

Table 3.4 shows the first branch of the first Foster circuit has the longest time constant due to the high resistance R_{11}. The effect of each branch on the total impedance is compared to the measured result are shown in Fig. 3.14 for both specimens, keyaki and sugi.

Table 3.4. The time constant-value for each branch of the first Foster circuit.

Element	Time Constant (τ)		
	1st Branch	2nd Branch	3rd Branch
Keyaki	1.3 ms	1.2 μs	0.1 μs
Sugi	0.2 s	14 μs	0.1 μs

Because the time constant of the third branch is far smaller than that of the other branches, the third branch can be neglected. The resistance R_{11} of the first branch of both specimens can be neglected because it is very high compared to the other resistances. The above investigation gives a simplified circuit as illustrated in Fig. 3.15. It consists of a capacitance C_0 and a parallel branch of resistance R_1 and capacitance C_1. The circuit parameters of the model, i.e., the resistance R_1 and capacitances C_0 and C_1, are obtained by ”Data solver” in MS Excel using the objective shown in (3.7). The calculated result of parameters C_0, R_1 and C_1 are shown in Table 3.5.

Table 3.5. The value of the R_k and C_k of the generalized circuit for distance of 0.05 m.

Element	C_0 [μF]	R_1 [MΩ]	C_1 [pF]	Time constant (τ) [μs]
Keyaki	0.26	4.14	1.01	4.2
Sugi	0.32	2.8	1.8	5.0

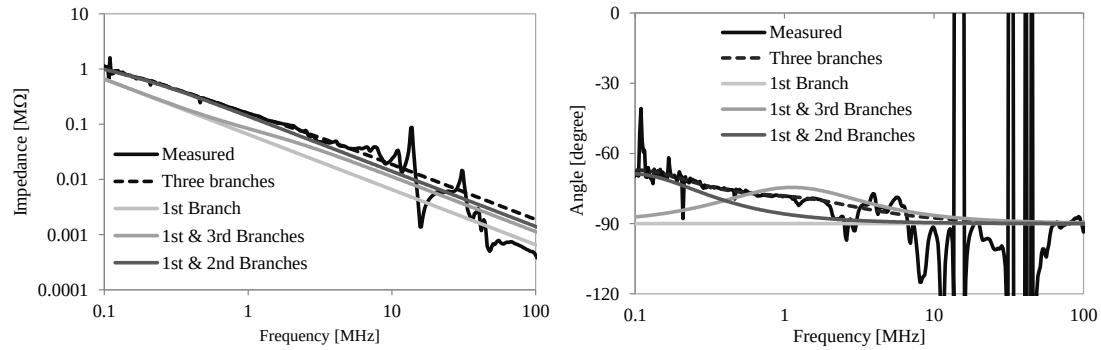

(a) Keyaki

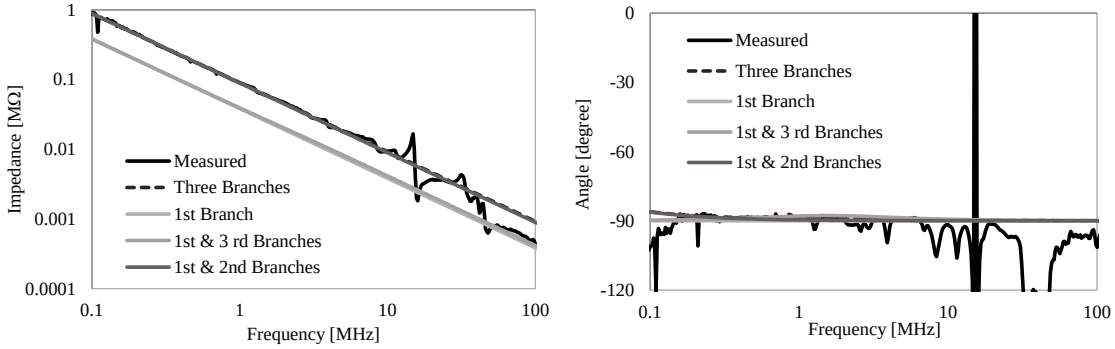

(b) Sugi

Fig. 3.14. Comparison of the impedance Z_{el} between branch elimination and the complete branches calculation with the measured result.

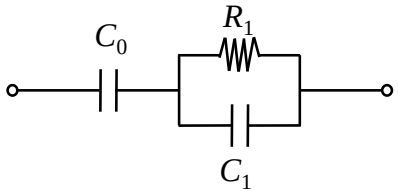

Fig. 3.15. A simplified circuit model for the impedance Z_{el}.

The impedance Z_{el} at a distance between the electrodes d of 0.05 m is calculated using (3.11) and is compared to the measured result illustrated in Fig. 3.16.

$$Z_{el} = \frac{1}{j\omega C_0} + \left[\frac{1}{1/R_1 + j\omega C_1} \right] = \frac{1}{G_{el}(\omega) + j\omega C_{el}(\omega)} \tag{3.11}$$

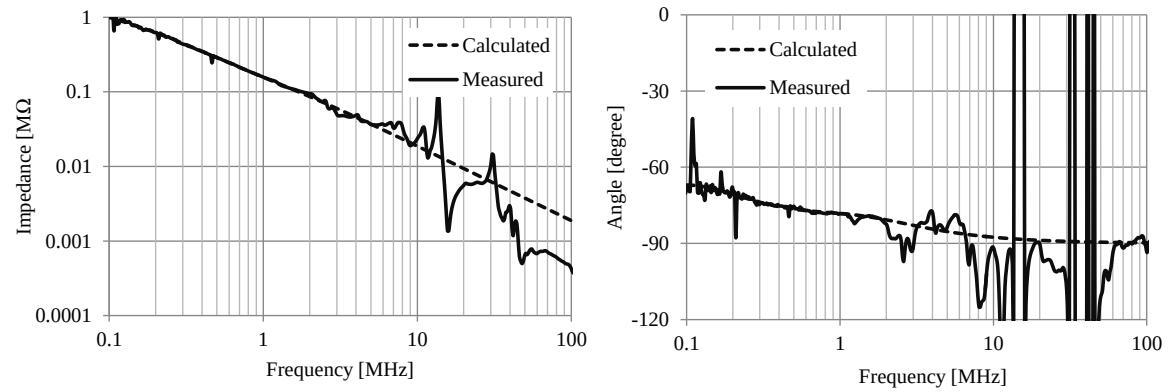

(a) Keyaki

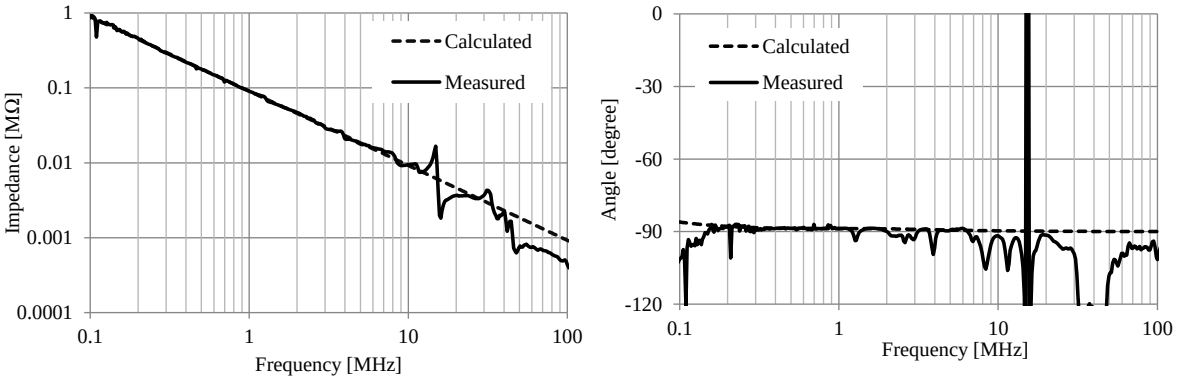

(b) Sugi

Fig. 3.16. Comparison of the branch impedance Z_{el} between calculated and the measured result using a simplified circuit.

Fig. 3.16 shows that the calculated results of the impedance between the electrodes Z_{el}, which is obtained by (3.11), agree well with the measured result up to 5 MHz.

The model of the impedance between the electrodes Z_{el} consists of a capacitor C_0 in series with a parallel *RC* circuit. This model with two branches of stray impedance to ground Z_g is used as the final circuit model of the electrodes implanted into a piece of wood as shown in Fig. 3.17.

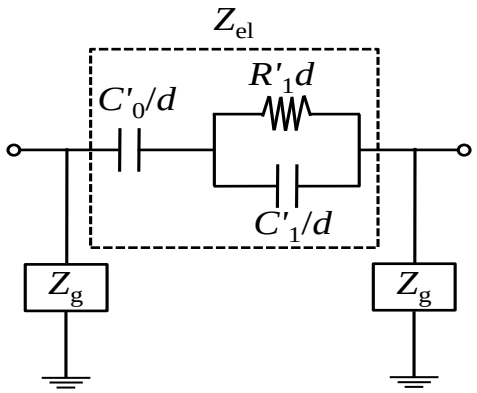

Fig. 3.17. Circuit model of impedance between electrodes

3.4 Application of Circuit Model in Transient Simulation

The aim to model the impedance between the electrodes is for a transient simulation. The usability of the pi-equivalent circuit (Fig. 3.17) is confirmed by comparisons with the measured results. The transient measurements for a distance between the electrodes d = 0.05 m are carried out using a circuit illustrated in Fig. 3.18. A voltage between the electrodes and an injected current is measured. This arrangement is simulated using Electromagnetic Transients Program (EMTP) to calculate the voltage and current response of the electrodes in a piece of wood. The parameters used in this simulation are shown in Table 3.6. The capacitance C_g and resistance R_g to ground are obtained from averaged measured values of those at a frequency range from 100 kHz to 10 MHz shown in Fig. 3.11. The comparisons between the measured and simulated results of both specimens for the distance between the electrodes d of 0.05 m are shown in Fig. 3.19.

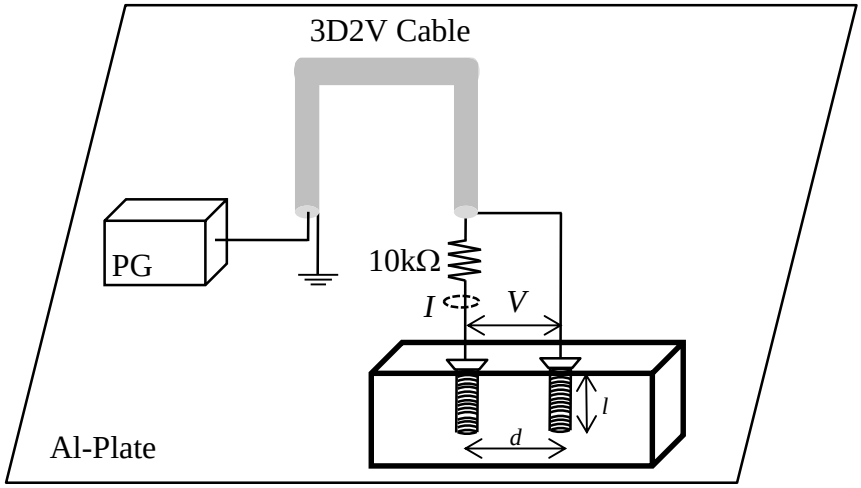

Fig. 3.18. Transient measurement set-up.

Table 3.6. The value of the R_k and C_k of the generalized circuit for distance of 0.05 m.

Element	C_0 [μF]	R_1 [MΩ]	C_1 [pF]	C_g [pF]	R_g [MΩ]
Keyaki	0.26	4.14	1.01	5	1
Sugi	0.32	2.8	1.8	5	1

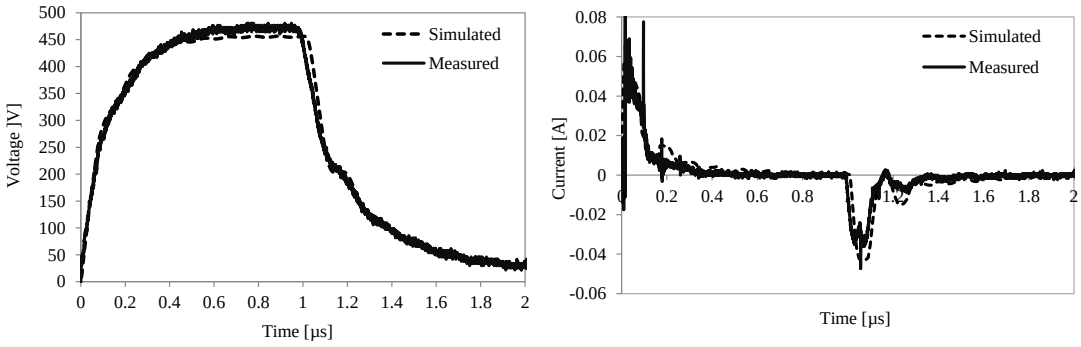

(a) Keyaki

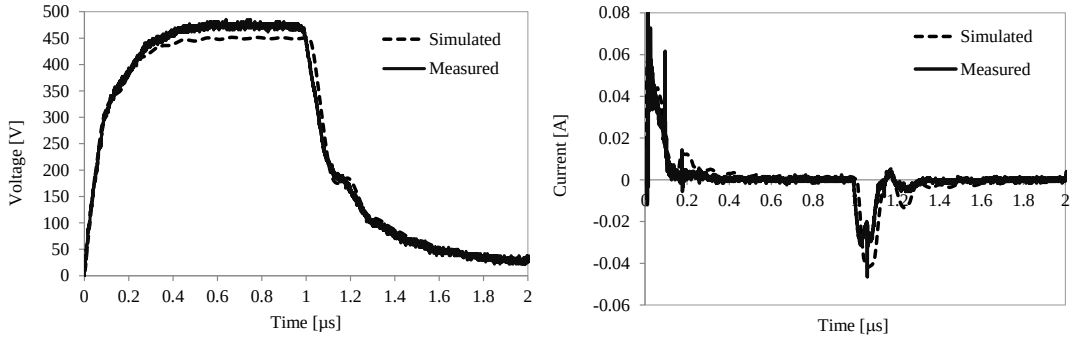

(b) Sugi

Fig. 3.19. Measured and simulated results for transient response of the electrode in a piece of wood, sugi and keyaki.

Fig. 3.19 shows that transient voltage and current obtained by the pi-circuit model with the parameters agree with the measured result.

3.5 Concluding Remarks

A circuit model of the impedance between the electrodes implanted into a piece of wood is proposed in this chapter. The model is a pi-circuit, which consists of a branch impedance between the electrodes implanted into the wood Z_{el} and two branches for expressing stray impedance to ground Z_g. An impedance between the electrodes Z_{el} is initially expressed by an *RC* network, such as either the first or second Foster circuits. The final model of impedance Z_{el} consists of a capacitor in series with a parallel *RC* circuit. The proposed model can be applied to a wide range of fields because the circuit parameters are expressed by a function of the

parameters of the electrode. The deviation of the impedance due to the species of woods is minor.

3.6 References

(1) R. Filter and J.D. Mintz, “An improve 60 Hz wood pole model,” *IEEE Trans. Power Del.,* vol. 5, no. 1, pp. 442-448, Jan. 1990.

(2) D. Permata, N. Nagaoka and A. Ametani:”A model circuit of impedance between electrodes in wood”, *Proc. 6th Int. Symp. EMC and Transients Infrastructures*, Hanoi, 2012, pp.87-88.

(3) D. Permata, N. Nagaoka and A. Ametani, ”A modeling method of impedance between the electrodes implanted into wood,” *The Papers of Technical Meeting on High Voltage Engineering IEEJ*, Kyoto, HV-13-035, pp. 59-63, 2013.

4 MODELING METHOD OF FAST TRANSIENT FOR A SMALL-CAPACITANCE CIRCUIT FOR LIGHTNING SURGE ANALYSIS

4.1 Introduction

Transient assessment is required in the field of power engineering to verify the immunity of electrical and/or electronic equipment connected to power systems. Lightning is one of the key phenomena for an insulation design of power systems. For an estimation of the lightning surge, stray capacitance has to be taken into account even if it is some pico-farads because the surge includes high frequency components. An accurate measurement of the small capacitance is indispensable. Many researches have been obtained the stray capacitances of the apparatuses by numerical simulations, such as finite element method [1-3], or by measurements [4-6], because the theoretical calculation of the stray capacitance is difficult. Furthermore, the measurement becomes harder with the decrease of the size of the apparatus due to the decrease of the capacitance.

Measured results of the small capacitance of a specimen by the steady-state measurement have been described in Chapter 3 [7]. Although the method is applicable in a laboratory test, it is difficult to apply it to the field of power systems whose measuring object is larger than the electronic devices. Instability due to radio interference is a problem when the method is applied to a practical system. The capacitance measurement is generally difficult by the impedance-measuring instrument for its small signal source and low immunity to noise.

On the other hand, the transient measuring method, which gives the impedance as a ratio between the voltage and current frequency responses transformed from time domain, can be easily applied to the high-voltage apparatus. However, the measurement of the small stray capacitance is difficult due to the low impedance of the voltage probe, which is indispensable to the transient voltage measurement. In this chapter, the disadvantage of the method will be described in detail.

Two modeling methods of a small-capacitance circuit is proposed in this chapter. The capacitance is estimated by using only transient currents to overcome the disadvantage of the

conventional method. The pi-circuit, which has been proposed in Chapter 3, is used to express stray capacitors between terminals and those from each terminal to ground [2, 5, 7].

4.2 Measurement of Small-Capacitance Circuit using Transient Voltage and Current Waveforms with Discrete Fourier Transform

A conventional method using voltage and current waveforms with discrete Fourier transform (DFT) is introduced in this section to see the effect of the parasitic capacitance of a voltage probe. The transient characteristics are measured using the circuits illustrated in Fig. 4.1. The common-mode to measure the voltage at the short-circuited electrode V_s and injected current I_s are used to obtain the stray impedance Z_s. The differential mode to measure the voltage between the electrodes V_t and injected current I_t is used to define impedance between the electrodes Z_t.

The transient voltage and currents are measured by a digital oscilloscope (Textronix DPO 4104, 1 GHz) with a voltage probe (Textronix P6139A, 500 MHz, 8pF 10 MΩ) and a current probe (Textronix CT-1). A step-like voltage is applied by a pulse generator (Noise Ken, PG, type INS-4040).

The same specimen with that used in steady-state measurement (Zelkova serrata, Keyaki) is used in the transient measurement. The measured results in the differential and common modes are shown in Figs. 4.2 and 4.3.

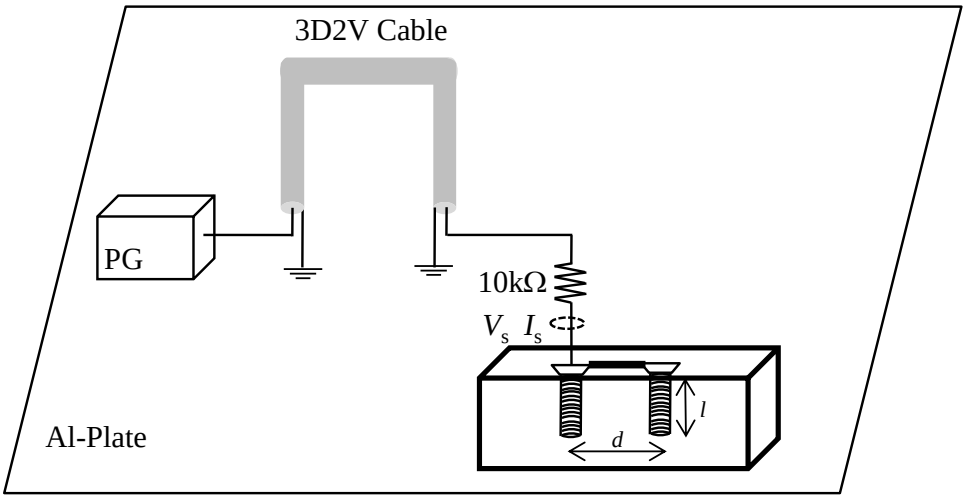

(a) Common mode

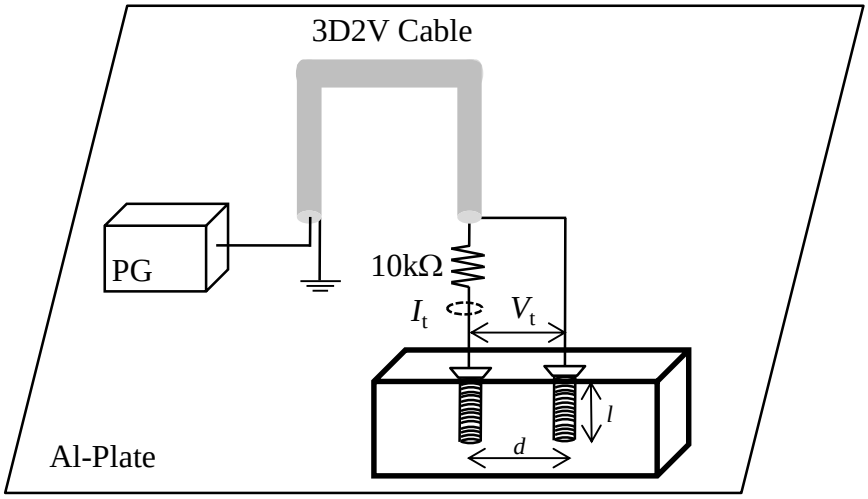

(b) Differential mode

Fig. 4.1. Measurement setup.

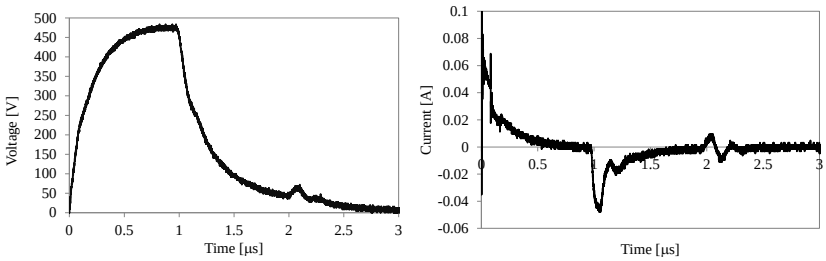

(a) Common mode

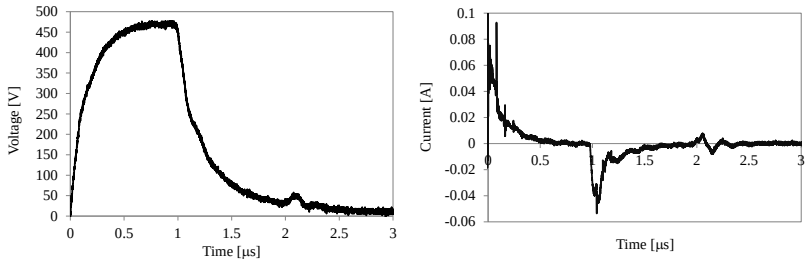

(b) Differential mode

Fig. 4.2. Measured transient characteristic, Keyaki d = 0.05 m.

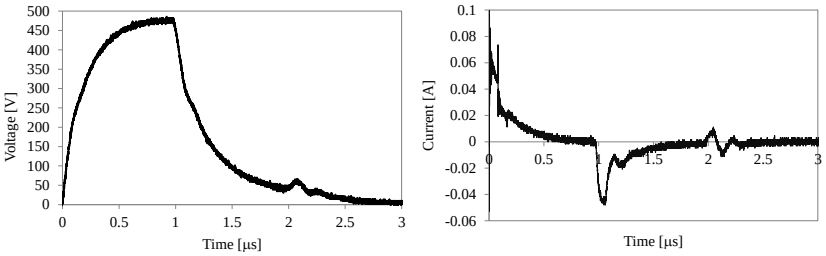

(a) Common mode

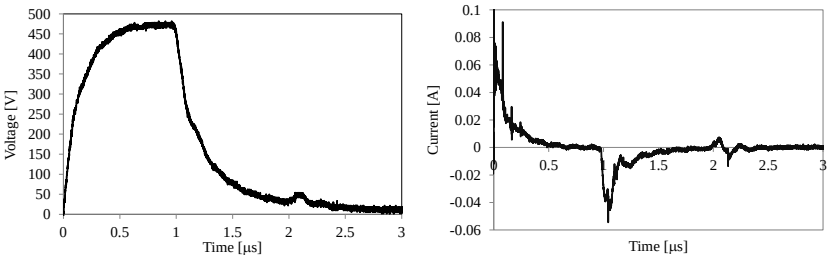

(b) Differential mode

Fig. 4.3. Measured transient characteristic, Keyaki d = 0.1 m.

A DFT [8] is used to convert the measured transient voltage and current from time to frequency domain. The stray impedance Z_s and the impedance between the electrodes Z_t, are

determined from the ratio between the corresponding voltage and current in a frequency domain as shown in (4.1) and (4.2).

$$Z_s(\omega) = \frac{V_s(\omega)}{I_s(\omega)} \tag{4.1}$$

$$Z_t(\omega) = \frac{V_t(\omega)}{I_t(\omega)} \tag{4.2}$$

Figs. 4.4 and 4.5 show the calculated impedances Z_s and Z_t with the measured result by the impedance analyzer instrument. The figures show that there is a notable difference between the numerical results by DFT and those by the steady-state measurement. This might due to the influence of parasitic capacitance of the measuring system. The investigation of this discrepancy is explained in the following section.

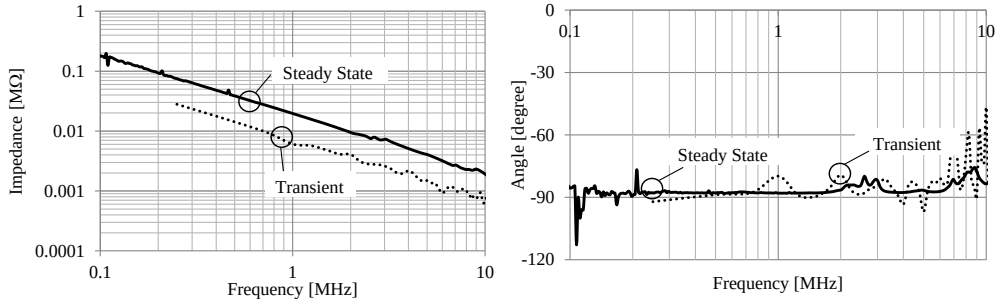

(a) The impedance Z_s and the angle

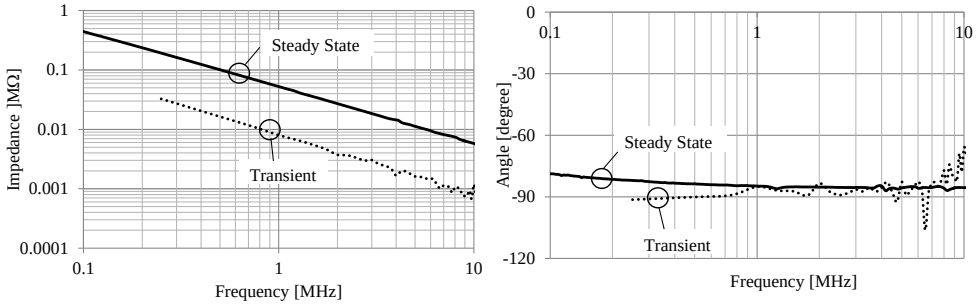

(b) The impedance Z_t and the angle

Fig. 4.4. Measured impedance by transient and steady-state methods, Keyaki d = 0.05m.

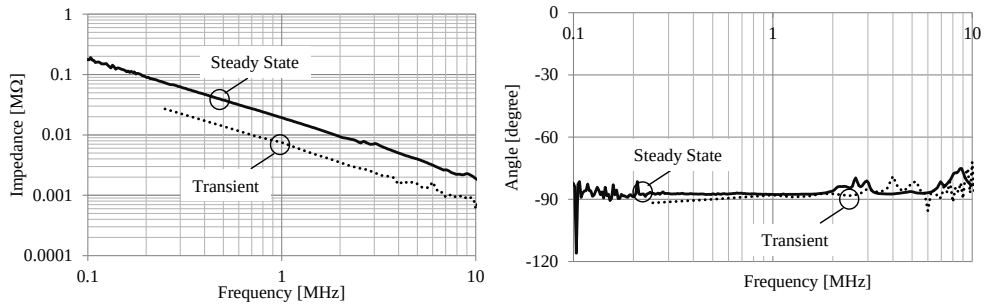

(a) Impedance Z_s and the angle

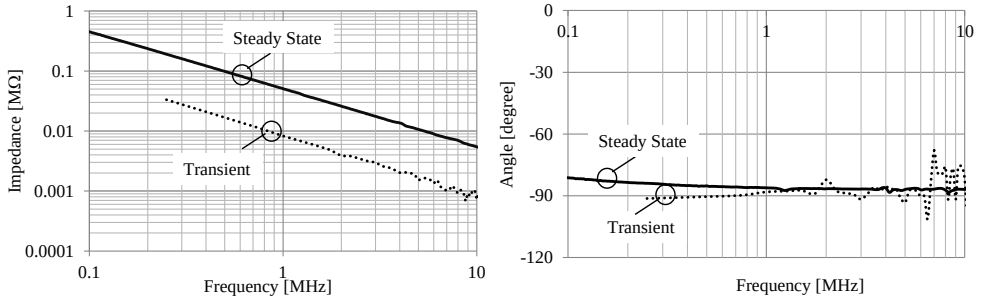

(b) Impedance Z_t and the angle

Fig. 4.5. Measured impedance by transient and steady-state methods, Keyaki d = 0.1m.

4.3 Effect of Measurement System on Small Capacitance Measurement [9]

The previous section has shown that there are discrepancies between the impedances obtained by DFT and by the steady-state measurement. The smaller impedances by the transient measurement are might be due to the effect of the measurement system. Three variables are identified affecting the measured result:

(1) A stray capacitance between each electrode and ground C_g

(2) A capacitance of a voltage probe C_p

(3) A sheath surge impedance of a current injecting cable R_{cs}

These parameters are important for an investigation on a high impedance measurement.

A capacitive circuit, which simulates the impedance between the electrodes implanted into a piece of wood, is tested to clarify the effect of the measuring system. When the practical electrodes are used, the investigation of the stray capacitance to ground is impossible because there is no common terminal in the practical electrodes implanted into a piece of wood. The

circuit under test (CUT) consists of a ceramic capacitor between the terminals C_{el} of 3 pF and two capacitors C_s of 10 pF as illustrated in Fig. 4.6. The capacitor to ground C_g in Fig. 4.7 expresses the stray capacitance to ground. However, the capacitance is unknown. The capacitor C_{ga} is an additional ceramic capacitor for the investigation of stray capacitance. The CUT is tested in a common and a differential mode as shown in Fig. 4.7.

The equivalent circuits for the two modes are illustrated in Fig. 4.8. The resistances R_{cc} and R_{cs} express the characteristic impedances of the coaxial and sheath modes of the cable, respectively. The stray capacitance to ground C_g and an input capacitance of a voltage probe C_p are taken into account. The voltage difference between the electrodes cannot be directly measured, because the stray capacitance to ground of the oscilloscope affects the voltage measurement. The fast transient voltage has to be measured by a "grounded" instrument. The voltages to ground of the electrodes are measured by an oscilloscope and the voltage between the electrodes is indirectly measured as the difference between the voltages. Nodal analysis is applied to analyze the equivalent circuits. The circuit equations for the common and differential modes are shown in (4.3) and (4.4), respectively.

$$\begin{bmatrix} s\left(Cp+\dfrac{2C_sC_g}{2C_s+C_g}\right)+\dfrac{1}{R_{sc}} & 0 & -\dfrac{1}{R_{sc}} \\ 0 & \dfrac{1}{R_{cs}}+\dfrac{1}{R_{cc}} & -\dfrac{1}{R_{cc}} \\ -\dfrac{1}{R_{sc}} & -\dfrac{1}{R_{cc}} & \dfrac{1}{R_{sc}}+\dfrac{1}{R_{cc}} \end{bmatrix} \begin{bmatrix} V_1 \\ V_2 \\ V_3 \end{bmatrix} = \begin{bmatrix} 0 \\ -I \\ I \end{bmatrix} \tag{4.3}$$

$$\begin{bmatrix} s\left(C_{el}+C_s+C_p\right)+\dfrac{1}{R_{sc}} & -sC_{el} & -sC_s & -\dfrac{1}{R_{sc}} \\ -sC_{el} & s\left(C_{el}+C_s+C_p\right)+\dfrac{1}{R_{cs}}+\dfrac{1}{R_{cc}} & -sC_s & -\dfrac{1}{R_{cc}} \\ -sC_s & -sC_s & s\left(2C_s+C_g\right) & 0 \\ -\dfrac{1}{R_{sc}} & -\dfrac{1}{R_{cc}} & 0 & \dfrac{1}{R_{sc}}+\dfrac{1}{R_{cc}} \end{bmatrix} \begin{bmatrix} V_1 \\ V_2 \\ V_3 \\ V_4 \end{bmatrix} = \begin{bmatrix} 0 \\ -I \\ 0 \\ I \end{bmatrix} \tag{4.4}$$

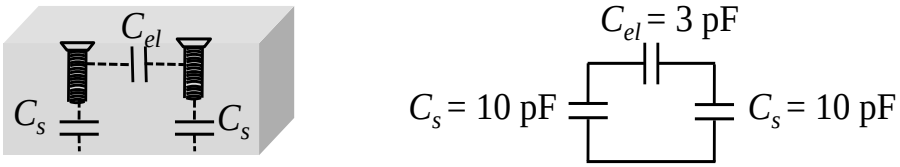

Fig. 4.6. Capacitive circuit, which represent the impedance between electrodes.

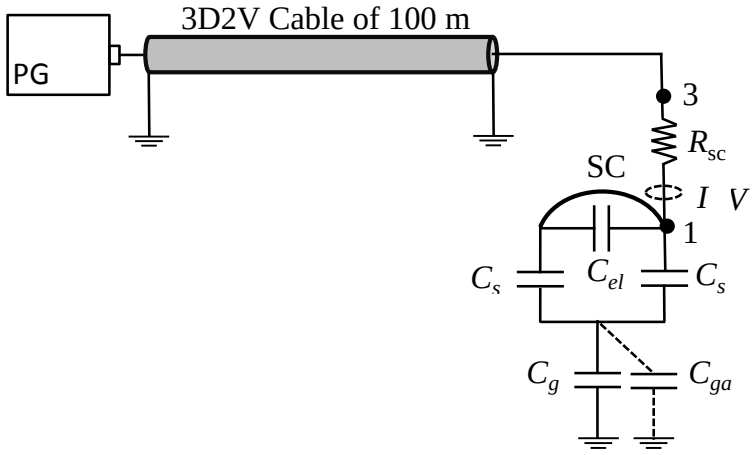

(a) Common Mode

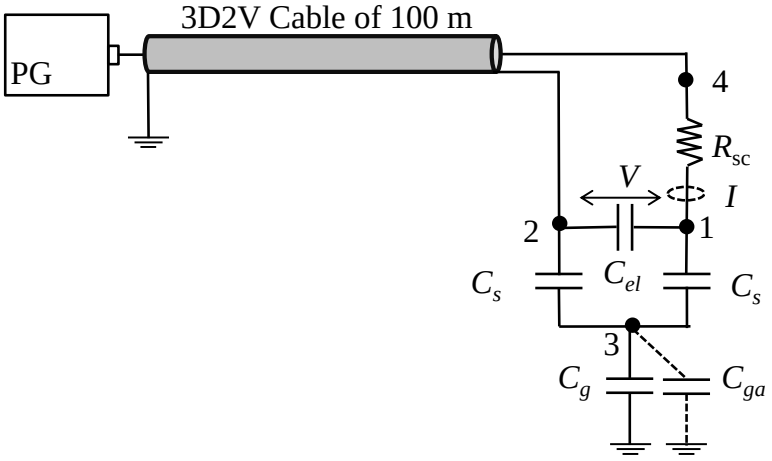

(b) Differential Mode

Fig. 4.7. Setup to investigate the effect of measurement system.

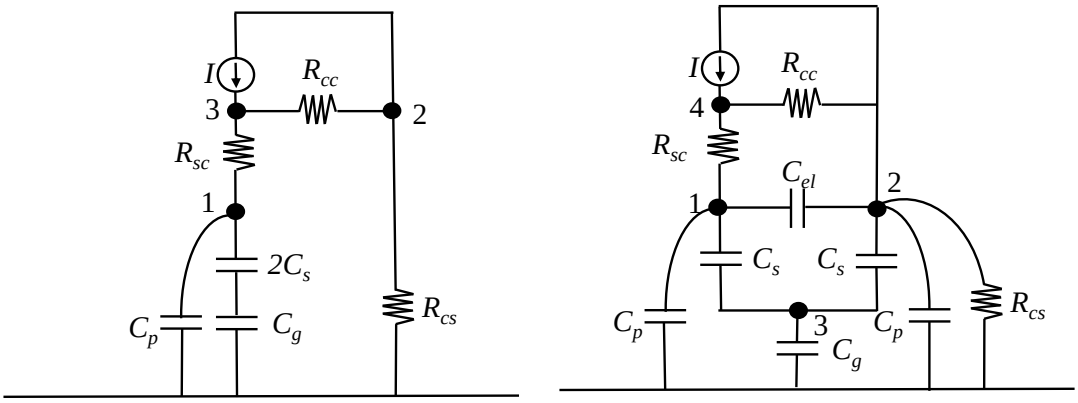

(a) Common mode (b) Differential mode

Fig. 4.8. Equivalent circuit.

To obtain the frequency characteristics of the impedances of the CUT from the transient voltage and current waveforms, a DFT is used to convert into a frequency domain. A time interval Δt in this study is 0.2 ns. The transient waveforms, which are used as input data for the DFT calculation, are truncated before a round trip time for the travelling wave (2τ) on the current injecting cable to neglect the effect of the impedance of the source (P.G.). To minimize the truncation errors, an exponential window function W with damping coefficient α as shown in (4.5) is applied to the time domain waveforms [10].

$$W = \exp(-\alpha i \Delta t) \tag{4.5}$$

In this paper, the damping coefficient of $\alpha=\Delta\omega=2\pi\Delta f$ is employed as shown in (4.6).

$$\begin{aligned} F(k\Delta f) &= 2\left(\sum_{i=0}^{N} f(i\Delta t)\exp(-\alpha i\Delta t)\exp(-j2\pi k\Delta f i\Delta t)\Delta t \right) \\ &= 2\Delta t\left(\sum_{i=0}^{N} f(i\Delta t)\exp(-(\alpha + j2\pi k\Delta) i\Delta t) \right) \\ &= 2\Delta t\left(\sum_{i=0}^{N} f(i\Delta t)\exp(-si\Delta t) \right) \end{aligned} \tag{4.6}$$

The DFT with the exponential window function (modified DFT) is called as Discrete Laplace Transform (DLT) because the equation is identical to the definition of Laplace transform with operator *s*.

Fig. 4.9 shows measured voltage and current waveforms. The transient voltage and current waveforms are truncated at 2τ = 1 μs, i.e., before arriving a reflected travelling wave from the terminal end of the cable. Since the length of the current injecting cable is 100 m and the traveling velocity of the coaxial mode is 198 m/μs, the travelling time τ becomes 0.5 μs. The window function is indispensable to reduce the truncation error on the voltage waveform which is converged to a non-zero voltage.

The impedances of the modes are obtained by the voltage and current in frequency domain as shown in (4.7) and (4.8).

$$Z_{comm}(f) = \frac{V_{comm}(f)}{I_{comm}(f)} \tag{4.7}$$

$$Z_{diff}(f) = \frac{V_{diff}(f)}{I_{diff}(f)} \tag{4.8}$$

Fig. 4.10 illustrates the impedances and their angles. The impedances in a frequency range between 1 MHz and 10 MHz are inversely proportional to the frequency and show a capacitive characteristic.

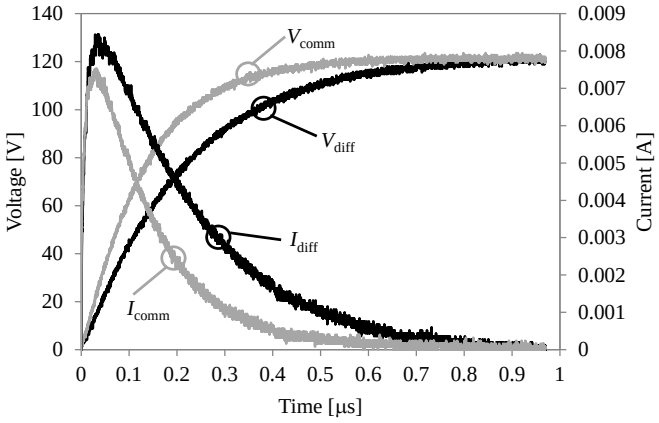

Fig. 4.9. Measured voltage and current waveforms.

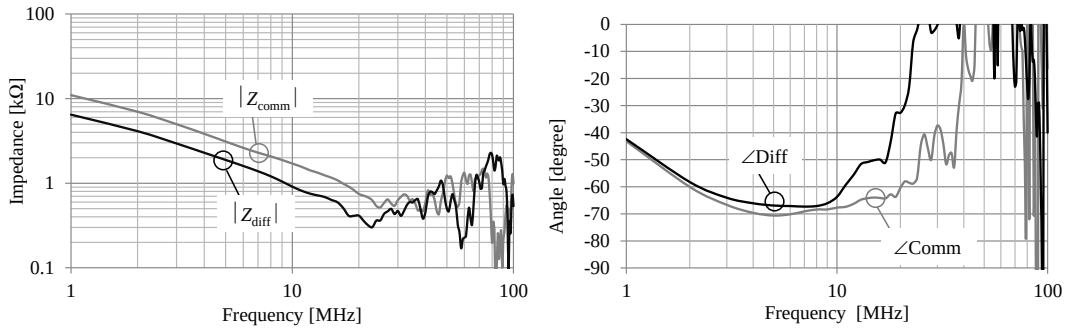

(a) Impedance (b) Angle

Fig. 4.10. Impedance and their angle obtained by DLT.

There is a series resonance at around 20 MHz and some oscillations are observed in the region higher than 10 MHz. It is assumed that the resonance is due to the stray inductance of the circuit and the oscillation is due to noise induced in the circuit.

The load capacitances seen from the source resistor R_{sc} are shown in Fig 4.11. The capacitances shown by bold lines are obtained from the imaginary parts of the impedances, which are determined from the measured results. It shows that the capacitances are affected by noise in a frequency range above 10 MHz. These values go to negative in the region.

The theoretical capacitances are also shown in Fig. 4.11 by the dashed lines. In the common mode, the capacitance is independent of the frequency, because the effect of the sheath surge impedance R_{cs} of the current injection cable is isolated by the high resistance R_{sc}.

$$C_{comm} = C_p + \frac{2C_sC_g}{2C_s + C_g} \tag{4.9}$$

The theoretical capacitances of the differential mode are easily obtained by applying Y - Δ conversion to the circuit consisting of C_s and C_g in Fig. 4.8 (b). By the conversion, a capacitance $C_1 = C_sC_g/(2C_s+C_g)$ is connected in parallel with C_p, and a capacitance $C_2 = C_s^2/(2C_s+C_g)$ is connected in parallel with C_{el}.

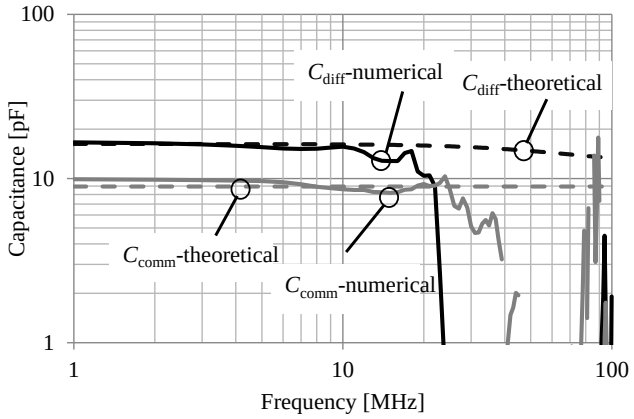

Fig. 4.11. The numerical and theoretical capacitances in differential and common modes.

The characteristic of the circuit is divided into two regions by the time constant τ of the parallel circuit of the capacitive branch (C_1//C_p) and the resistance R_{cs} ($\tau = (C_1+C_p)R_{cs}$). In this study, a frequency region up to 10 MHz is defined as a low frequency region ($f << 1/2\pi\tau$), and a high frequency region becomes a band above 100 MHz.

In the low frequency region, the parallel capacitive branch (C_1//C_p) can be neglected since the sheath surge impedance R_{cs} is far lower than the impedance of the branch. Node 2 in Fig. 4.8 (b) is grounded via the resistor R_{cs}. The equivalent capacitance is given by a parallel connected two branches, as shown in (4.10).

$$\begin{aligned} C_{diff-LF} &= \left(C_p + C_1\right) + \left(C_{el} + C_2\right) \\ &= \left(C_p + \frac{C_s C_g}{2C_s + C_g} \right) + \left(C_{el} + \frac{{C_s}^2}{2C_s + C_g} \right) \\ &= C_p + C_{el} + \frac{C_s (C_s + C_g)}{2C_s + C_g} \end{aligned} \tag{4.10}$$

In the high frequency region, the sheath surge impedance R_{cs} can be neglected due to the low impedance of the parallel connected capacitive branch (C_1//C_p). The differential mode-capacitance in the high frequency region is shown in (4.11).

$$C_{diff-HF} = \frac{1}{2}\left(C_p + C_1\right) + \left(C_{el} + C_2\right)$$
$$= \frac{1}{2}\left(C_p + \frac{C_s C_g}{2C_s + C_g}\right) + \left(C_{el} + \frac{C_s^2}{2C_s + C_g}\right)$$
$$= \frac{1}{2}\left(C_p + C_s\right) + C_{el} \tag{4-11}$$

Since the measured results are affected by noise at a frequency above 10 MHz, the circuit parameters aforementioned are analyzed in the frequency range from 1 MHz to 10 MHz. Although the sheath surge impedance R_{cs} theoretically affect the differential-mode capacitance, the capacitance is independent of R_{cs} in the frequency range. The curve of the differential-mode capacitance C_{diff} in Fig. 4.11 also shows that the sheath surge impedance R_{cs}, is negligible in a frequency range below 10 MHz. The other parameters will be discussed in the following subsections.

(1) *Stray capacitance between CUT and ground C_g*

To investigate the stray capacitance between the CUT and ground C_{g}, an additional capacitance C_{ga} of 47 pF is connected between the common terminal to ground, i.e., in parallel with the unknown stray capacitance C_{g} as shown in Fig. 4.7. The additional capacitance C_{ga} is expressed by dotted lines in the figure. The effect of C_{g} is discussed using a capacitance difference ΔC between the capacitances with and without C_{ga}. The equivalent capacitances with the additional capacitance C_{ga} are obtained as shown in (4.12) and (4.13) by substituting C_{g}+C_{ga} into C_{g} in (4.9) and (4.10). The difference in the common mode ΔC_{comm} is given by the difference between (4.12) and (4.9) as shown in (4.14). In the same manner, the difference in the differential mode ΔC_{diff} is obtained as (4.15) by subtracting (4.10) from (4.13). The stray capacitance to ground C_{g} is obtained by solving (4.14) or (4.15) and substituting the measured ΔC. The theoretical equations (4.14) and (4.15) shows that the ratio of the capacitance difference ΔC in the common and differential mode is four at a low frequency. The measured ratio converges to four with decrease of the frequency as shown in

Fig. 4.12. The C_g for both modes are shown in Fig. 4.12. The very small stray capacitance of 1 to 2 pF can be estimated by the proposed method.

$$C_{comm-withCga} = C_p + \frac{2C_s\left(C_g + C_{ga}\right)}{2C_s + C_g + C_{ga}} \tag{4.12}$$

$$C_{diff-withCga} = C_p + C_{el} + \frac{C_s(C_s + C_g + C_{ga})}{2C_s + C_g + C_{ga}} \tag{4.13}$$

$$\Delta C_{comm} = \frac{4{C_s}^2 C_{ga}}{(2C_S + C_g + C_{ga})(2C_S + C_g)} = 4\Delta C_{diff} \tag{4.14}$$

$$\Delta C_{diff} = \frac{{C_s}^2 C_{ga}}{(2C_S + C_g + C_{ga})(2C_S + C_g)} \tag{4.15}$$

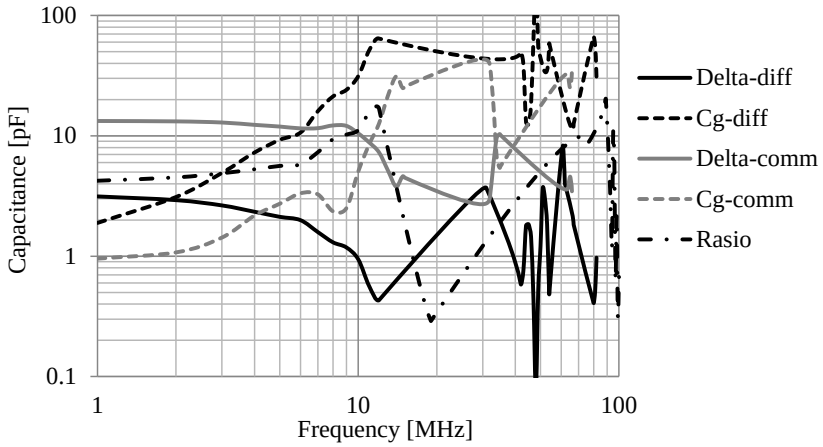

Fig. 4.12. ΔC, C_g and ratio of capacitance differences between common and differential modes.

(2) *Voltage probe capacitance* C_p

Equations (4.16) and (4.17) show a capacitance of a voltage probe C_p obtained from (4.9) and (4.10). These results are calculated by substituting the capacitances obtained from

the results shown in Fig. 4.11 into (4.16) and (4.17). The voltage probe capacitances C_p of the common and differential modes are shown in Fig. 4.13. The specification of the probe capacitance provided by the manufacturer is 8 pF. The result shows the accuracy of the proposed method. Even if the probe capacitance is unknown, it can be estimated by the method.

$$C_{p-comm} = C_{comm} - \frac{2C_s C_g}{2C_s + C_g} \tag{4.16}$$

$$C_{p-diff} = C_{diff} - C_{el} - \frac{C_s\left(C_s + C_g\right)}{2C_s + C_g} \tag{4.17}$$

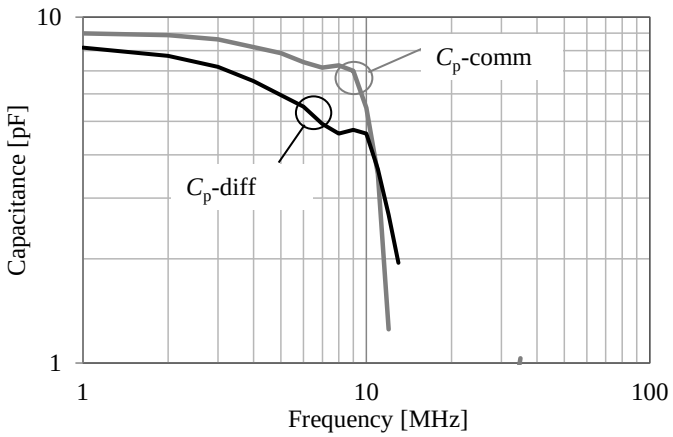

Fig. 4. 13. C_p in common and differential modes.

(3) *Comparison between numerical and theoretical result*

The driving point capacitance ((4.9) and (4.10)) calculated using the measured parameters is shown in Fig. 4.11 by dashed lines. The capacitances C_g and C_p are assumed to be 1 pF and 8 pF, respectively. The parameters C_g and C_p are taken at the low frequency. A comparison between the theoretical and measured results illustrated in Fig. 4.11 shows a satisfactory accuracy of the estimated parameters in a frequency range below 10 MHz. The range is enough to analyze a lightning surge simulation.

4.4 Modeling of Impedance between Electrodes using Numerical Electromagnetic Field Analysis [11, 12]

The previous section has shown the effect the parasitic capacitances on transient measurement. The capacitances consist of a stray capacitance from the circuit to ground, and of the voltage probe capacitance. Since the capacitance of the probe is assumed to be 8 pF, which is comparable or larger than the capacitance of the circuit, the measuring voltage across the small-capacitance circuit will be affected by the parasitic capacitance. The effect has a fatal disadvantage for the transient method. The low impedance estimated in the previous section (Figs. 4.4 and 4.5) is due to the parasitic capacitance. The high sensitivity to noise and the truncation error of the numerical Fourier transform are other disadvantages for the conventional transient measurement method [9].

To overcome these limitations, a method to measure the small-capacitance circuit without voltage information across the circuit is proposed. As a preliminary study, the impedance between the electrodes in a piece of wood is modeled using numerical electromagnetic field analysis. A capacitance is obtained as a ratio of the amplitude of the step current response in a steady-state condition and the slope of the ramp voltage [11, 12].

Virtual Surge Test Lab (VSTL) based on Finite Difference Time Domain (FDTD) method is used as an electromagnetic field analysis in this study. The specimen is modeled using a rectangular dielectric with a relative permittivity of three and dimensions of 140×140×250 mm. The electrodes are expressed by a thin-wire model and their radius r, length l and distance d are 5 mm, 100 mm and 50 mm, respectively. The dimension of the wood and the electrode arrangement is equal to that of the real specimen. The analysis space is 1.25×1.14×1.35 m with a space step Δs of 10 mm.

The capacitance of the electrodes is investigated in the following cases:

(case-a) the wood with electrode, i.e., the specimen in a free space

(case-b) the wood above an aluminum plate with a gap of 21 cm

FDTD simulations are carried out in a common and a differential mode to investigate the capacitance between the electrodes and those to the ground as illustrated in Fig. 4.14.

A ramp-voltage with a slope of 250 V/μs ($=V_{ts}$) is used as a voltage source. The current

response of a capacitive circuit theoretically becomes a step function. The voltage and current responses are shown in Fig. 4.15. The capacitance can be obtained by the current amplitude I and the voltage slope V_{ts} as shown in (4.18).

$$C = \frac{I}{V_{ts}} \tag{4.18}$$

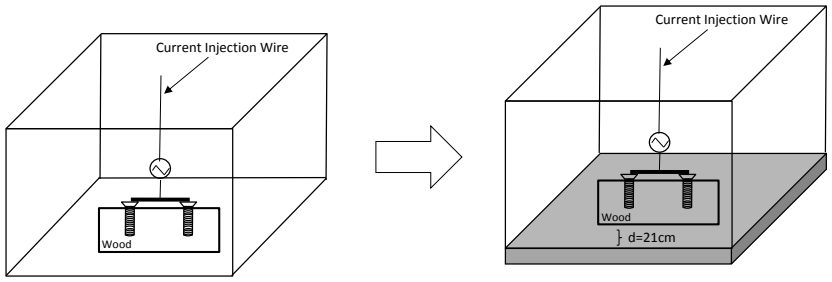

(a-1) In free space, common mode (b-1) Above an aluminum plate, common mode

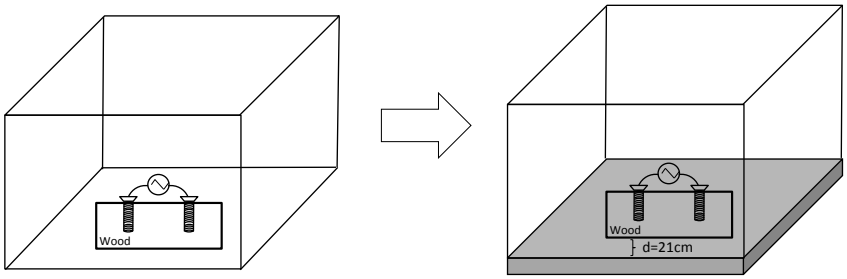

(a-2) In free space, differential mode (b-2) Above an aluminum plate, differential mode

Fig. 4.14. Simulation setup, common and differential modes.

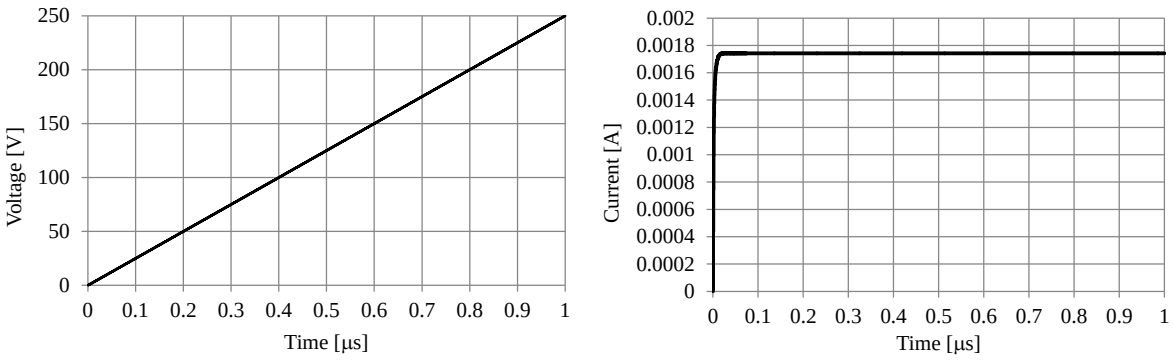

Fig. 4.15. Applied ramp-voltage and current response.

The capacitances between the electrodes in the differential and common mode are shown in Table 4.1. The common mode simulation is carried out in free space and above the ground modeled by an aluminum plate. The difference between two cases is assumed to be stray capacitance $2C_g = C'_{comm} - C_{comm} = 0.2$pF, hence the capacitance for each electrode C_g is 0.1pF.

In the differential mode (Fig 4.14 (a-2)), the capacitance in free space is determined by the sum of the capacitance between the electrodes (C_{el}) and that from the lead wire to the electrode (C_{lw}), i.e, $C_{lw} + C_{el}$. Because the voltage is supplied through the lead wire, i.e, thin wire representation, the capacitance established between the lead wire and the electrode C_{lw} is taken into account. In the experiment, the coaxial cable 3D2V is used to supply the voltage, the effect of the coaxial cable is taken into account by its coaxial surge impedance and sheath surge impedance as will be explained later in the next section. To obtain the capacitance C_{el}, the capacitance C_{lw} has to be removed from the calculated capacitance in free space. The capacitance C_{lw} is obtained by a simulation (Fig. 4.14 (a-2)) without the electrodes. The capacitance between the electrodes C_{el} becomes 3.55 pF (=4.06-0.51). Its accuracy is confirmed by a comparison with a theoretical capacitance between two parallel wires shown in (4.19). The difference between the theoretical and measured capacitance is 6.78 %.

$$C = \left[\frac{\pi \varepsilon_0 \varepsilon_r}{\ln\left(\frac{(d-r)}{r}\right)} \right] l = 3.80\,\text{pF} \tag{4.19}$$

Table 4.1. Capacitance in differential and common modes.

No.	Configuration	Capacitance [pF]			
		Common		Differential	
(a)	Electrodes inserted into wood (in free space)	C_{comm}	6.77	C_{lw} $C_{lw}+C_{el}$	0.51 4.06
(b)	On Al-plate with gap	C'_{comm}	6.97	C_{diff}	4.06

The capacitances from common and differential mode are used to compose a pi-type circuit of the electrodes inserted into a piece of wood on a conductive plate as illustrated in Fig. 4.16. The circuit parameters C_g = 0.10 pF are determined by the common mode, C_{el} = 3.55 pF and C_{lw} = 0.51 pF by the differential mode. Total capacitance of the pi-circuit seen from the terminals can be obtained theoretically ($C_{tot} = C_{el} + C_{lw} + C_g / 2 =$ 4.11 pF). The simulated capacitance C_{diff} (Fig. 4.14 (b-2)) is 4.06 pF. The small difference between the theoretical and calculated capacitance (C_{tot}-C_{diff}) confirms the accuracy of the simulation. From the investigations, it is clarified that the capacitance can be obtained from a set of step-like current and a slope of a ramp-type voltage. The slope of transient waveform can be used to determine the capacitance.

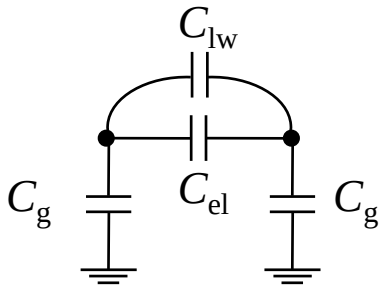

Fig. 4.16. Pi-circuit of impedance between electrodes.

4.5 Measurement of Small-Capacitance Circuit using Transient Current Waveform and Slope of its Wave-tail [13]

The study on the modeling of the impedance between the electrodes by means of numerical electromagnetic-field analysis shows that the capacitance can be determined using a transient waveform. However, it is difficult to apply the ideal ramp voltage at a field measurement.

A comprehensive method to measure a small capacitance with a loss is proposed in this section. The parameters are determined using a set of transient current waveforms. As an application example, the method is applied to a composition of an equivalent circuit expressing the impedance between the electrodes implanted into a piece of wood.

A specimen used in this investigation is a cubic wood (Japanese cypress, Hinoki) of 140 × 140 × 250 mm. Two screws are used as the electrodes whose radius r is 5 mm, distances between the electrodes d is 50 mm and length l is 100 mm. Fig. 4.17 illustrates a measuring circuit. The resistor R_{sc} of 10 kΩ, 51 kΩ or 100 kΩ is attached to the core of the current injecting cable. The 3D2V coaxial cable of 100 m length is used for injecting a current. A voltage is applied using a pulse generator (P.G., Noiseken INS-4040). The transient currents are measured using a digital oscilloscope (Tektronix DPO 4104, 1 GHz) with a current probe (Tektronix CT-1).

The measurements are carried out in the common- and differential-mode. The first setup is for a measurement of the impedance to ground modeled by an aluminum plate. The sheath of the current injecting cable is connected to the plate and the core to the short-circuited electrodes. The second one is for a measurement of the impedance between the electrodes by connecting the electrodes to the core and sheath of the current injecting cable.

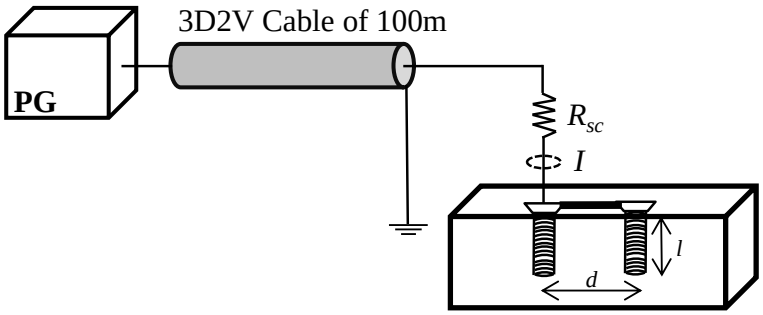

(a) Common mode

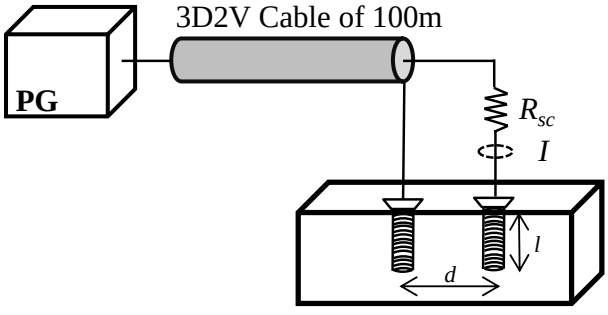

(b) Differential mode

Fig. 4.17. Measurement setup.

The measured results are shown in Fig. 4.18. The vertical axis is displayed in logarithmic scale. The current waveform is truncated before a round trip time for the travelling wave (2τ) on the current injecting cable to neglect the effect of the impedance of the source (P.G.). The time constant (τ) for the common and differential modes obtained from the slope of the current waveforms in Fig. 4.18 are shown in Table 4.2. These data will be further analyzed to determine the circuit parameters as shown in the following subsection 4.5.2.

Table 4.2. Measured time constants (τ) in μs.

	Common Mode			Differential Mode		
R_{sc} [kΩ]	10	51	100	10	51	100
τ [μs]	0.162	0.668	1.262	0.152	0.590	1.068

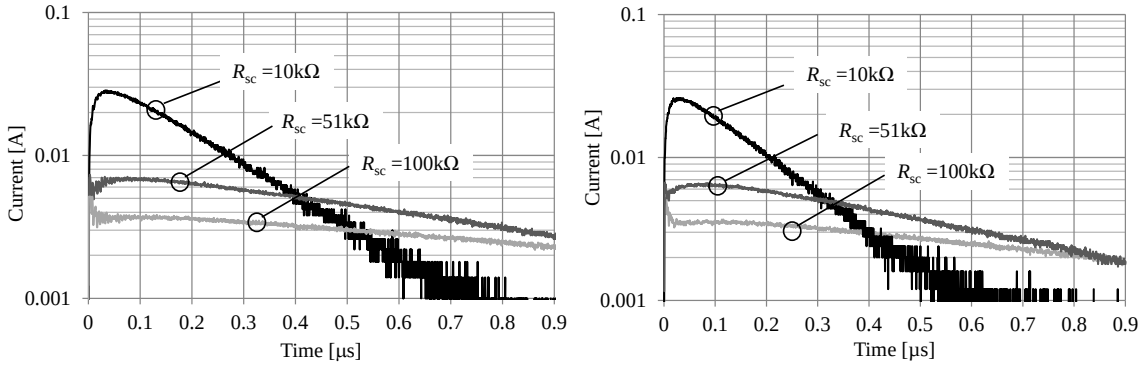

(a) common mode (b) differential mode

Fig. 4.18. Semi logarithmic chart of measured transient current.

4.5.1 Effect of sheath surge impedance

The transient measurement requires a current injecting cable. A coaxial cable should be used from a viewpoint of the high immunity to noise. Since the coaxial surge impedance (R_{cc} = 50 Ω for 3D2V cable) is connected in series to the high source resistor R_{sc}, the effect of the surge impedance is negligible. The sheath surge impedance of the current injecting cable R_{cs} is also negligible. In other words, the current injecting cable can be neglected when a high

resistance R_{sc} is connected in series to the core. However, the low impedance of the sheath surge impedance R_{cs} affects the transient voltage and current in the differential mode. The sheath surge impedance is approximately given by the following equation, and it becomes some hundred ohms.

$$R_{cs} = 60 \ln\left(\frac{2h}{r_s}\right) \tag{4.20}$$

where h and r_s are height and outer radius of the cable, respectively.

The effect of the sheath surge impedance R_{cs} on the transient measurement is confirmed using a source circuit with two source resistors connected either to the core R_{sc}' or to the sheath R_{ss}' as shown in Fig. 4.19 (b). If the sum of the resistances R_{sc}' and R_{ss}' is equal to R_{sc}, i.e., $R_{sc}' + R_{ss}' = R_{sc}$, the injecting current of the circuit in Fig. 4.19 (b) should be identical with that of the circuit shown in Fig. 4.19 (a) if the sheath surge impedance can be neglected. The injected current from the core flows back to the source through the resistor R_{ss}'.

The measured results of a specimen, when the series resistors R_{sc}' and R_{ss}' have the same resistance of 5.1 kΩ, 27 kΩ or 51 kΩ ($\approx R_{sc}/2$), are illustrated in Fig. 4.20. If the source circuit is expressed by Fig. 4.19 (b), the current in the case $R_{sc}' = R_{ss}' = 51$ kΩ should be almost identical to that in the case $R_{sc} = 100$ kΩ. However, there is a 26 % difference between these currents in Fig. 4.20. It shows that the other current path exists. The sheath surge impedance R_{cs}, which is neglected in the circuit shown in Fig. 4.19, has to be taken into account. The modified source circuit is shown in Fig. 4.21.

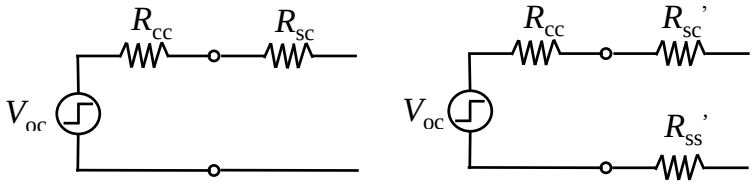

(a) Single resistor (core only) (b) Series resistors (core and sheath)

Fig. 4.19. Equivalent circuit of source and source resistors.

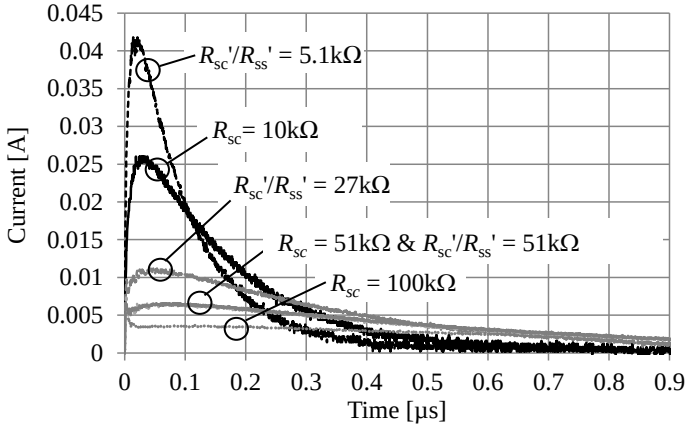

Fig. 4.20. Measured differential currents.

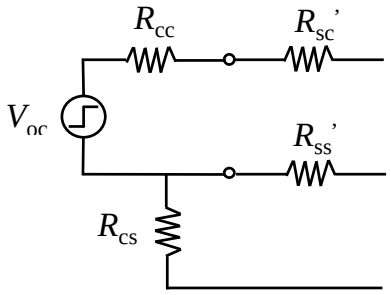

Fig. 4.21. Modified source circuit with sheath surge impedance R_{cs}.

When a device under test (DUT), the electrodes implanted into a piece of wood, for example, is connected to the measurement system through the current injecting cable; an equivalent circuit expresses the arrangement of the measurement system and the DUT is shown in Fig. 4.22. The differential mode impedance shown in Fig. 4.22 is obtained from the modified source circuit (Fig. 4.21) with R_{ss}' = 0 and the pi-circuit of the impedance between the electrodes (Fig. 3.7 (a)). The grounding impedance Z_g is in parallel with the sheath surge impedance R_{cs}. For the 3D2V cable placed on the floor, the sheath surge impedance R_{cs} is 130 Ω, which is far smaller than the impedance Z_g. Therefore, the grounding impedance Z_g connected in parallel with the sheath surge impedance can be negligible when R_{ss}' = 0. The sheath surge impedance R_{cs} is connected in series with the other grounding impedance Z_g. The impedance of the differential mode can be approximately expressed by an equivalent circuit shown in Fig. 4.23. The series connected R_{cs} is also negligible due to the high impedance of the ground branch Z_g. For the common mode test, the sheath surge impedance R_{cs} can be

negligible because the sheath is directly grounded.

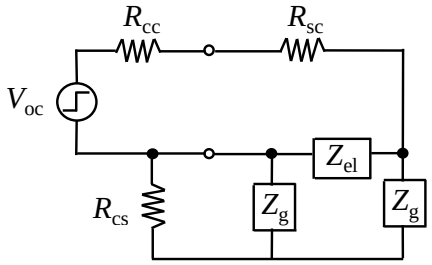

Fig. 4.22. Equivalent circuit of measuring system in differential mode.

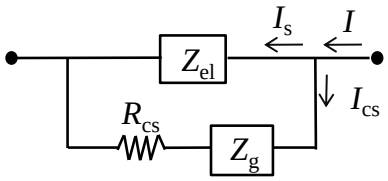

Fig. 4.23. A modified circuit of impedance in differential mode taking into account the effect of sheath surge impedance R_{cs}.

The effect of the sheath surge impedance is confirmed by the measured and theoretical results. Fig. 4.23 is used for the theoretical calculation. The core current I is divided by the parallel-connected branches, the electrodes (Z_{el}) and the other branch. The later impedance is approximately expressed by a series connection of the sheath surge impedances R_{cs} and the grounding impedance Z_g ($Z_g + R_{cs} // Z_g \approx Z_g + R_{cs}$).

The ratio between the current flowing through the sheath (I_s) and that into the sheath surge impedance R_{cs} (I_{cs}) can be calculated using (4.21). The theoretical ratio I/I_s is obtained as 2.7. The parameter R_{el} and R_{g1} are obtained from Table 4.4, as will be explained in the subsection 4.5.2. A measured result of the sheath and core currents (I_s and I) is shown in Fig. 4.24. The ratio between their peak values I/I_s is 2.7, which is identical to the theoretical result.

$$\frac{I_{cs}}{I_s} = \frac{Z_{el}}{R_{cs} + Z_g} \approx \frac{Z_{el}}{Z_g} \approx \frac{2R_{el1}}{R_{g1}} = \frac{2 \cdot 1.41\text{k}\Omega}{1.68\text{k}\Omega} \approx 1.7 \tag{4.21-a}$$

$$\frac{I}{I_s} = \frac{I_s + I_{cs}}{I_s} = 1 + \frac{Z_{el}}{R_{cs} + Z_g} \approx 1 + \frac{Z_{el}}{Z_g} \approx 2.7 \tag{4.21-b}$$

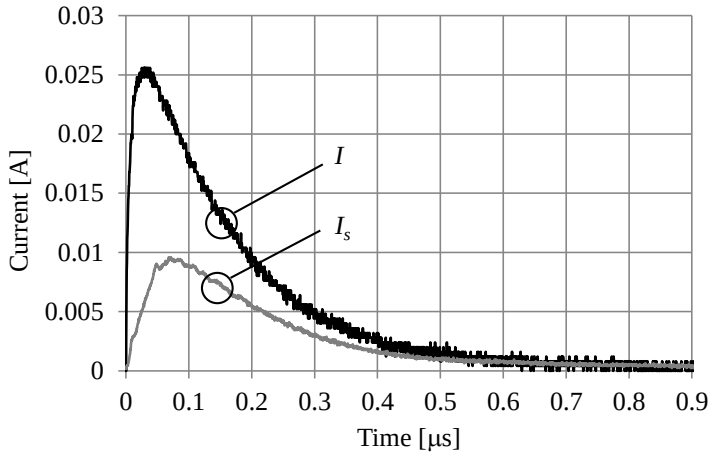

Fig. 4.24. Core current I and sheath current I_s.

4.5.2 Equivalent circuit composition

If the impedance can be modeled by a capacitive circuit illustrated in Fig. 4.25, the time constant (τ) for the RC circuit is expressed by (4.22)

$$\tau = \frac{(R_{cc} + R_{sc} + R_{ac})R_{bc}}{R_{cc} + R_{sc} + R_{ac} + R_{bc}} C_{bc}, \quad \text{for common mode} \tag{4.22-a}$$

$$\tau = \frac{(R_{cc} + R_{sc} + R_{ad})R_{bd}}{R_{cc} + R_{sc} + R_{ad} + R_{bd}} C_{bd}, \quad \text{for differential mode} \tag{4.22-b}$$

where R_{ac}, R_{bc} and C_{bc} are for the common mode, and R_{ad}, R_{bd} and C_{bd} are for the differential mode.

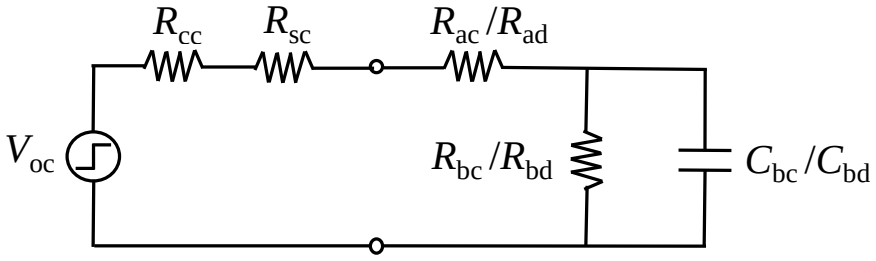

Fig. 4.25. An equivalent circuit of capacitive impedance.

In order to obtain three unknown variables R_{ac}, R_{bc}, and C_{bc} for the common mode, or R_{ad}, $R_{bd,}$ and C_{bd} for the differential mode, (4.22-a) or (4.22-b) is simultaneously solved for three cases with the different source resistors (R_{sc} = 10 kΩ, 51 kΩ or 100 kΩ). The circuit parameters of the impedance in the common and differential modes are shown in Table 4.3.

Table 4.3. Circuit parameters of equivalent circuit.

Mode	Parameter	
Common Z_{comm} (=Z_g/2)	R_{ac} [kΩ]	3.0
	R_{bc} [MΩ]	5.2
	C_{bc} [pF]	12.5
	τ_{bc}=$R_{bc}C_{bc}$ [μs]	65.0
Differential Z_{diff}	R_{ad} [kΩ]	3.4
	R_{bd} [MΩ]	0.9
	C_{bd} [pF]	11.5
	τ_{bd}=$R_{bd}C_{bd}$ [μs]	10.4

Tabel 4.3 shows the impedance characteristic can be divided into three frequency regions. In the low frequency region ($f << f_{b,}$ $f_b = 1/2\pi\tau_b$, $\tau_{bc} = R_{bc}C_{bc}$ or $\tau_{bd} = R_{bd}C_{bd}$) the impedance are principally determined by the resistance R_{bc} for the common mode and by the resistance R_{bd} for the differential mode, respectively. In the middle frequency region (higher than frequency f_b) the capacitance C_{bc} or C_{bd} determined the characteristic. However, in the high frequency region ($f >> f_a$, $f_a = 1/2\pi\tau_a$, $\tau_{ac} = R_{ac}C_{bc}$ or $\tau_{ad} = R_{ad}C_{bd}$), the resistance R_{ac} or R_{ad} determined the impedance characteristics, because the resistance R_{ac} and R_{ad} is far smaller than R_{bc} and R_{bd}.

The pi-type circuit (Fig. 4.22) is composed based on the impedance characteristic, and it becomes as shown in Fig. 4.26. In the high frequency region, the impedance is represented by a resistor R_{g1} for a grounding capacitor Z_g and by $2R_{el1}$ for a branch of impedance between the electrodes Z_{el}. On the other hand, in the low to middle frequency region, it's represented by a parallel *RC* circuit; R_{g2} and C_{g2} for a grounding capacitor Z_g, and R_{el2} and C_{el2} for a branch of

impedance between the electrodes Z_{el}.

The series resistances R_{el1} and R_{g1} are assumed to be the contact resistances of the electrodes. The parallel circuit of R_{el2} and C_{el2} expresses the insulating resistance of the wood and the capacitance between the electrodes. The resistance and stray capacitance of the electrodes to ground are expressed by R_{g2} and C_{g2}. The relations between the circuit parameters (R_{g1}, R_{g2}, R_{el1}, R_{el2}, C_{g2} and C_{el2}) and the parameters shown in Table 4.3 will be explained in the following subsections.

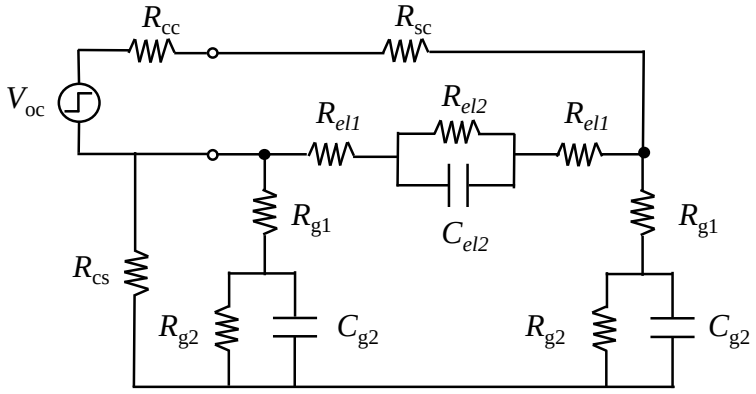

Fig. 4.26. A circuit of impedance between the electrodes implanted into a piece of wood.

4.5.2.1 Derivation of circuit parameters in high frequency region

Since the circuit parameters shown in Table 4.3 are determined by the low and middle frequency components, i.e., the time-constants of the wave-tail shown in Table 4.2, the uncertainty of the series resistor R_{ac} for common mode and R_{ad} for differential mode should be examined. In the example of the impedance between the electrodes implanted into a wood, the reliability of the parameter R_{ac} (R_{ad}) ($<<R_{bc}$ (R_{bd})) can be improved using information in the high frequency region.

The voltage source V_{oc} shown in Figs. 4.21, 4.22, and 4.25 is the open-circuited voltage at the end of the current injection cable. The voltage can be measured without the effect of the parasitic capacitance in the voltage probe because the internal impedance of the source determined by the coaxial-mode surge impedance of the current injection cable (50 Ω) is far lower than the input impedance of the probe.

The impedance in a high frequency region is theoretically obtained as the ratio between

the open-circuited voltage and the current injected into the circuit with some kind of time-to-frequency transformation, such as Fourier transform. However, the noise induced into the measured results and quantization error of a waveform recorder reduce the estimation reliability of the high-frequency characteristic. The impedance in the high frequency region, i.e., the resistance in the region, can be obtained from the voltage and current ratio at the wave-front in a time-domain. This is a practical way comparing with the sophisticated numerical time-to-frequency transformation. Since the open-circuited voltage V_{oc} is known, the series resistance can be obtained from equivalent circuits in the high frequency region shown in Fig. 4.27 and (4.23).

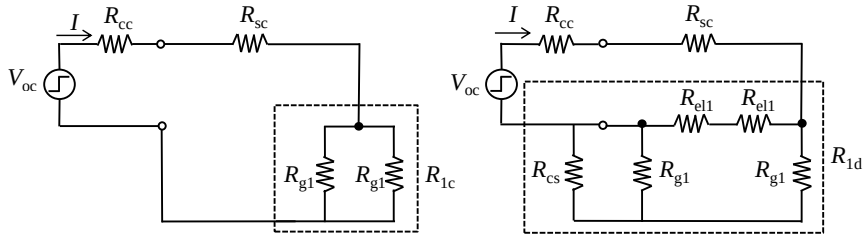

(a) Common mode (b) Differential mode

Fig. 4.27. Equivalent circuit in a high-frequency region.

$$\frac{V_{oc}}{I} = R_{cc} + R_{sc} + R_{1c} = R_{cc} + R_{sc} + {R_{g1}}/{2} \tag{4.23-a}$$

$$\frac{V_{oc}}{I} = R_{cc} + R_{sc} + R_{1d} = R_{cc} + R_{sc} + 2R_{el1} \,//\left(R_{cs} \,//\, R_{g1} + R_{g1}\right) \tag{4.23-b}$$

A small source resistance R_{sc} is preferable for an accurate estimation of the series resistance R_{g1} (R_{el1}) because the resistances given in (4.23) have a term of the source resistances R_{cc}+R_{sc}. The difference between the estimated result (4.23-a) and the source resistances (R_{cc}+R_{sc}) becomes a series resistance in a common mode R_{1c}. The resistance for a differential mode R_{1d} can be obtained in a similar way using (4.23-b). The resistances are obtained as averaged values between the half of the wave-front time of the current waveform (T_f/2=8 ns) and T_f(8 < t < 16 ns). The results for the series resistances R_{1c} and R_{1d} using measured data at R_{sc} = 10 kΩ are 0.8 kΩ and 1.1 kΩ, respectively. These resistances will be used to obtain the circuit parameters R_{g1} and R_{el1} as shown in (4.24), instead of those from

information in the middle and low frequency regions (R_{ac} and R_{ad} in Fig. 4.25 and Table 4.3).

$$R_{g1} = 2R_{1c} \tag{4.24-a}$$

$$R_{el1} = \frac{(R_{cs} \,//\, R_{g1} + R_{g1})R_{1d}}{2[(R_{cs} \,//\, R_{g1} + R_{g1}) - R_{1d}]} \tag{4.24-b}$$

4.5.2.2 Derivation of circuit parameters in low frequency region

In the middle and low frequency regions, the common mode impedance consists of a *RC* parallel circuit, i.e., R_{g2} and C_{g2} connected in parallel (Fig. 4.28 (a)). The circuit parameters are obtained by (4.25) with the results shown in Table 4.3.

$$R_{g2} = 2R_{bc} \tag{4.25-a}$$

$$C_{g2} = \frac{C_{bc}}{2} \tag{4.25-a}$$

As illustrated in Fig. 4.23, the differential mode impedance can be expressed by a parallel connection of Z_g and Z_{el} as shown in Fig. 4.28 (b) and (4.26).

$$R_{el2} = \frac{R_{g2}R_{bd}}{R_{g2} - R_{bd}} \tag{4.26-a}$$

$$C_{el2} = C_{bd} - C_{g2} \tag{4.26-a}$$

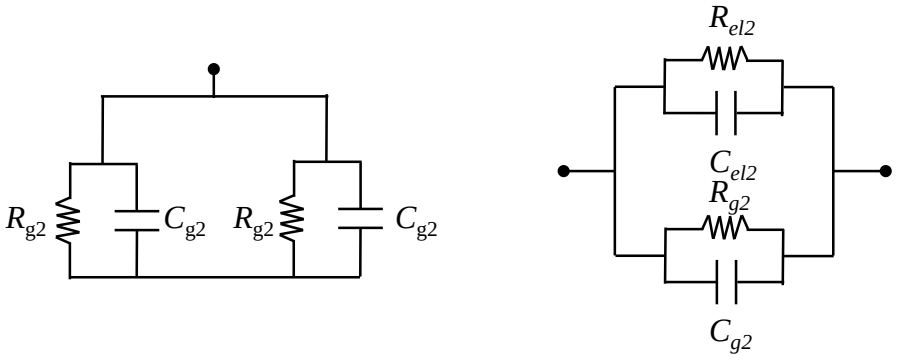

(a) Common mode (b) Differential mode

Fig. 4.28. Equivalent circuit in a low-frequency region.

The circuit parameters of the equivalent circuit (Fig. 4.26) obtained by (4.24) to (4.26) are shown in Table 4.4.

Table 4.4. Circuit parameters of equivalent circuit.

	Parameters	
Z_g (=2Z_{comm})	R_{g1} [kΩ]	1.7
	R_{g2} [MΩ]	10.0
	C_{g2} [pF]	6.3
Z_{el}	R_{el1} [kΩ]	1.4
	R_{el2} [MΩ]	1.0
	C_{el2} [pF]	5.3

4.5.3 Effect of unsymmetrical stray capacitance to ground [14]

The method to measure a small-capacitance circuit and to present an equivalent pi-type circuit model to express the stray capacitors between two electrodes implanted into a wood has been proposed in the previous subsection. The stray capacitances to ground of the terminals have been assumed to be equal, i.e. symmetrical. In general, power apparatuses have unsymmetrical stray capacitances to ground. A method to create an equivalent pi-type circuit model for unsymmetrical stray capacitance to ground is described in this subsection.

A miniature circuit breaker (MCB) is taken as an example of the unsymmetrical stray capacitance to ground. The stray capacitances from the incoming and outgoing terminals are different. In addition to the capacitances, the MCB has stray capacitances between contacts. A measurement method for the unsymmetrical circuit is proposed by a modification of the method for the symmetrical stray capacitance. The modification is achieved in the differential-mode measurements.

This study uses a two-pole low-voltage MCB, whose rated voltage U_e is 220 V and rated short-circuit current I_{cn} is 2.5 kA. The measurements are carried out in the differential- and common-mode as shown in Figs. 4.29 and 4.30.

The common mode test is for a measurement of the impedance to ground. In the test, all terminals are short-circuited (switched “ON”).

The differential modes are for measurements of the impedances between terminals. For an unsymmetrical circuit, two impedances have to be measured to obtain the stray capacitances for the incoming and outgoing terminals. The arrangement of the core and sheath of the current injecting cable is swapped. For the measurements, the terminals at the incoming and outgoing sides are respectively short-circuited to exclude the impedance between phases and the contacts are opened (switched “OFF”).

The sending-end resistor R_{sc} is attached to the core of the current injecting cable of 3D2V. Its cable length is 100 m. A voltage is applied using a pulse generator (P.G., Noiseken INS-4040). The transient currents are measured using a digital oscilloscope (Tektronix DPO 4104, 1 GHz) with a current probe (Tektronix CT-1).

The equivalent circuit of the MCB impedance is similar to that in the electrodes implanted into a piece of wood,.i.e., a pi-circuit. The model of the MCB can be expressed by some capacitors, because the MCB has a high insulating resistance, i.e., its leakage current is negligible. The circuit is illustrated in Fig. 4.31. The capacitor C_{ct} expresses the capacitance between contacts. The capacitors C_{gi} and C_{go} represent the stray capacitors to ground at the incoming and outgoing terminals, respectively.

The common mode characteristic is expressed by the parallel-connected stray capacitors between the MCB and the ground (C_{gi} and C_{go}) as shown in Fig. 4.32 (a) since all terminals are short-circuited. The sheath surge impedance of the current injection cable has no effect on the measurement because the high resistance is connected between the cable core and the circuit.

The effect of the sheath surge impedance in the differential mode has already been explained in the previous subsection. In the mode, the sheath of the current injecting cable is connected to one of the terminals. The stray capacitor grounding from the terminal connected to the sheath, is short-circuited by the low sheath surge impedance. In the incoming-differential mode measurement, the outgoing-stray capacitor to ground C_{go} can be neglected because the outgoing terminal is connected to the sheath. On the other hand, the incoming-stray capacitor to ground C_{gi} is short-circuited in the outgoing-differential mode measurement.

The differential modes are expressed by two equivalent circuits as shown in Fig. 4.32 (b). The circuit consists of a capacitor between contact C_{ct} and a capacitor to ground C_{gi} or C_{go}.

The stray capacitances to be measured in these modes, C_{in}, C_{out} and C_{comm} are derived from the circuits shown in Fig. 4.32. The capacitances can be obtained by analyzing the current waveforms using the slope of the wave-tail as described in the previous subsection or a nonlinear fitting method, which will be described in the next section. The parameters of the pi-type circuit model are obtained by solving (4.27) simultaneously.

$$C_{comm} = C_{gi} + C_{go} \tag{4.27-a}$$

$$C_{in} = C_{ct} + C_{gi} \tag{4.27-b}$$

$$C_{out} = C_{ct} + C_{go} \tag{4.27-c}$$

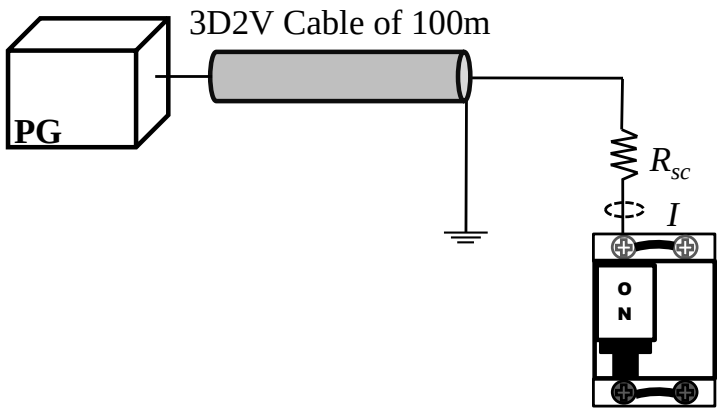

Fig. 4.29. Common mode measurement set-up.

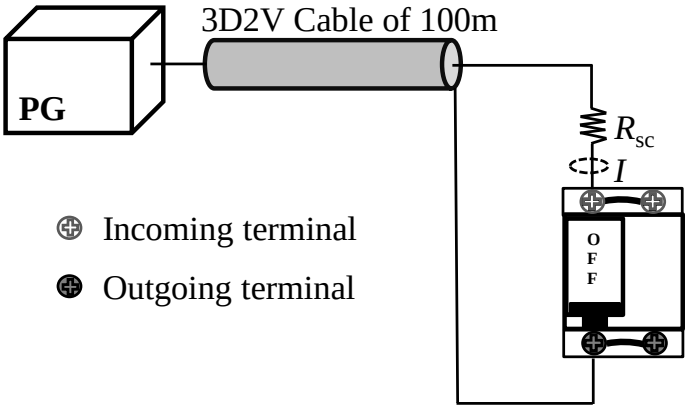

(a) Incoming-differential mode

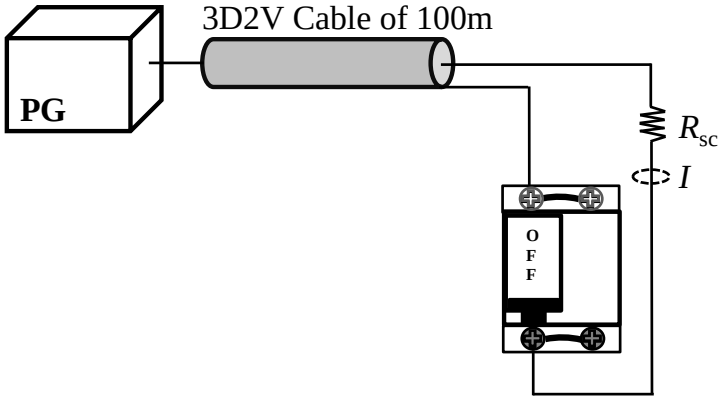

(b) Outgoing-differential mode

Fig. 4.30. Two types of measurement setup: incoming- and outgoing-differential mode.

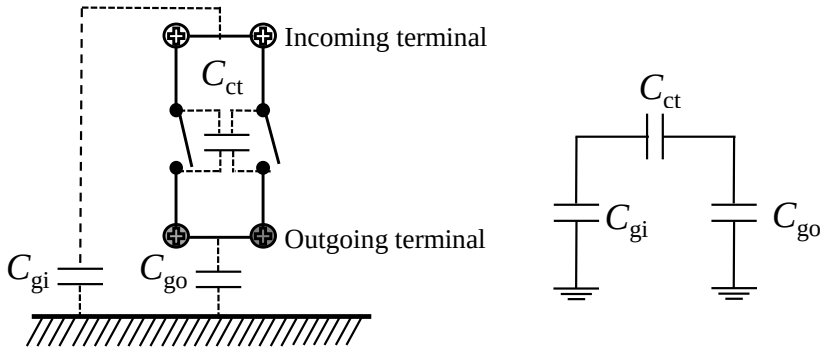

Fig. 4.31. Pi-type circuit of impedance between contacts in MCB.

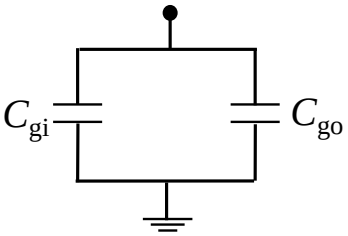

(a) Common mode

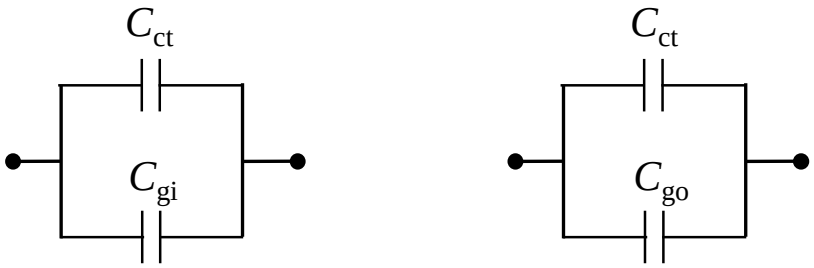

(b-1) Incoming-differential mode (b-2) Outgoing-differential mode

Fig. 4.32. Capacitance circuits in MCB, common- and differential- mode.

4.6. Curve Fitting Method [14]

In subsection 4.5.2, a method to define the circuit parameters using the slopes of a set of transient current waveforms have been proposed. Since the slope is taken from the wave-tail of the current waveforms, the parameters only represent the characteristic in a low frequency region. The characteristic in a high frequency region has been defined as averaged ratio between the open-circuited voltage V_{oc} at the terminal and the injected current waveform at its wave-front. In the previous subsection, the averaged value from the half of the wave-front time $T_f/2$ to the wave-front time T_f is used.

Another method to estimate the circuit parameters using transient current waveforms is proposed. A curve fitting method based on a non-linear least squares method is used to estimate the circuit parameters of the equivalent circuit. A numerical modeling procedure is shown in Fig. 4.33. Two input data are required to define the parameters of each circuit, i.e., an open-circuited voltage V_{oc} and a current flowing through the circuit I. The circuit parameters are obtained by an analysis of the transient waveforms as shown below.

The first step is an analysis of the applied voltage waveform, which is given as sampled data $V_{\mathrm{meas}}(t_i)$. The voltage can be measured by a conventional voltage measurement with a voltage probe because the source impedance, i.e., the coaxial surge impedance of the current injecting cable is far lower than that of the voltage probe. The voltage is assumed to be a step-like voltage whose voltage rise is expressed by a double exponential function shown in (4.28).

$$V_{fit}(t) = V_m\left[1 - Ae^{-t/\tau_1} - (1-A)e^{-t/\tau 2}\right] \tag{4.28}$$

The parameters in (4.28) are obtained by minimizing the object function S given in (4.29).

$$S = \sum_{i=1}^{n}\left[V_{meas}(t_i) - V_{fit}(t_i, \beta_V)\right]^2 = \text{minimum} \tag{4.29}$$

where β_V is a vector of parameters: V_{m}, A, τ_1, τ_2.

The residual sum of squares S is minimized by finding the elements of the vector β_{V}. The fitting should be carried out with reasonable initial values of the parameters [15]. The initial values for V_{m}, and τ_1 are taken from the maximum voltage and half of the rising time of the open-circuited voltage, respectively. The initial values of A and τ_2 are assumed to be A=0.7 and τ_2=10 τ_1. The fitness of the curve, i.e., whether the residual reaches to a local minimum or not has to be confirmed by a plot of the measured and estimated voltages. However, the proposed initial values give a good approximation.

In the second step, the current waveforms are approximated to obtain the circuit parameters. The procedure for the nonlinear fitting of the measured data with a model is similar to that of the first step. The current function $I_{\mathrm{fit}}(t_i, \beta_{\mathrm{I}})$ depends on the applied voltage shown in (4.28) and the impedance of the circuit. The circuit investigated in this paper is assumed to be an *RC* series circuit, and the current is expressed by (4.30) and (4.31) using Laplace operator *s*.

$$I(s) = \frac{V_{fit}(s)}{Z(s)} \tag{4.30}$$

Where

$$Z(s) = R + \frac{1}{sC} \tag{4.31}$$

Since the current function given in (4.30) is in a frequency domain, the current must be transformed into a time domain prior to the estimation of the unknown parameter β_I. The current function $I_{fit}(t, \beta_I)$ in time domain is shown in (4.32). Because the parameters for the voltage $\beta_V = [A, V_m, \tau_1, \tau_2]$ has been obtained, the unknown parameters in β_I become R and C. The fitting to the measured current I_{meas} gives the circuit parameters R and C.

$$i(t) = \frac{V_m C\left[\begin{array}{c} A(\tau_2 - RC)e^{-t/\tau_1} + (A-1)(RC - \tau_1)e^{-t/\tau_2} \\ +\left((A-1)\tau_1 - A\tau_2 + RC\right)e^{-t/RC} \end{array}\right]}{(RC - \tau_1)(RC - \tau_2)} \tag{4.32}$$

The nonlinear curve fittings are carried out using Maple (Ver. 17). The example of the fitted results with the corresponding parameters are shown in Fig. 4.34 with the measured data.

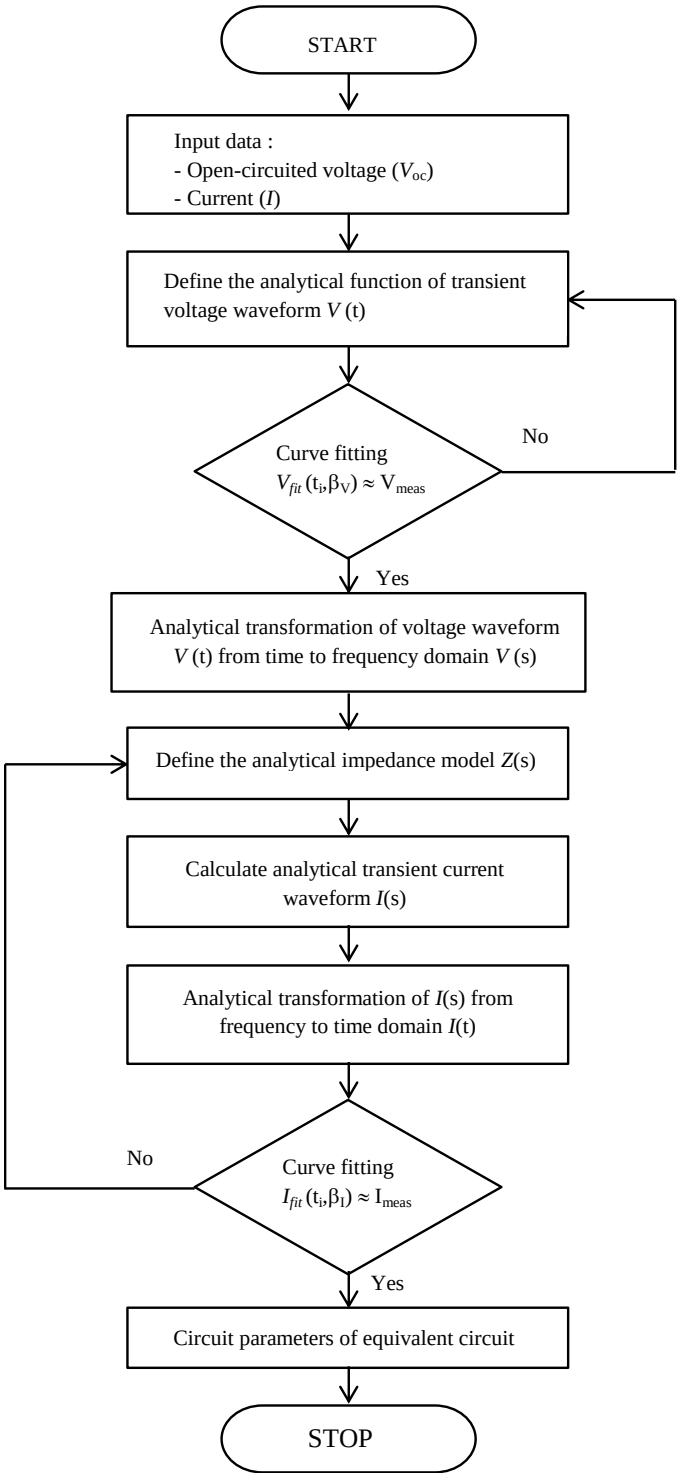

Fig. 4.33. Numerical procedure of curve fitting.

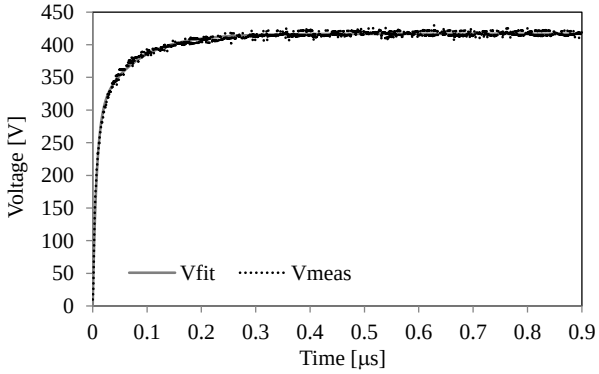

(a) Voltage waveform

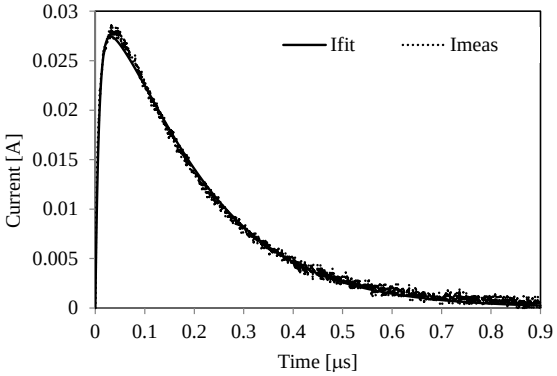

(b) Current waveform

Fig. 4.34. Comparison between measured and fitted waveforms.

4.7 Concluding Remarks

The disadvantage of the conventional method to obtain the impedance as a ratio between the voltage and current frequency responses transformed from time domain using DFT has been shown in this chapter. The parasitic capacitance of the measuring system, such as a voltage probe, obscures the small capacitance. The derivation of the circuit parameter using the voltage information will be affected by the parasitic capacitance.

A method to measure a small capacitance using a set of transient current waveforms has been proposed in this chapter. The method enables a measurement without voltage information across the small capacitance. The effect of the parasitic capacitance of the voltage probe, which has a fatal disadvantage for the transient method, is removed.

In addition, the effect of the sheath surge impedance on the transient measurement, which is one of factors reducing the reliability, is investigated and a correction method is proposed.

The circuit parameters are determined by analyzing the injected current waveform with the open-circuited voltage. Two methods can be used to estimate the circuit parameters:

1. The Slope of wave-tail.

The circuit parameters, which represent the low frequency, are obtained from the slope of wave-tail of the current waveform. The parameters in a high frequency region are defined by a ratio between the open-circuited voltage V_{oc} and the slope of the current at its wave-front. This method is simple and handy, because it does not require any transformation tools.

2. Least squares fitting.

A nonlinear fitting method is applied to the transient waveforms. The circuit parameters are determined by analyzing the injected current waveform with the open-circuited voltage. The reasonable initial values, which are indispensable to the nonlinear fitting for a stable estimation of the circuit parameters, are given by the method using the slope of wave-tail method.

4.8 References

[1] P. Valsalal, S. Usa, and K. Udayakumar, "Modelling of metal oxide arrester for very fast transients," *IET Sci. Meas. Technol*., vol.5, no.4, pp.140-146, Feb. 2011.

[2] Qin Yu and Thomas W. Holmes, "A study on stray capacitance modeling of inductor by using the Finite Element Method," *IEEE Trans. on Electromagn. Compat.*, vol.43, no.1, pp.88-93, Feb. 2001.

[3] Z.J. Csendes and J.R. Hamann, "Surge arrester voltage distribution analysis by the finite element method," *IEEE Trans. Power App. Syst*., vol.PAS-100, no.4, pp.1806-1813, April 1981.

[4] Z. Zhongyuan, L. Fangcheng, and L. Guishu, "A high-frequency circuit model of a potential transformer for the very fast transient simulation in GIS," *IEEE Trans. Power Del.,* vol.23, no.4, pp.1995-1999, Oct. 2008.

[5] G. Grandi, M. K. Kazimierczuk, A. Massarini, and U. Reggiani, “Stray capacitances of single-layer solenoid air-core inductors,” *IEEE Trans. Ind. Appl.*, vol.35, no.5, pp.1162-1168, Sept./Oct. 1999.

[6] S. R. Naidu and A. F. C. Neto, “The stray-capacitance equivalent circuit for resistive voltage dividers,” *IEEE Trans. Instrum. Meas*., vol.34, no.3, pp.393-398, Sept. 1985.

[7] D. Permata, N. Nagaoka and A. Ametani, ”A modeling method of impedance between the electrodes implanted into wood,” *The Papers of Technical Meeting on High Voltage Engineering IEEJ*, Kyoto, HV-13-035, pp.59-63, 2013.

[8] E. Oran Brigham, *The Fast Fourier Transform*, NJ:Prentice Hall,1974.

[9] D. Permata and N. Nagaoka, “Effect of measuring system on small-capacitance measurement using transient waveforms,” *The Science and Engineering Review of Doshisha University*, vol.55, no.4, pp.55-60, Jan 2015.

[10] P. Moreno, and A. Ramirez, “Implementation of the numerical Laplace transform: a review”, *IEEE Trans. on Power Del.*, vol.23, no.4, pp.2599-2608, Oct. 2008.

[11] D. Permata and N. Nagaoka, “A modeling of an impedance between electrodes in a wood using a numerical electromagnetic analysis,” *Proc. 7th Int. Symp. EMC and Transients Infrastructures*, Koh Samui, 2013.

[12] D. Permata, N. Nagaoka and A. Ametani, “A method to determine an impedance between electrodes implanted into a wood using transient current waveform,” *The Papers of Technical Meeting on High Voltage Engineering IEEJ*, Wakayama, HV-14-028, pp.57-61, 2014.

[13] D. Permata and N. Nagaoka, “An impedance measurement of a small-capacitance circuit using transient waveforms for lightning surge analysis,” *IEEJ Trans. Electrical and Electronic Engineeering*, vol.9, no.S1, pp.S37-S43, Oct. 2014.

[14] D. Permata and N. Nagaoka : “Modeling method of fast transient for unsymmetrical stray capacitance to ground”, *IEEJ Trans. Electrical and Electronic Engineeering*, vol.10, Supplement, Oct. 2015 (accepted for publication).

[15] S. Venkatesan, P. Vanaja Ranjam, and D. Ashokaraju, “A comparative study on methods for evaluation of lightning impulse parameters,” *Proc. 2003 Conf. Convergent Technologies for Asia-Pacific Region*, vol.4, 2003, pp.1562-1566.

5 APPLICATION OF MEASUREMENT METHOD FOR SMALL-CAPACITANCE CIRCUIT

5.1 Introduction

Transient analysis is essential in power system studies. Transient phenomena may be the result of lightning strike, some malfunction of the system or the switching of a circuit [1]. Since transient analysis by digital simulation has enough accuracy in comparison with that by experiment, numerical simulation tools have been widely used to study the various phenomena such as transient overvoltage due to lightning or switching. For a circuit-theory-based digital simulation, equivalent circuit and its parameters are indispensable [2]. The users have to define every circuit parameters even if the capacitance is very small for a fast transient simulation. In general, the stray capacitance cannot be obtained by theoretical equation, and its measurement is difficult. The measurement method of small-capacitance circuit has been proposed [3], and is explained in Chapter 4.

This chapter will demonstrate the application of the proposed method in power system apparatus. The highlighted point of the method is an assumption that sheath surge impedance R_{cs} is far smaller than that of the ground impedance Z_g. Hence, one of the ground impedances Z_g, which is connected in parallel to sheath surge impedance R_{cs}, has been neglected. When the ground impedance Z_g is comparable with the sheath surge impedance R_{cs}, the ground impedance Z_g cannot be omitted as shown in Fig. 5.1. Although the circuit parameters can be theoretically estimated, the proposed method may lose its practicality. The limitation in the capacitance can be easily calculated by (5.1). If the sheath surge impedance is assumed to be 130 Ω (placed on the ground), the capacitance at a frequency of 1 MHz becomes about 1 nF. As the same manner, the capacitance at 10 MHz becomes 100 pF. The small capacitance defined by (5.1) is the target of the measurement of this thesis.

$$C << \frac{1}{\omega R_{cs}} = \frac{1}{2\pi f R_{cs}} [\mathrm{F}]$$

$$<< \frac{1}{2\pi 130} [\mu\mathrm{F}] = 1.2[\mathrm{nF}], \text{ at } 1\,\mathrm{MHz} \tag{5.1}$$

$$<< \frac{1}{2\pi 1300} [\mu\mathrm{F}] = 0.12[\mathrm{nF}], \text{ at } 10\,\mathrm{MHz}$$

If the grounding capacitance is far greater than that of the above value, any conventional steady-state and transient methods can be applied to the measurement.

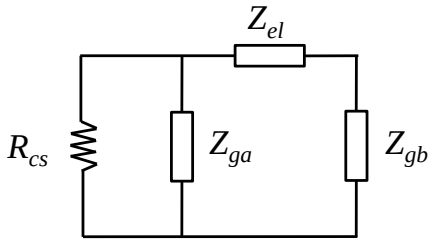

Fig. 5.1. An equivalent circuit of impedance between the electrodes in case ground impedance Z_g is comparable with the sheath surge impedance R_{cs}.

The small-capacitance is a typical property of stray capacitor. Hence, the proposed method is applied to measure the stray capacitance in the following apparatus.

(1) Electrodes implanted into a piece of wood.

Wooden poles and cross-arms are still used in distribution system across the world [4, 5]. Flashover through the wood can be occurred in case the wood is aging or has high moisture content [6]. The transient characteristic of the wooden insulator against a lightning strike is important to insulation design. One of the factors determining the characteristic is the impedance between the electrodes implanted into a piece of wood.

(2) Miniature circuit breaker (MCB).

In an MCB, the stray capacitors are formed between contacts, phases, and to ground. The MCB has to be precisely modeled in a transient overvoltage studies. The circuit breaker has been conventionally represented by an ideal switch [7]. Recently, behaviors of the

dielectric insulation during its open/close operation were presented [8, 9]. In this study, the stray capacitance, which is important for the transient characteristic of the MCB, is measured using the proposed method. When the contacts are closed, the MCB is modeled by a stray capacitor between phases and two symmetrical stray capacitors to ground. If the contacts are opened, the MCB is represented by stray capacitors between contacts and phases, and two unsymmetrical stray capacitors to ground [3, 10].

(3) Gas-filled arrester (GA).

An inherent property of a gas-filled arrester before its flashover is a small capacitance [11]. For example, it is required to model the internal impedance of GA to estimate the breakdown voltage. The equivalent circuits of the MCB and GA are useful to evaluate overvoltage in communication system such as telephone system as well as in low-voltage distribution system [11].

5.2 Impedance between Electrodes Implanted into a Piece of Wood

The specimen used in this investigation is a cubic wood (Japanese cypress, Hinoki) of 140 × 140 × 250 mm. Two screws are used as electrodes. The screw has radius r of 5 mm, distance between the electrode d of 30 or 50 mm and length l of 80 or 100 mm. There are four cases of the electrode arrangement shown in Table. 5.1. The specimens are tested in the common and differential mode as shown in Fig. 4.16 in Chapter 4.5. The measured current waveforms are analyzed by the following two methods: the slope of wave-tail method and the nonlinear fitting method.

Table 5.1. Parameters of measurement.

	Distance d [mm]	Length l [mm]
Case 1	30	80
Case 2	50	80
Case 3	30	100
Case 4	50	100

5.2.1 Slope of wave-tail method

The measured results in semi-logarithmic charts are shown in Fig. 5.2. The time constants (τ) for the differential and common modes obtained from the slope of the current waveforms illustrated in Fig. 5.2 are shown in Table 5.2. These data are used to determine the parameters of the equivalent circuit shown in Fig. 5.3 by the slope of wave-tail method described in subsection 4.5.2. The circuit parameters of the impedance in the common and differential modes are shown in Table 5.3.

Table 5.2. Measured time constants (τ) in μs.

	Common Mode			Differential Mode		
R_{sc} [kΩ]	10	51	100	10	51	100
Case 1 [d30,l80]	0.148	0.602	1.109	0.146	0.579	1.050
Case 2 [d50,l80]	0.143	0.616	1.169	0.133	0.505	0.915
Case 3 [d30,l100]	0.158	0.639	1.200	0.156	0.636	1.163
Case 4 [d50,l100]	0.162	0.668	1.262	0.152	0.590	1.068

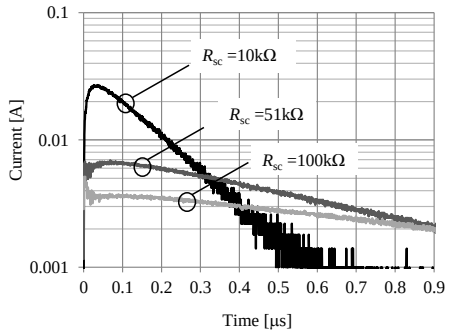

(a-1) case 1 - common mode

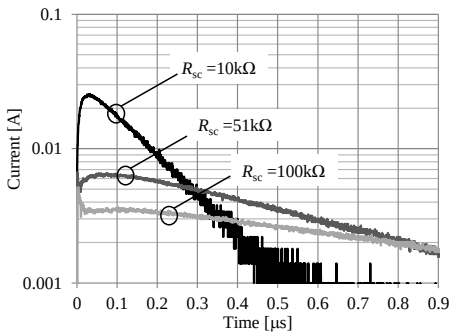

(b-1) case 1 – differential mode

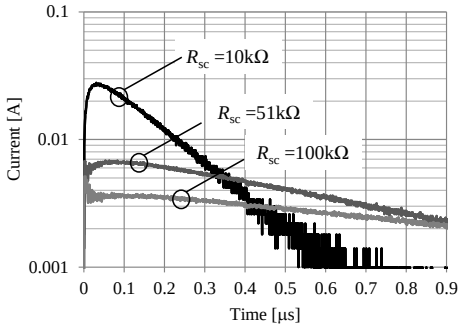

(a-2) case 2 - common mode

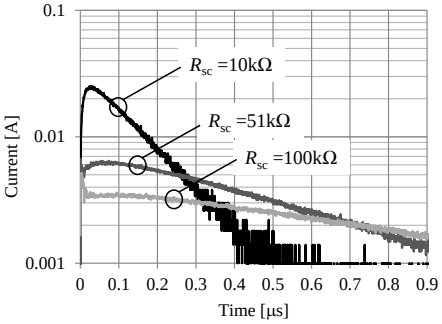

(b-2) case 2 – differential mode

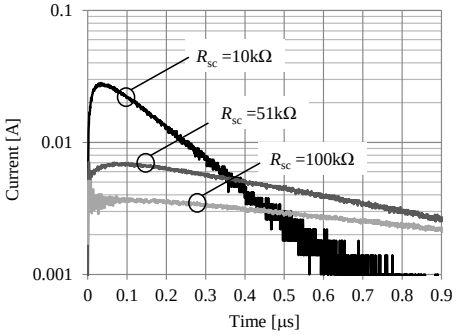

(a-3) case 3 - common mode

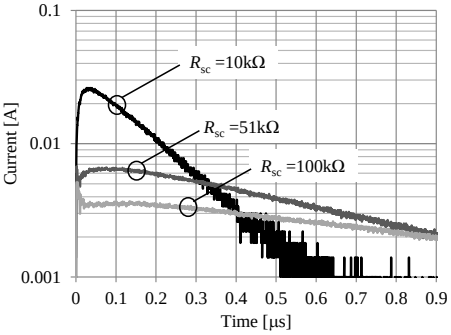

(b-3) case 3 – differential mode

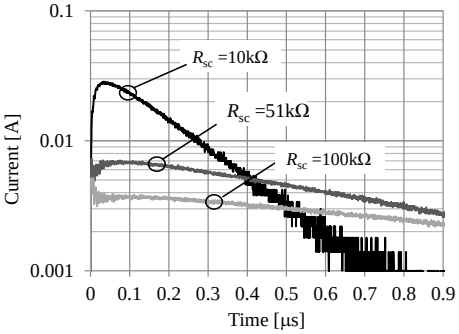

(a-4) case 4 - common mode

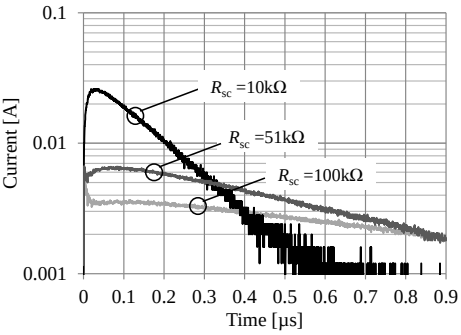

(b-4) case 4 – differential mode

Fig. 5.2. Semi logarithmic chart of measured results of transient current.

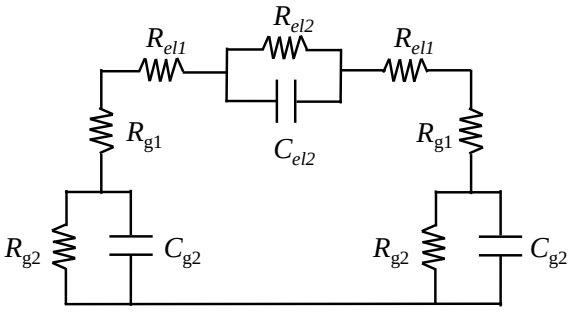

Fig. 5.3. A circuit of impedance between the electrodes implanted into a piece of wood.

Table 5.3. Circuit parameters determined by the slope of the wave-tail method.

	Parameter	Case 1 [d30,l80]	Case 2 [d50,l80]	Case 3 [d30,l100]	Case 4 [d50,l100]
Z_g (=2Z_{comm})	R_{g1} [kΩ]	2.0	1.9	1.8	1.7
	R_{g2} [MΩ]	2.5	7.7	6.6	10.0
	C_{g2} [pF]	5.8	5.9	6.0	6.3
Z_{el}	R_{el1} [kΩ]	2.0	1.9	1.4	1.4
	R_{el2} [MΩ]	1.4	1.2	1.2	1.0
	C_{el2} [pF]	5.6	3.8	6.5	5.3

5.2.2 Nonlinear fitting method

An open-circuited applied voltage and the current are analyzed using the nonlinear fitting method. Since a reduction of the number of parameters will stabilize and speed up the convergence calculation, the impedance of the circuit shown in Fig. 5.3 is simplified. Resistances R_{el2} and R_{g2}, which represent the insulating resistance of the wood and resistance between the electrodes and the ground, are neglected. These resistances are very high, and have a minor effect on the impedance characteristics in the region ($f<f_1$, $f_1=1/2\pi\tau_1$, $\tau_1=R_{g1}C_{g2}$ or $\tau_1=R_{el1}C_{el2}$) and ($f>f_2$, $f_2=1/2\pi\tau_2$, $\tau_2=R_{g2}C_{g2}$ or $\tau_2=R_{el2}C_{el2}$). The equivalent circuit is reduced as shown in Fig. 5.4. The resistance R_{el} and R_g are assumed to be the contact resistance of the electrodes, whereas the capacitances C_{el} and C_g represent the capacitance between the electrodes and the stray capacitance of the electrodes to ground, respectively.

The voltage waveform is analyzed by the nonlinear fitting in the same manner as described in section 4.6. The impedance model changes to the circuit expressed in Fig. 5.4. In the common mode (Fig. 5.4(a)), the impedance is still assumed to be an *RC* circuit as shown in (4.32), where the resistance *R* becomes a series resistance, i.e, $R_{comm} = R_{cc} + R_{sc} + R_g/2$. Since R_{cc} and R_{sc} are 50 Ω and 10 kΩ, respectively, the resistance R_g can be obtained, i.e, $R_g = 2(R_{comm}-(R_{cc} + R_{sc}))$. The common mode-capacitance C_{comm} is equal to a parallel branches of capacitance to ground C_g, i.e, $C_{comm} = 2C_g$.

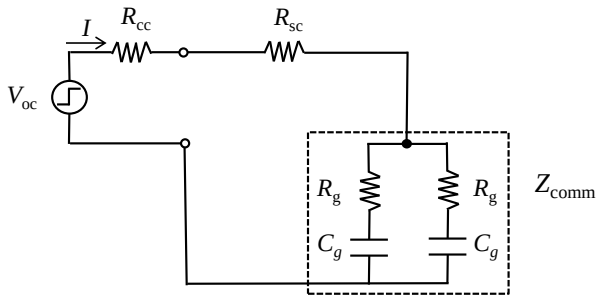

(a) Common mode

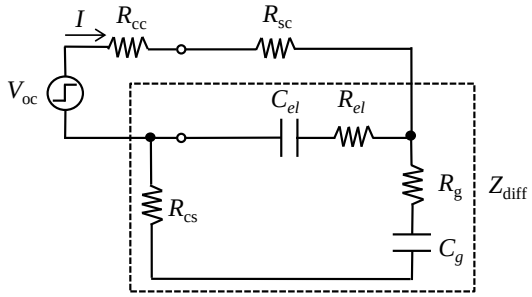

(b) Differential mode

Fig. 5.4. The simplified circuit of impedance between the electrodes implanted into wood used for nonlinear fitting.

In the differential mode, one of branches of the stray impedances to ground is short-circuited by the low sheath surge impedance as shown in Fig. 5.4(b). The impedance is shown in (5.2) as a function of Laplace operator *s*.

$$Z(s) = \frac{(1+sR_{el}C_{el})(1+sR_gC_g+sR_{cs}C_g)}{s(sR_{cs}C_{el}C_g+sR_{el}C_{el}C_g+sR_{el}C_{el}C_g+sR_gC_{el}C_g+C_g+C_{el})} + (R_{cc}+R_{sc}) \qquad (5.2)$$

The resistances R_{cc}, R_{sc} and R_{cs} are known from the measurement circuit, and the parameters R_g and C_g are obtained from the common mode calculation. The nonlinear fitting to the current waveform gives the parameters R_{el} and C_{el}. The circuit parameters obtained by the nonlinear fitting method are shown in Table 5.4. The fitted results with the corresponding parameters are shown in Figs. 5.5 and 5.6 with the measured data.

Table 5.4. Circuit parameters determined by the nonlinear fitting method.

	Common Mode		Differential Mode	
	R_g [kΩ]	C_g [pF]	R_{el} [kΩ]	C_{el} [pF]
Case 1 [*d*30,*l*80]	1	5.8	1.5	5.1
Case 2 [*d*50,*l*80]	1	5.8	1.5	4.2
Case 3 [*d*30,*l*100]	1	6.1	1.4	6.1
Case 4 [*d*50,*l*100]	1	6.9	1.4	4.6

Theoretically, the contact resistance should be inversely proportional to the surface area. Table 5.3 shows the contact resistance R_{g1} or R_{el1} have a decreasing tendency with the increase of the electrode length. It expresses the fact that the contact resistance is inversely proportional to the surface area. However, the resistance R_g or R_{el} in Table 5.4 is nearly equal for all cases. It shows that the contact resistance is independent of the length of the electrode. In this study, the clear trend of the contact resistance cannot be observed because a stable contact between the wood and the electrode is not achieved.

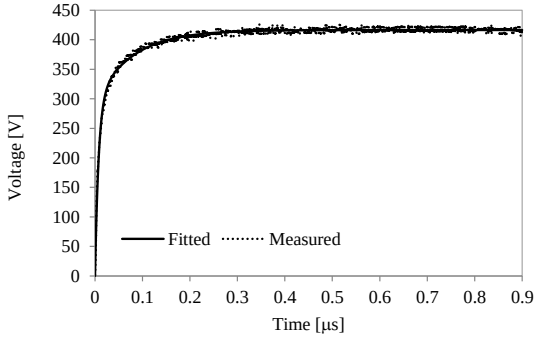

Fig. 5.5. Fitted model with measured data for applied voltage V_{oc}.

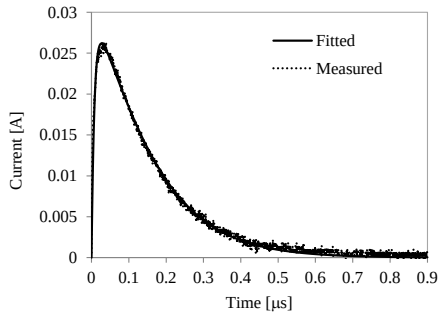

(a-1) case 1 – common mode

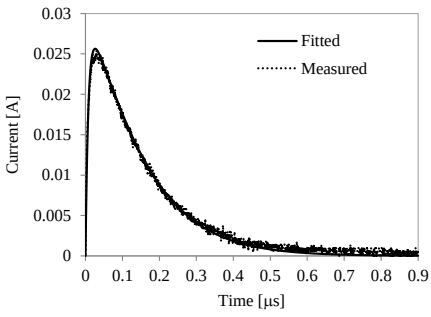

(b-1) case 1 – differential mode

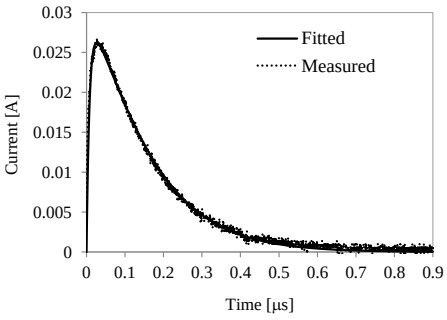

(a-2) case 2 – common mode

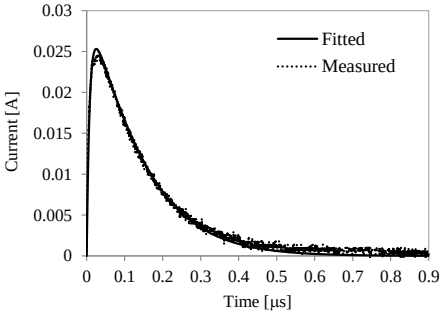

(b-2) case 2 – differential mode

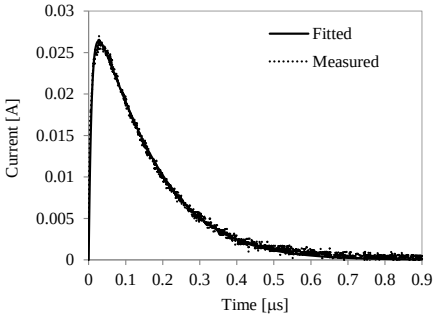

(a-3) case 3 – common mode

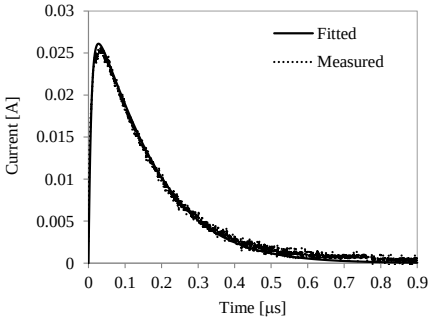

(b-3) case 3 – differential mode

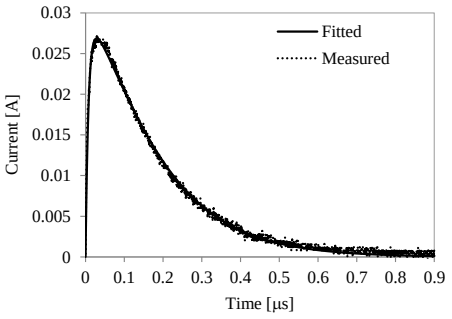

(a-4) case 4 – common mode

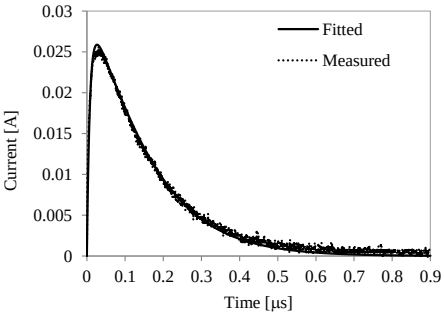

(b-4) case 4 – differential mode

Fig. 5.6. Fitted-model of injecting current I_c with measured data, with the R_{sc} = 10kΩ.

5.2.3 Theoretical parameters

The measured-capacitances between the electrodes C_{el} shown in Tables 5.3 and 5.4 are verified by a theoretical calculation. The capacitances can be approximately calculated using a theoretical equation for a parallel-wire shown in (4.19).

The measured capacitances between the electrodes C_{el} with the theoretical capacitance are listed in Table 5.5. The estimated capacitances between the electrodes C_{el} are confirmed to be in accordance with the theoretical equation as shown in Fig. 5.7.

Table 5.5. Capacitance between the electrodes C_{el} obtained by measured result and theoretical calculation.

Case			Measured		Theoretical*
	Distance d [mm]	Length l [mm]	Slope	Curve fit	
Case 1	30	80	5.6	5.1	5.5
Case 2	50	80	3.8	4.2	4.1
Case 3	30	100	6.5	6.1	6.9
Case 4	50	100	5.3	4.6	5.1

*: radius r: 5 mm, distance d: 30 mm, 50 mm, relative permittivity ε_r: 4 [12]

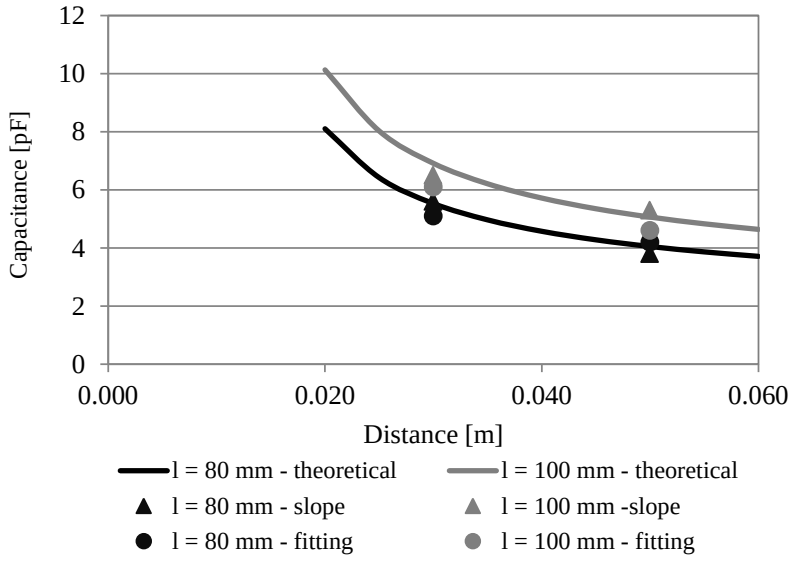

(a) C_{el} versus distance

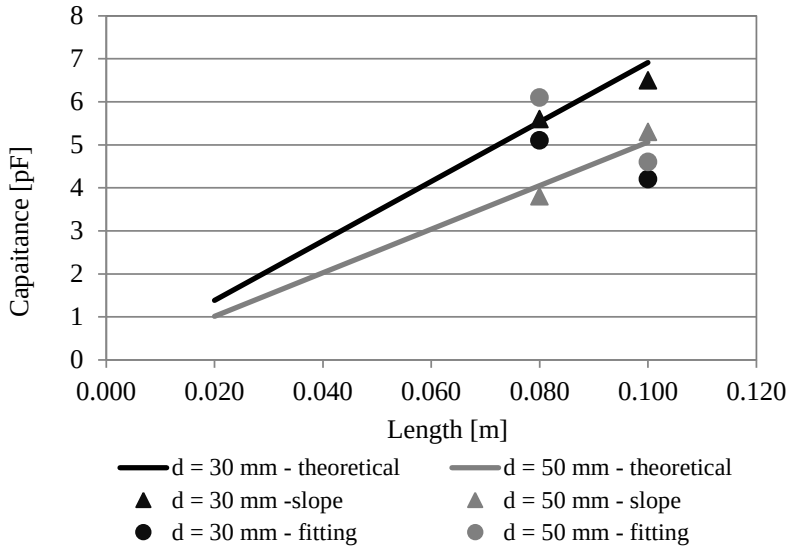

(b) C_{el} versus length

Fig. 5.7. Measured and theoretical C_{el}.

5.2.4 Transient simulation

Transient currents flowing into the electrodes implanted into a piece of wood are simulated using Electromagnetic Transients Program (EMTP). To verify the reliability of each method, the circuit parameters listed in Tables 5.3 and 5.4 with the equivalent circuit shown in

Figs. 5.3 (for slope of wave-tail method) and 5.4 (for nonlinear method) are used in the EMTP simulation. The results for cases 2 and 3, which have the minimum distance d with the longest length l, and the maximum distance d with the shortest length l are presented. Comparisons between simulated and measured results for source resistance R_{sc} of 10 kΩ are shown in Figs. 5.8 to 5.11.

In these simulations, the current injection cable 3D2V is expressed by a Semlyen's line model to takes into account its frequency dependent effect [13].

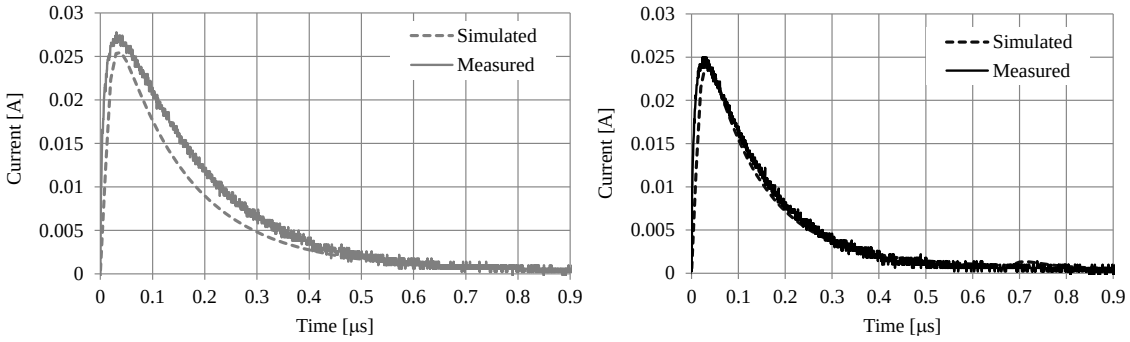

(a) Common mode (b) Differential mode

Fig. 5.8. Simulated results for R_{sc} = 10 kΩ in Case 2 (slope of wave-tail method).

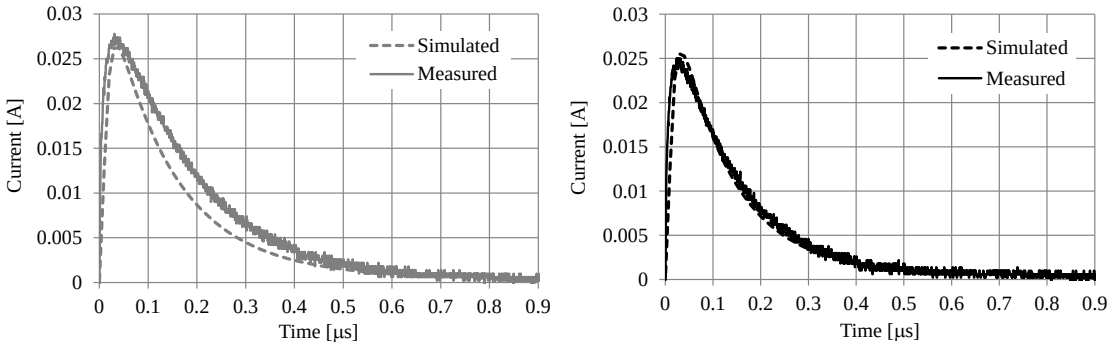

(a) Common mode (b) Differential mode

Fig. 5.9. Simulated results for R_{sc} = 10 kΩ in Case 2 (nonlinear fitting method).

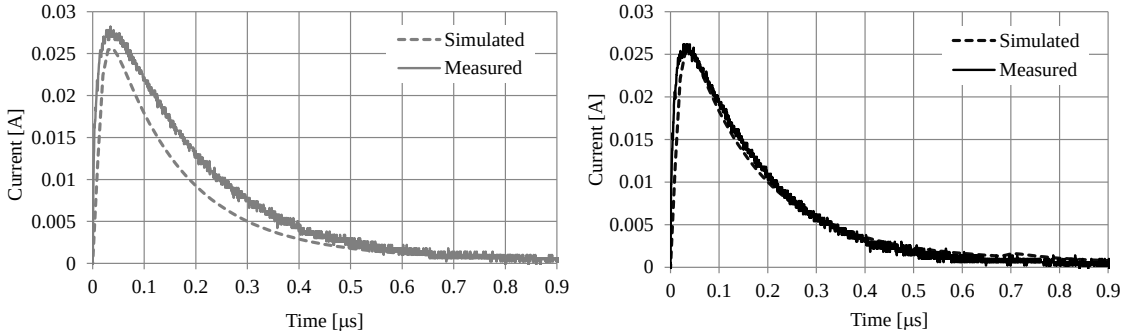

(a) Common mode (b) Differential mode

Fig. 5.10. Simulated results for R_{sc} = 10 kΩ in Case 3 (slope of wave-tail method).

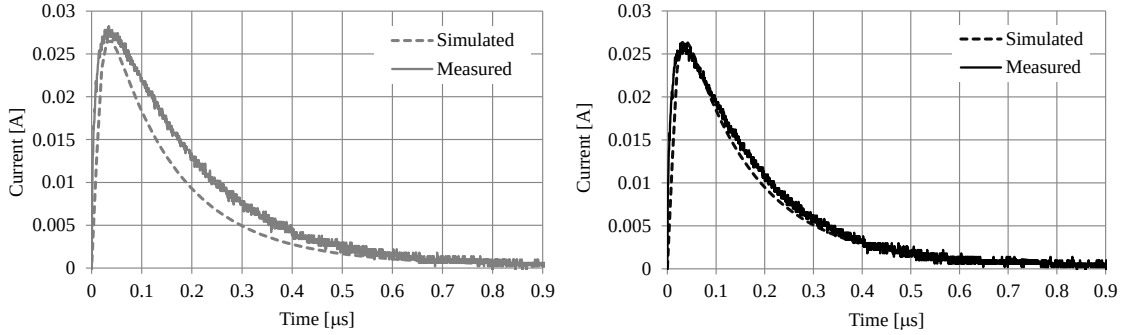

(a) Common mode (b) Differential mode

Fig. 5.11. Simulated results for R_{sc} = 10 kΩ in Case 3 (nonlinear fitting method).

From Figs. 5.8 to 5.11, it is clear that the circuit with the parameters obtained by both methods can satisfactorily reproduce the measured results. The slope of wave-tail method is useful because no numerical calculation is required and its accuracy is satisfactory. Although the nonlinear method requires a numerical calculation, the method gives better approximation.

5.3 Miniature Circuit Breaker (MCB)

A two-pole low-voltage MCB, whose rated voltage U_e and rated short circuit current I_{cn} is 2.5 kA, is used in this study. The equivalent circuit of the MCB impedance is similar to that in the electrodes implanted into a piece of wood. A pi-type circuit is composed of three branches: an impedance between phases or between contacts and two impedances from those

to ground. The model of the MCB can be expressed by some capacitors, because the MCB has a high insulating resistance, i.e., its leakage current is negligible.

Two pi-type circuits will be investigated in this study. The first one is for an MCB, which has symmetrical stray capacitors from its terminals to ground. The second circuit has unsymmetrical stray capacitors. In the later equivalent circuit, a capacitor between contacts are taken into account.

5.3.1 Stray capacitor between phases

To obtain the stray capacitance between phases, the MCB is tested in the common and differential modes as shown in Fig. 5.12. In the common mode test, every terminals are short-circuited. For the measurement of the capacitance between the phases, the contacts are closed ("ON") to exclude the capacitance between the contacts. A pi-type circuit consisting of the stray capacitors is shown in Fig. 5.13. Since the MCB has a symmetric structure, the circuit has symmetrical stray capacitances to ground C_{gp}.

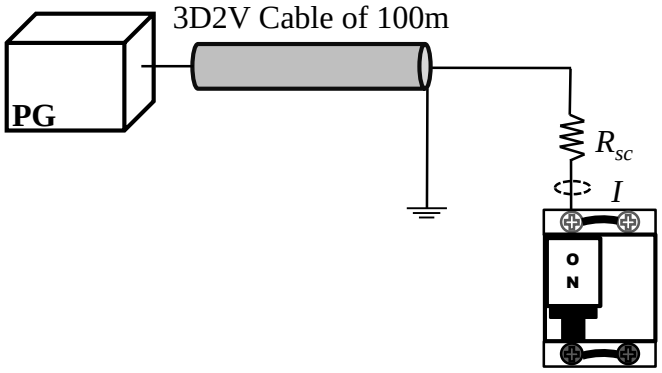

(a) Common mode

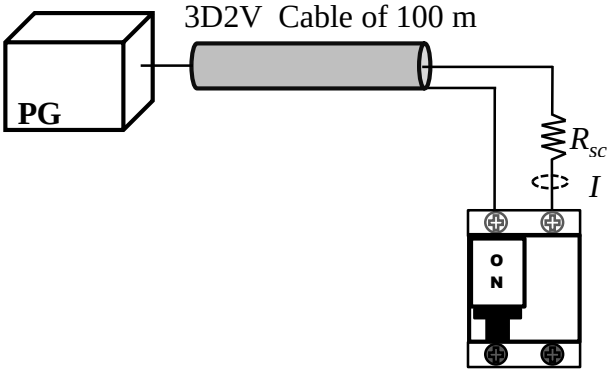

(b) Differential mode

Fig. 5.12. Measurement setup for investigating stray capacitor between phases.

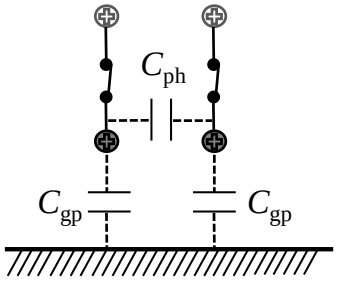

Fig. 5.13. Pi-type equivalent circuit of stray capacitor between phases in MCB.

The measured transient currents in a semi-logarithmic charts and their time constants at the wave-tail are shown in Fig. 5.14 and Table 5.6. The time constants are analyzed using the slope of the wave-tail method as described in subsection 4.5.2.

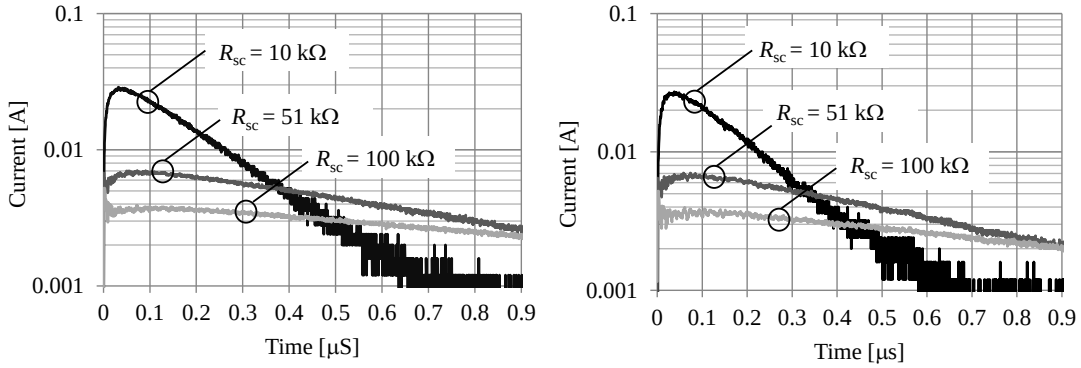

(a) Common mode (b) Differential mode

Fig. 5.14. Semi logarithmic plot of measured transient current, stray capacitor between phases.

Table 5.6. Measured time constants (τ) in μs.

	Common Mode			Differential Mode		
R_{sc} [kΩ]	10	51	100	10	51	100
τ (μs)	0.191	0.827	1.569	0.172	0.373	0.652

The fitted transient currents with the measured data are shown in Fig. 5.15. To approximate the measured result in the differential- and common-mode, the circuit is assumed to be an *RC* series circuit. The resistance *R* either in the common- or differential-mode represents the sending end resistance R_{cc} in series with the coaxial surge impedance R_{sc}, ($R_{comm} = R_{diff} = R_{cc} + R_{sc}$, $R_{cc} = 50\,\Omega$, $R_{sc} = 10\,\text{k}\Omega$). The capacitance in the common mode C_{comm} expresses the stray capacitance to ground ($C_{comm} = 2C_{gp}$) as shown in Fig. 5.16 (a). In the differential mode, the stray capacitor grounding from the terminal connected to the sheath is short-circuited by the low sheath surge impedance. The circuit in the mode is shown in Fig. 5.16(b) ($C_{diff} = C_{ph} + C_{gp}$). The measured stray capacitances, C_{comm}, C_{diff}, C_{ph}, and C_{gp}, are shown in Table 5.7.

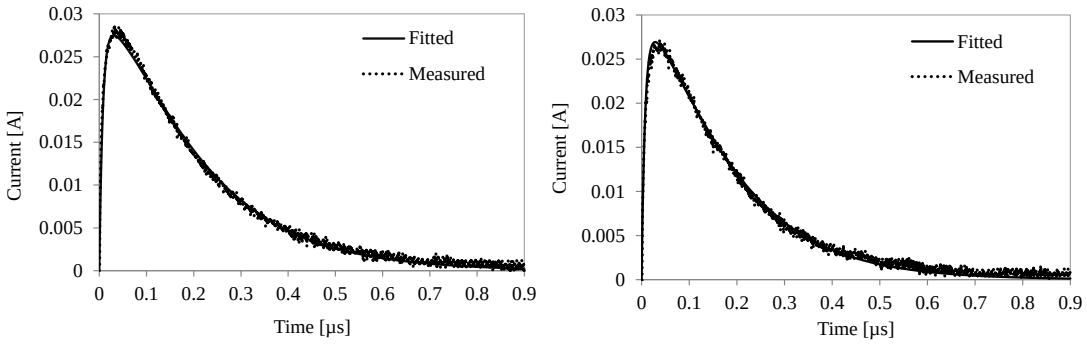

(a) Common mode (b) Differential mode

Fig. 5.15. Fitted models of injecting current and measured data, stray capacitor between phases with R_{sc} = 10kΩ.

(a) Common mode (b) Differential mode

Fig. 5.16. Capacitance circuit of stray capacitors between phases in MCB.

Table 5.7. The parameters of stray capacitors between phases circuit.

	Capacitance [pF]	
	Slope	Nonlinear Fitting
C_{comm} (=2C_{gp})	15.8	16.2
C_{diff} (=C_{ph}+C_{gp})	12.1	14.0
C_{gp}	7.9	8.1
C_{ph}	4.2	5.9

In the common mode, the stray capacitance to ground measured by an impedance analyzer (Agilent 4294A) at a frequency of 1 MHz is 16.3 pF. Both the methods estimate the stray capacitance to ground with small difference. In the differential mode, the stray capacitance between phases measured by the instrument is 4.02 pF. The capacitance between

phases C_{ph} obtained by the nonlinear fitting method is greater than that measured by the instrument. However, the capacitance obtained by the nonlinear fitting method is insensitive to the noise. It is independent from time span of observation.

5.3.2 Stray capacitor between contacts

The stray capacitor between contacts is established when the contacts of MCB are opened. At that time, the MCB has two terminals, i.e., incoming and outgoing terminals. The stray capacitances to ground at the incoming and outgoing terminals are unequal, i.e., unsymmetrical. A measurement method for the unsymmetrical circuit is proposed in this subsection. The technique has been applied to the MCB in subsection 4.5.3. The equivalent circuit and the capacitance circuit of the MCB for this case are illustrated in Figs. 5.17 and 5.18.

The stray capacitances to be measured are shown in Fig. 5.18 and (5.3). The capacitances between contacts (C_{ct}), and the stray capacitance to ground at the incoming and outgoing terminals (C_{gi} and C_{go}) are obtained as a solution of the following simultaneous equations.

$$C_{comm} = C_{gi} + C_{go} \tag{5.3-a}$$

$$C_{in} = C_{ct} + C_{gi} \tag{5.3-b}$$

$$C_{out} = C_{ct} + C_{go} \tag{5.3-c}$$

The measured injected currents using semi-logarithmic scale and their time constants (τ) are shown in Fig. 5.19 and Table 5.8. The fitted results are shown in Fig. 5.20. Since the common mode setup is identical to that for the stray capacitor between phases as shown in Fig. 5.12 (a), the common mode capacitance C_{comm} shown in Table 5.7 is substituted to (5.3-a).

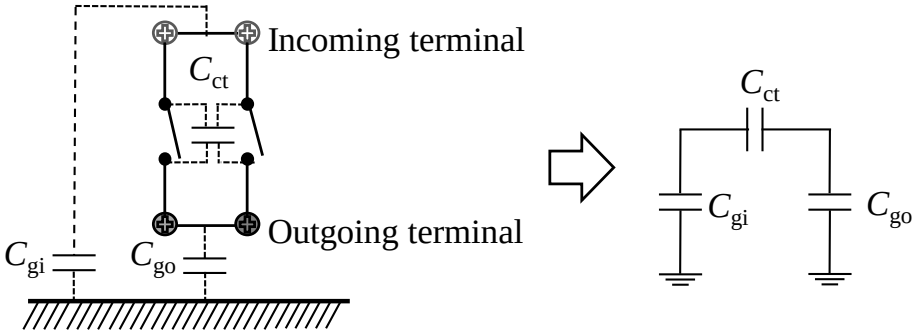

Fig. 5.17. Pi-equivalent circuit of impedance between contacts in MCB.

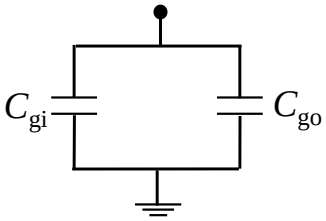

(a) Common mode

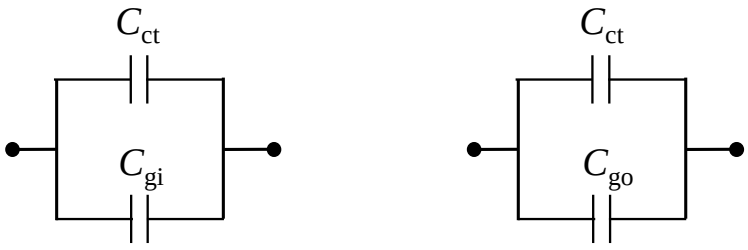

(b-1) Incoming-differential mode (b-2) Outgoing-differential mode

Fig. 5.18. Capacitance circuits in MCB, differential- and common mode.

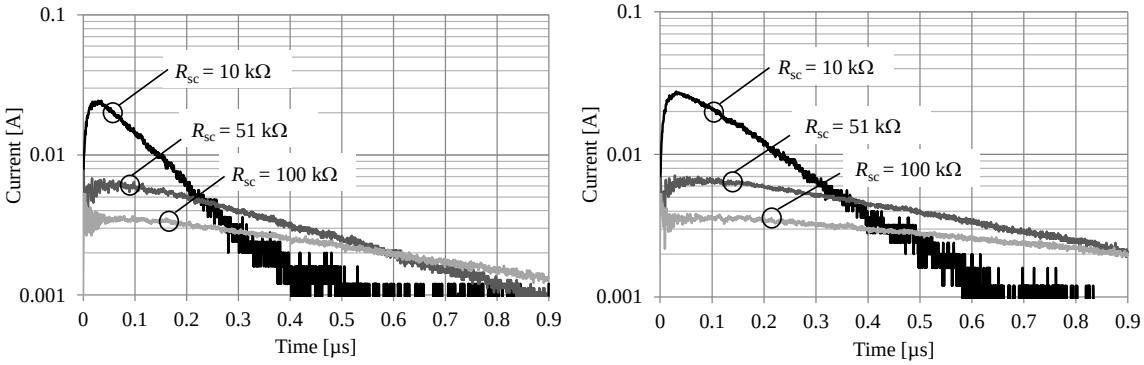

(a) Incoming-differential mode (b) Outgoing-differential mode

Fig. 5.19. Semi logarithmic plot of measured transient current, stray capacitor between contacts.

Table 5.8. Measured time constants (τ) in μs.

	Incoming-Differential Mode			Outgoing-Differential Mode		
R_{sc} [kΩ]	10	51	100	10	51	100
τ (μs)	0.120	0.430	0.790	0.175	0.687	1.288

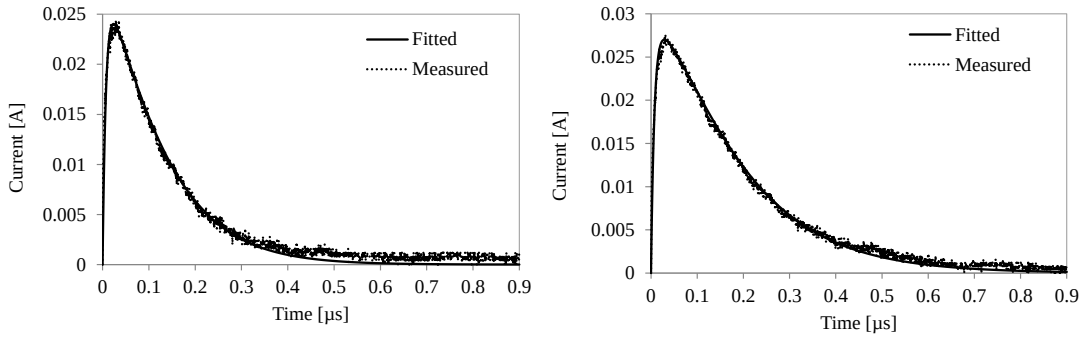

(a) Incoming-differential mode (b) Outgoing-differential mode

Fig. 5.20. Fitted model with the measured result, in the case of stray capacitor between contacts, with R_{sc} = 10 kΩ.

Fig. 5.21 shows that the stray capacitors in the MCB can be divided into two according to the symmetry between its phases.

- The capacitance C_{ct} between the contacts measured by the circuit shown in Fig. 4.30 is equally divided into two, $C_{ct\text{-}a}$ and $C_{ct\text{-}b}$.
- Each stray capacitance from the incoming or outgoing terminal to ground is separated into two phases, $C_{gi\text{-}a}$ and $C_{gi\text{-}b}$, or $C_{go\text{-}a}$ and $C_{go\text{-}b}$.
- The capacitors between phases $C_{ph\text{-}i}$ and $C_{ph\text{-}o}$ are short-circuited as shown in Fig. 4.30 in subsection 4.5.3.

The calculated results of the circuit parameters obtained by the slope of the wave-tail and the nonlinear fitting method are listed in Table 5.9. The total capacitance between the contacts C_{ct} is 2.3 pF by the slope of the wave-tail methods and 3.4 pF by the nonlinear fitting method, and it is the smallest. The stray capacitances to ground at both terminals C_{gi} and C_{go} are different, because the MCB has the unsymmetrical stray capacitance. The stray capacitance at the outgoing terminal is twice of that at the incoming terminal.

One of the methods to evaluate the reliability of the equivalent circuit of the MCB is a measurement of the voltage across the terminal of the MCB. However, the voltage across the stray capacitor cannot be measured, since the stray capacitance is smaller than the capacitance of the voltage probe. The voltage is indirectly measured using a GA as shown in the next section.

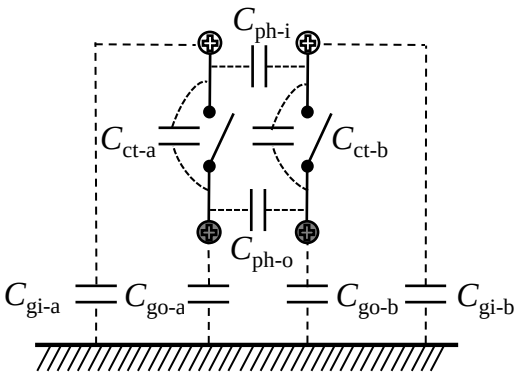

Fig. 5.21. Equivalent circuit of stray capacitors in MCB

Table. 5.9. The parameters of stray capacitors between contacts circuit.

	Capacitance [pF]	
	The Slope Method	The Nonlinear Fitting Method
C_{in}	7.7	8.7
C_{out}	12.7	14.2
C_{comm}	15.8	16.2
C_{ct}	2.3	3.4
C_{gi}	5.4	5.4
C_{go}	10.4	10.8
$C_{ct\text{-}a} = C_{ct\text{-}b} = C_{ct}/2$	1.1	1.7
$C_{gi\text{-}a} = C_{gi\text{-}b} = C_{gi}/2$	2.7	2.7
$C_{go\text{-}a} = C_{go\text{-}b} = C_{go}/2$	5.2	5.4

5.4 Gas-filled Arrester (GA)

A gas-filled arrester (GA) consists of two or more metallic electrodes that are separated by a gap in a hermetically sealed envelope containing an inert gas [11]. A gas-filled arrester EC90X manufactured by EPCOS is used in this study. Its transient characteristic is measured using a circuit shown in Fig. 5.22 [10]. The sending-end resistor of R_{SC}=10 kΩ is attached to the core of the current injecting cable of 3D2V. Its cable length is 100 m. A voltage is applied using a pulse generator (P.G., Noiseken INS-4040). The transient currents are measured using a digital oscilloscope (Tektronix DPO 4104, 1 GHz) with a current probe (Tektronix CT-1).

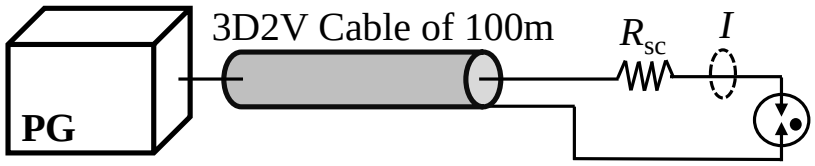

Fig. 5.22. Transient measurement setup for GA.

The transient current waveform is used to define the internal impedance of the GA before a flashover using the proposed nonlinear fitting method. The measured result of the transient current waveforms can be divided into two: with and without a flashover as shown in Fig. 5.23(a) and 5.23(b), respectively. Fig. 5.23 (b) shows a typical current waveform of the gas arrester with a flashover. The waveform before the flashover represents the transient response of the GA. The waveform after a flashover expresses a short-circuited response due to an arc discharge. The transient current waveform before the flashover shown in Fig. 5.23(a) is used to obtain the impedance of the gas arrester using the nonlinear fitting method with the corresponding open-circuited voltage. The fitted results with the measured data of the open-circuited (applied) voltage and the injected current are shown in Figs 5.24 and 5.23 (a).

The impedance of the gas arrester before the flashover can be represented by a capacitor with a resistor connected in series as shown in Fig. 5.25. The capacitance C_{ga} is determined by the configuration of the GA, which consists of two metallic electrodes insulated by dielectric-gases. The resistor correlates to the losses of the dielectric material before the flashover of the GA.

Voltage-time (*V*-t) or time-lag curves is one of the characteristics of GA. It determines the characteristic of the breakdown voltage across the gap of the GA. Two parameters are required to obtain a volt-time curve: time to flashover and voltage across the gap at the flashover. The time and voltage at the flashover are observed using the measurement setup shown in Fig.5.22. To obtain the flashover time, the applied voltage is increased until a flashover is observed in the current waveform. Since the impedance of the GA is higher than that of a voltage probe, any voltage measurement will result in error due to the probe capacitance [3]. The flashover voltage is estimated by the simulation result by EMTP instead by the voltage measurement. In the simulation, the GA is represented by its internal impedance shown in Fig. 5.25. The calculated voltage across the *RC* series circuit at the measured flashover time is assumed to be the flashover voltage, since the voltage represents the gap-voltage. Table 5.11 shows a set of time to flashover and their corresponding voltages. The *V-t* characteristic can be approximated by (5.4), and it is illustrated in Fig. 5.26.

$$f(t) = 0.82t^{-0.39} + 84 \tag{5.4}$$

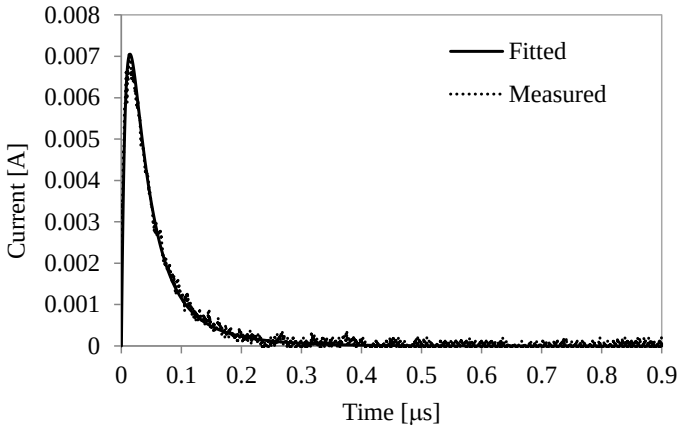

(a) Measured current, at V_{oc} = 170 V

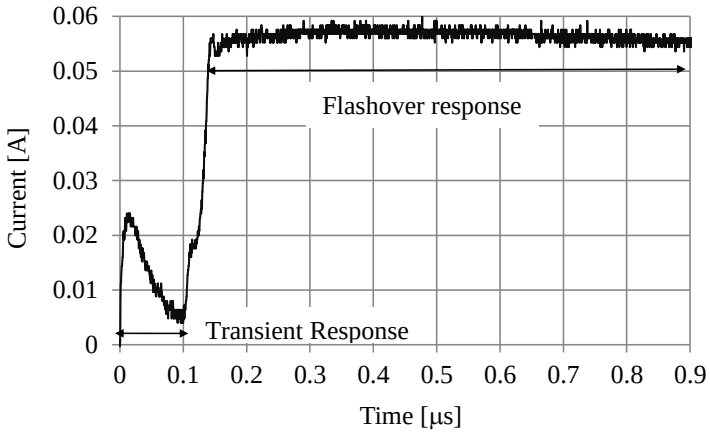

(b) Measured current, at V_{oc} = 680 V

Fig. 5.23. Measured transient current waveforms of GA.

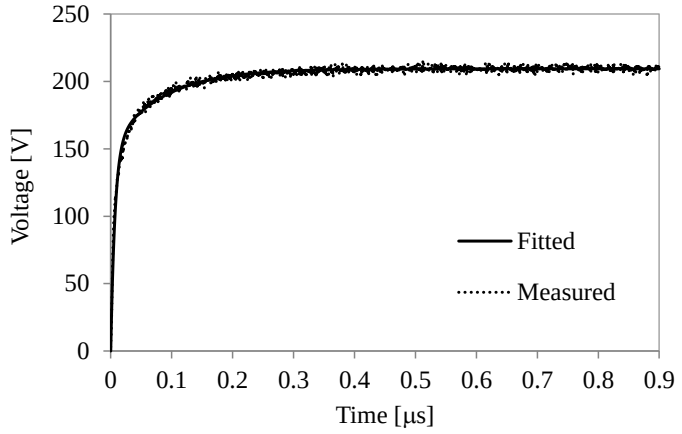

Fig. 5.24. Open-circuited voltage, at V_{oc} = 170 V.

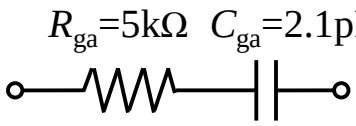

Fig. 5.25. Equivalent circuit of GA.

Table 5.11. Time to flashover and their corresponding voltage.

No.	Applied voltage, V_{oc} [V]	Time [μs]	Gap Voltage [V]
1	372	0.55	276
2	416	0.36	311
3	500	0.21	361
4	680	0.10	460

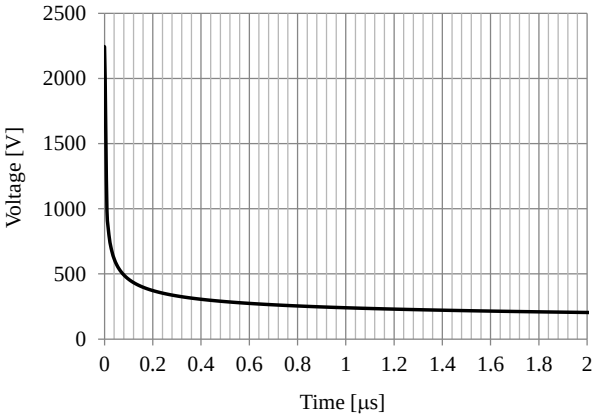

Fig. 5.26. Voltage-time curve of GA.

The characteristic of the flashover can be expressed by an equivalent circuit shown in Fig. 5.27. The switch is closed according to the *V-t* curve to express the flashover, and the *RC* series circuit expresses the internal impedance of the GA before the flashover. The circuit can be simulated by EMTP. Transient Analysis Control System (TACS), which is one of the models for expressing control systems, is used to represent the flashover. The TACS controls the closing time of the switch according to the *V-t* curve. In the simulation of this study, the resistance R_{ga} can be negligible because the time constant of the *RC* series circuit (10.5 ns) is

far smaller than that of the transient response of the test circuit illustrated in Fig. 5.22. Fig. 5.28 shows the simulated current is identical to the time of flashover of the measured result at the applied voltage of 680 V. The simulated times to flashover with the measured ones for the applied voltages are listed in Table 5.12.

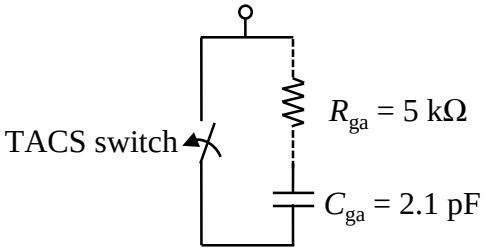

Fig. 5.27. Equivalent circuit of GA for studying the flashover phenomena.

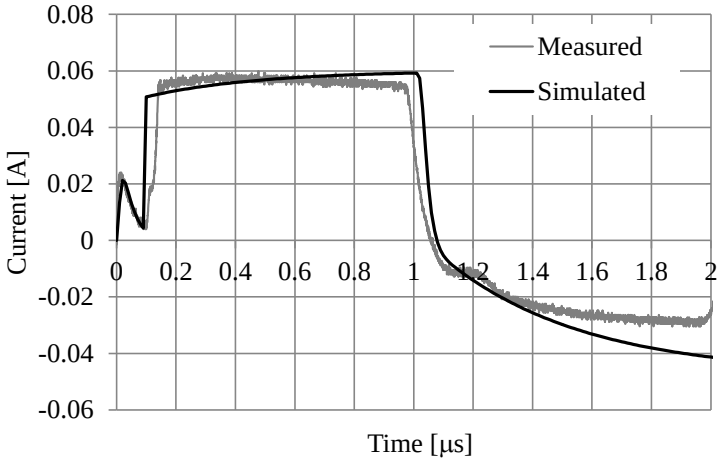

Fig. 5.28. Simulated core current with measured result, at V_{oc} = 680 V

Table 5.12. Time to flashover in μs, simulated and measured results.

No.	Applied voltage, V_{oc} [V]	Measured	Simulated	% Difference
1	372	0.55	0.58	5.3
2	416	0.36	0.37	2.7
3	500	0.21	0.22	4.6
4	680	0.10	0.10	0

One of the methods to evaluate the reliability of the equivalent circuit of the MCB is a measurement of the voltage across the terminal of the MCB. However, the voltage across the stray capacitor cannot be measured, since the stray capacitance is smaller than the capacitance of the voltage probe. The voltage is indirectly measured using a GA. Even if the MCB is opened, some voltage is induced on the terminal connected to the GA via the stray capacitor between contacts. From the time to flashover of the GA, the voltage across the GA can be estimated using a voltage-time (*V-t*) curve of the GA shown in Fig.5.26.

A pulse voltage is applied by a generator (PG, Noiseken INS-4040) to the GA and MCB via a current injection cable 3D2V and a resistor of 10k□ as shown in Fig. 5.29. The mode can be represented by the circuit short-circuited between phases of the MCB because the surge voltages on both lines are assumed to be equal [14].

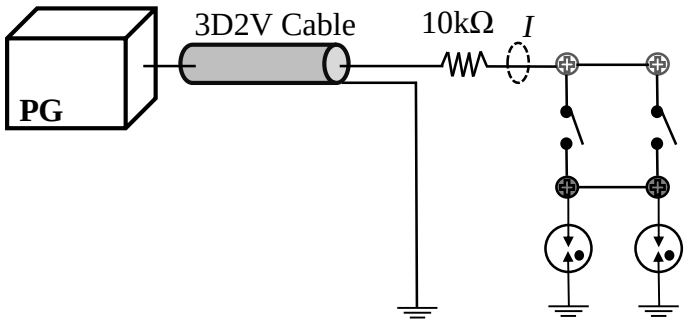

Fig. 5.29. Measurement setup for common mode surge.

Since a measurement of the voltage across a small-capacitance circuit is difficult due to the low impedance of the voltage probe, an EMTP simulation is used to estimate the voltage instead of the voltage measurement. In this simulation, the current injection coaxial-cable 3D2V is expressed by a Semlyen's line model to take into account its frequency dependent effect [13]. The MCB is represented by the pi-type circuit consisting of stray capacitors between contacts as shown in Fig. 5.17. The parameters of the MCB model used in the simulation are determined by the nonlinear fitting method as shown in Table 5.9. The GAs are represented by a parallel circuit of its internal impedance and a TACS controlled switch as shown in Fig. 5.27. The applied voltage at the incoming terminal of the MCB and the voltage across the GA, which are estimated by the simulation, are shown in Figs. 5.30 and 5.31.

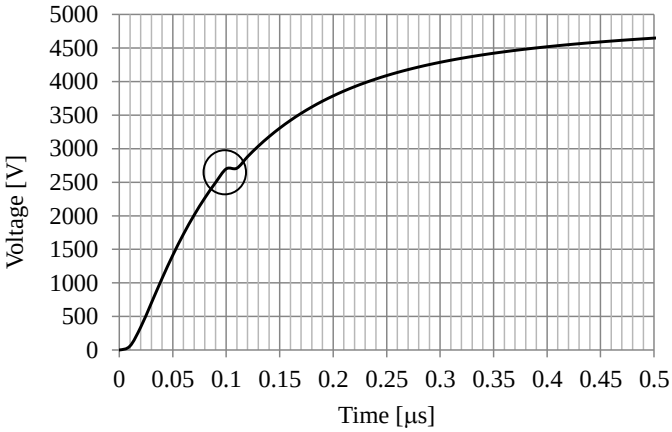

Fig. 5.30. Simulated voltage at incoming terminal of MCB.

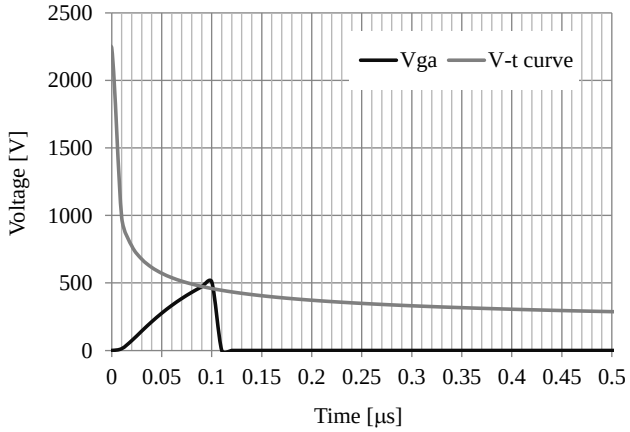

Fig. 5.31. Simulated voltage across the GA and the *V*-t curve

Fig. 5.30 shows that the applied voltage becomes flat at the time of flashover. It is the time at which the voltage across the GA exceeds the *V-t* curve as shown in Fig. 5.31. After the flashover, the switch connected in parallel with the internal impedance of the GA (Fig. 5.27) is closed. The GA is short-circuited to the ground by the TACS switch. It is also confirmed in the simulated current as follows.

The simulated and the measured injected currents *I* are illustrated in Fig. 5.32. The difference in the peak current is 8%. The peak current is observed before the flashover of the GAs. The current is determined by the capacitances of the MCB and the internal impedance of the GA. The stray capacitance to ground by the nonlinear fitting method at the outgoing terminals C_{go} is 10.8 pF as shown in Table 5.9 and the total capacitance of the GA is 4.2 pF,

which is connected in parallel with the stray capacitance C_{go} (Fig. 5.33). Although the effect of the GA cannot be negligible, it can be said that the MCB and the GA models have a satisfactory accuracy. The times at the flashovers, which determine the voltage across the GA, are shown in Fig. 5.32 by circles. The gray and black circles are for the measured and simulated time, respectively. The figure shows that the flashover can be detected by the current waveform without any voltage measurement. The measured waveform shows a strong oscillation after the flashover. However, there is no oscillation in the calculated result, because the flashover is modeled by a switch and the discharge characteristic of the GA is neglected in the simulation. The measured and simulated flashover times are 0.13 μs and 0.11 μs, respectively. These times can be converted to the voltages using the *V*-t curve of the GA. The times correspond to the voltages of 423 V and 445 V, respectively. The differences between the measured and simulated voltages are 5 %.

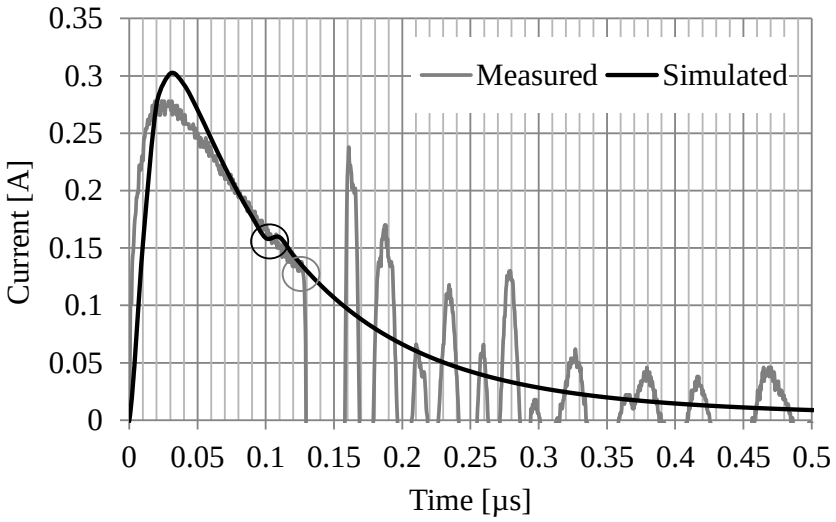

Fig. 5.32. Measured and simulated results for common mode surge.

The proposed equivalent circuit of the MCB and GA enables to predict the applied voltage at the flashover. The MCB as well as the GA is represented by the stray capacitors as shown in Fig. 5.33. The ratio between input and output voltage is shown in (5.5). The applied voltage is higher by 5.4 times than the flashover voltage.

$$V_{in} = \frac{2C_{ga} + C_{ct} + C_{go}}{C_{ct}} V_{out} = \frac{(2 \times 2.1) + 3.4 + 10.8)}{3.4} V_{out} \approx 5.4 V_{out} \tag{5.5}$$

The ratio agrees well with that between the voltages just before the flashover shown in Figs. 5.30 and 5.31.

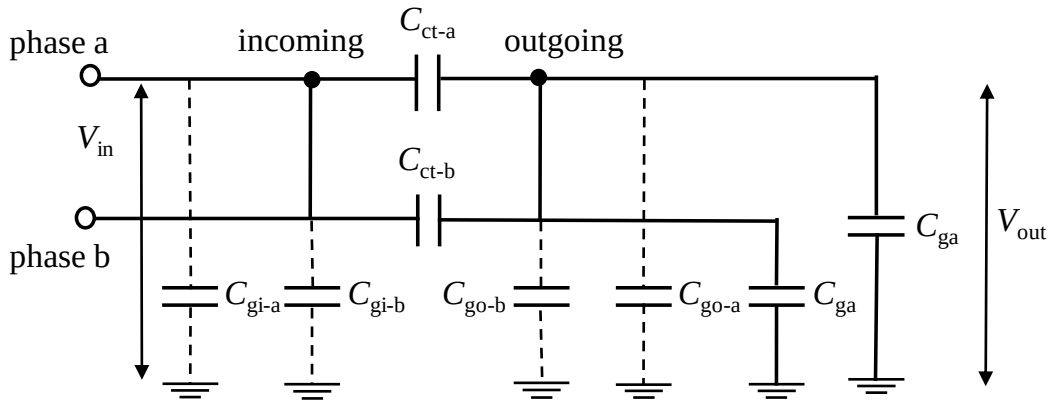

Fig. 5.33. Equivalent circuit of MCB and GA for calculating ratio of applied voltage and the output voltage, i.e., flashover-voltage of GA.

The proposed simulation method is applicable to low-voltage power systems and telecommunication systems.

In a low-voltage power system, various modes of surge can be generated. The common mode surge is defined that the surge on each conductor is in phase and equal in magnitude as shown in Fig. 5.34. Thus, a voltage is not generated between these conductors. The common mode surge is more troublesome than the differential mode surge. In the power distribution system, the surge is always invades through a distribution transformer as a common mode surge, regardless of the mode in which it was generated [14].

The common mode surge is also known as longitudinal mode surge. The surge generated by a lightning strike travels along a telecommunication line. Even if the lightning strikes far from a customer and the surge voltage are attenuated, the surge is a threat to an electronic circuit whose withstand voltage is low. The proposed simulation method is valuable for an insulation design of the communication system.

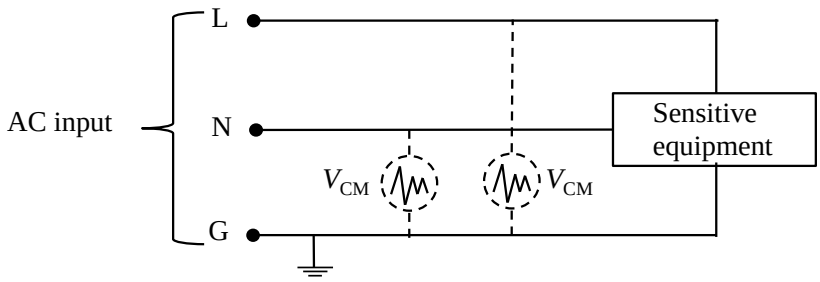

Fig. 5.34. Common mode surge [14].

5.5 Concluding Remarks

The proposed techniques were applied to several power apparatus, which have a small capacitance such as a stray capacitance.

(1) The impedance between electrodes implanted into a wood.

The measured impedance between electrodes implanted into a piece of wood was compared with that obtained by the theoretical equation for a capacitance between parallel wires. Two methods to determine the parameters, i.e, the slope of the wave-tail and the nonlinear fitting, were used. The good agreement between the simulated and measured results shows that the proposed equivalent circuit for the electrodes and the estimation method for its circuit parameters are reliable for fast transient simulation.

(2) Gas-filled arrester.

The internal impedance and the flashover model of a gas-filled arrester (GA) have been developed. The flashover circuit model is used in EMTP to simulate the flashover phenomena. The simulated time to flashover agrees well with the measured result. The maximum difference is 5.3 %.

(3) Miniature Circuit Breaker and Gas-filled arrester.

A measuring method of the stray capacitances in an MCB has been proposed. The accuracy of the model parameters has been confirmed by an indirect measurement of the voltage across the terminal of the MCB via the flashover-voltage of the GA. The difference between the simulated terminal voltages and the measured results are 5%. It shows that the

stray capacitor model of the MCB has enough reliability to reproduce the measured result, especially in a common mode interference.

5.6 References

[1] J. P. Bickford and A. G. Heaton, "Transient overvoltages on power systems," *IEE Proc.*, vol.133, no.4, pp.201-225, May 1986.

[2] WG C4.501, "Guideline for numerical electromagnetic analysis method and its application to surge phenomena," *CIGRE*, June 2013.

[3] D. Permata and N. Nagaoka, "An impedance measurement of a small-capacitance circuit using transient responses for lightning surge analysis," *IEEJ Trans. Electrical and Electronic Engineering*, vol.9, no.S1, pp. S37-S43, Oct. 2014.

[4] K. L. Wong and M. F. Rahmat, "Study of leakage current distribution in wooden pole using ladder network model, " *IEEE Trans. Power App. Syst*., vol.25, no.2, pp. 995-1000, April 2010.

[5] K. L. Wong, S. Pathak and M. F. Rahmat, "Aging effect on leakage current flow in wooden poles", *IEEE Trans. Dielectr. Electr. Insul.*, vol.16**,** no.1, pp.133-138, Feb. 2009.

[6] *IEEE guide for improving the lightning performance of electric power overhead distributions lines*, IEEE Std 1410-1997, pp.16, 1997.

[7] IEEE Modeling and Analysis of System Transients WG, "Modeling guidelines for fast front transients," *IEEE Trans. Power Del.*, vol.11, no.1, pp.493-506, Jan. 1996.

[8] G. Bizjak, P. Zunko, and D. Povh, "Combined model of SF6 circuit breaker for use in digital simulation programs," *IEEE Trans. Power Del*., vol.19, no.1, pp.174-180, Jan. 2004.

[9] B. Badrzadeh, M. H. Zamastil, and E. Isabegovic, "Transients in wind power plants-part1:modeling methodology and validation," *IEEE Trans. Ind. Appl*., vol.48, no.2, March/April 2012.

[10] D. Permata and N. Nagaoka, “Modeling method of fast transient for unsymmetrical stray capacitance to ground,” *IEEJ Trans. Electrical and Electronic Engineering*, vol.10, Supplement, Oct. 2015 (accepted for publication).

[11] *IEEE guide for the application of gas tube and air gap arrester low voltage surge protective devices*, IEEE Std C62.42-1992, pp.1-24, 1993.

[12] W. Simpson, A. Tenwolde: *Physical properties and moisture relations of wood*, Wood Handbook, pp.3.1-3.4, 1999.

[13] D. Permata, Y. Ikeda, and N. Nagaoka: “Effect of current injection cable on lightning surge measurement for scaled circuit,” *The Science and Engineering Review of Doshisha University*, vol.55, no.4, pp.61-67, Jan. 2015.

[14] Dev Paul, “Low-voltage power system surge overvoltage protection,” *IEEE Trans. Ind. Appl.*, vol. 37, no.1, pp.223-229, Jan/Feb 2001.

6 CONCLUSION

Nowadays, numerical simulation tools have been widely used to study the various phenomena such as transient overvoltage due to lightning or switching. Transient analysis by digital simulation has enough accuracy in comparison with that by experiment. Circuit parameters are required in the calculation using a circuit-theory-based simulation tools. The users have to define every circuit parameters even if the circuit has small capacitance such as stray capacitance for a fast transient simulation. In general, the capacitance cannot be obtained by theoretical calculation and its measurement is difficult.

The obstacles in measuring small-capacitance circuit are minimizing the effect of parasitic capacitance of the measuring system. The parameters that affect the measured result have been investigated in this study. Effects of the current injection cable, which is indispensable to the transient measurement, is also investigated. The correction method of the effect of the sheath surge impedance on the measurement, which is one of the factors reducing the reliability, is proposed.

This thesis has developed a method to measure a high-impedance using transient waveforms. A pi-type circuit is used to represent the stray capacitors between electrodes and those to ground. The circuit parameters are obtained by analyzing the current waveform using two methods, i.e., the slope of the wave-tail method and the nonlinear fitting method. The method has been applied in some circuits: impedance between electrodes implanted into a piece of wood, stray capacitor of MCB, and gas-filled arrester.

Chapter 2 describes a literature review of transient overvoltage and its classification. A transient measurement is briefly reviewed. Since this thesis emphasizes the overvoltage due to lightning surge, the models for a fast transient in some power apparatuses are described.

In Chapter 3, the pi-type circuit to model the impedance between electrodes implanted into a piece of wood has been developed. The circuit consists of an impedance between electrodes and ground impedances. In this chapter, a steady state measurement by an impedance analyzer instrument is used. These measured data, i.e., the impedances and their angles, are used to estimate the circuit parameters.

In Chapter 4, a modelling method for fast transient simulation has been proposed. It is well known in a power system that the transient assessment is required to verify the immunities of electrical and/or electronic equipment. The transient measurement is practical compared to the steady state measurement, since the arbitrary voltage can be applied. However, the conventional transient measuring method heavily influenced by a probe-capacitance and a sheath surge impedance of the current injection cable. In the proposed method, there is no effect of the probe-capacitance, because the measured impedance is obtained without any voltage information across a small capacitance. The circuit parameters are determined by an open-circuited voltage at the end of the current injection cable and the injected current. The voltage measurement is not influenced by the probe impedance due to low impedance of the cable. However, the effect of the sheath surge impedance of the current injection cable, which is indispensable for the transient measurement, cannot be negligible. A correction method is proposed in this chapter.

Two methods have been proposed to analyze the transient waveforms, i.e., using the slope of the wave-tail of the current waveform and a nonlinear fitting method. The former method is handy because it gives the capacitances without any numerical time-to-frequency transformation. In the nonlinear fitting method, the time-to-frequency transformation is analytically carried out. The proposed methods have a high immunity to noise and numerical errors such as a truncation error due to the removal of the numerical time-to-frequency transformations.

Applications of the proposed method are described in Chapter 5. The application circuit of the proposed method is a capacitive circuit, whose grounding impedance is far higher than the sheath surge impedance. The reliability of the method is confirmed by a theoretical analysis and/or transient simulation. Some circuits are tested and modeled by the method:

(1) *Impedance between electrodes implanted into a piece of wood*: the capacitances obtained from the measured result agree with those from theoretical analysis. In addition, the transient simulation using the circuit parameters can reproduce the measured results with a satisfactory accuracy.

(2) *Miniature circuit breaker and gas-filled arrester*: the internal impedance before its flashover is obtained by the proposed method. Transient responses of the arrester are calculated using EMTP. The calculated-flashover times agree with the measured results. A circuit of an MCB with a GA is used to confirm the accuracy of the proposed method. The breakdown voltage of the GA is obtained by EMTP simulation, and it was confirmed by the measured result. The models of the fast transient of the MCB with the GA can reproduce the measured result satisfactorily. The result shows that the induced voltage determined by the small capacitances accurately modeled by the proposed method. The models also useful to predict the applied voltage at the flashover.

The results show the proposed method has enough reliability to determine the circuit parameters, which are difficult to obtain by conventional methods. In addition, the proposed method is applicable to communication system as well as low voltage distribution system. The results in this thesis may contribute a reasonable insulation design of these systems.

Remark for future research:

- The circuit model of the electrodes implanted into a piece of wood is developed in a dry condition. To obtain the detailed insulation characteristics of the wood, it is required to get its response in wet conditions at a special-purpose laboratory for the wet conditions. The circuit parameters of the contact and leakage resistors as well as the stray capacitors can be estimated by the proposed measuring method. The circuit model is useful to investigate the flashover through the wood such as in wooden cross arm, wooden house, and wooden PV structure.

- This thesis enables a measurement of small capacitances of power apparatus. However, the method is applicable to the other fields, such as communication equipment. Reasonable insulation design is enabled by an accurate simulation taking into account the small capacitances. Lightning surge on communication system should be estimated taking into account both the telecommunication system and power system, because the difference of

the grounding potentials on these systems has much effect on the transient voltage. The difference heavily depends on their stray capacitances to ground.

- The models of wood as an insulator, a switch (MCB) and a gas-arrester have been developed in this thesis. These components are basic elements not only for power system but also electronic and/or communication system. In addition to this, the proposed method is applicable to the other elements. This thesis opens up a new field in a transient simulation. These models are applicable to practical systems, such as low voltage distribution system, telecommunication system, and control system. The transient characteristics have to be clarified by the models with the circuit parameters determined by the proposed method.

APPENDIX: EFFECT OF CURRENT INJECTION CABLE ON LIGHTNING SURGE MEASUREMENT FOR SCALED CIRCUIT [1]

A.1 Transient Characteristics

In this appendix, the transient characteristic of a current injection cable, which is used for a surge measurement, is investigated. An experimental setup for a measurement of the transient characteristic of a current injection cable is illustrated in Fig. A.1. A coaxial cable, 3D2V, is used as the current injection cable. The transient characteristic is investigated in three cable arrangements; Case I: a horizontal cable with a length of 2.6 m, and Cases II: a vertical inverted-L type cable of 6 m length, and Cases III: a vertical inverted-U type cable of 8 m length. The configuration of Case II is used to feed a current to a measuring object (scaled model of a tower or building).

In all cases, the sheath of the current injection cable is connected to the ground at the sending-end, i.e., the cold terminal of the PG is grounded. The core of the current injection cable is open- or short-circuited at the receiving-end (Case C_o or C_s) in Cases I and III. The core cannot be grounded in Case II. The applied voltages from the PG for the open- and short-circuited conditions are 500 V and 100 V, respectively.

The transient voltage and currents are measured by a digital oscilloscope (Textronix DPO 4104, 1 GHz) with a voltage probe (Textronix P6139A, 500 MHz, 8pF 10 MΩ) and a current probe (Textronix CT-2). A step-like voltage is supplied from a pulse generator (Noise Ken, PG, type INS-4040).

EMTP is used to calculate the transient voltage and current. The current injection cable is modeled by a recursive convolution line model, which is known as Semlyen's frequency dependent line model [2,3].

For an investigation of the effect of the sheath grounding at the receiving-end of a cable, the sheath is grounded (Case S_s) or open-circuited (Case S_o), i.e., only the sheath at the sending-end of the cable is grounded (case S_o) and the sheath both at the sending-end and the receiving-end are grounded (case S_s).

The effect of a voltage reference wire is taken into consideration in the measurement of the voltage at the receiving-end (Case II).

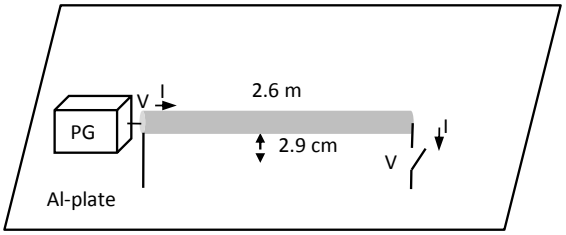

(a) Case I

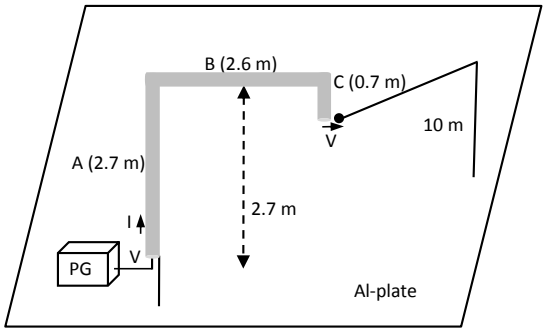

(b) Case II

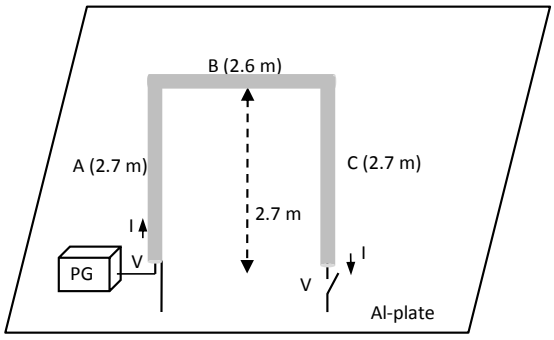

(c) Case III

Fig. A.1. Three configurations of a current injection cable.

The measured and simulated results at the sending-end and the receiving-end for the three circuits-configurations are shown in Figs. A.2 and A.3. The measured results for Case S_o are represented by the bold lines and the simulated results are shown by the dashed lines for case S_o and the dashed-dotted lines for case S_s.

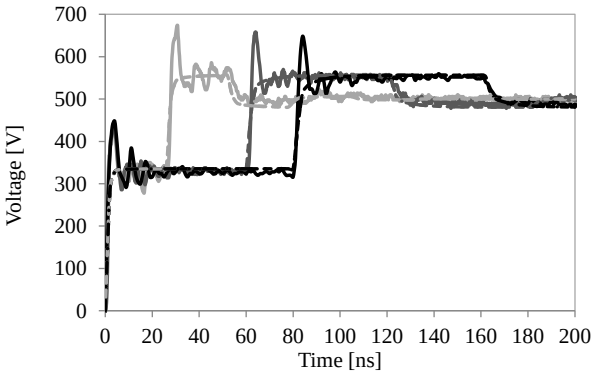

Sending-end core voltage

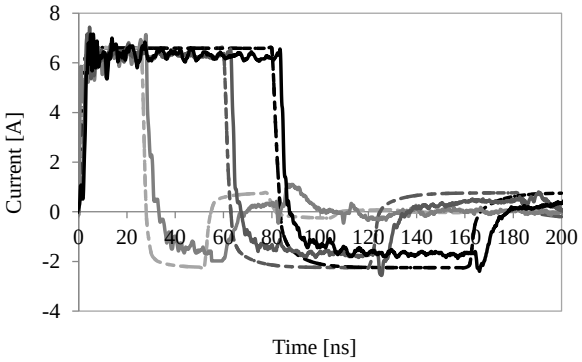

Sending-end core current

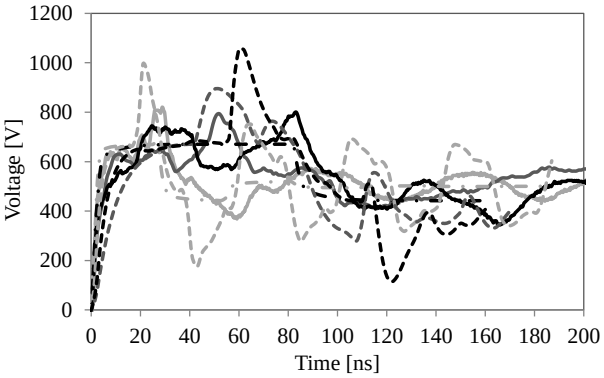

Receiving-end core voltage

Cable 2.6 Cable 6 m Cable 8 m

Fig. A.2. Measured and simulated results core at the receiving-end is open circuited (case C_o).

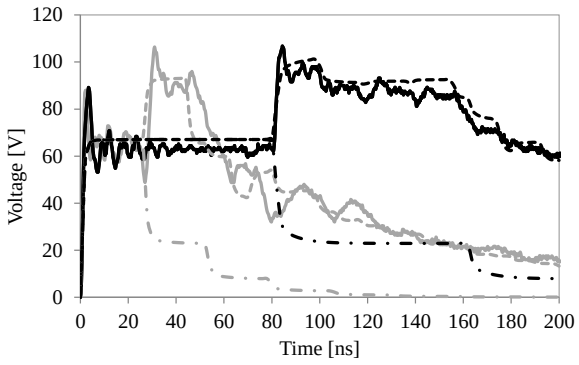

(a) Sending-end core voltage

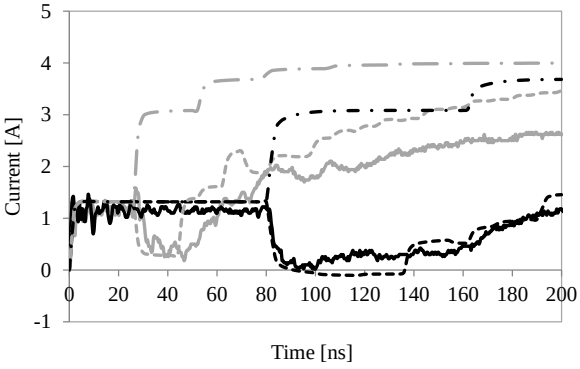

(b) Sending-end core current

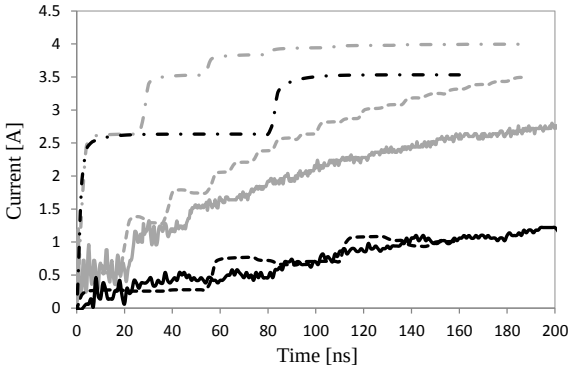

(c) Receiving-end core current

Cable 2.6 m Cable 8

Fig. A.3. Measured and simulated results core at the receiving-end is short circuited (case C_s).

The simulated results show that there is no difference in the sending-end voltage and current (Fig. A.2 (a) and (b)) whether the sheath is grounded (Case S_s, dashed-dotted) or ungrounded (Case S_o, dashed) if the core at the receiving-end is open-circuited (Case C_o).

There is no similarity between the core voltages of the current injection cable at the receiving-end shown in Fig. A.2 (c). The receiving-end voltages oscillate due to the capacitance of the probe, which is used to measure the core voltage. The effect of the capacitance of the probe can be negated by grounding the sheath at the receiving-end (Case C_o-S_s). Fig. A.2 (c) in Case III also shows a travelling wave observed before one round trip ($t<2\tau=2l/v$=16m/200m/μs, at around t=80 ns) which is not found in the other cases. It is due to a reflected wave from the connecting point of sections C and B illustrated in Fig. A.1.

The effect of the sheath grounding at the receiving-end is clearly observed if the core at the receiving-end is short-circuited (case C_s, Fig. A.3). The sending-end voltage and current (Fig. A.3 (a) and A.3 (b)) change to the opposite direction at one round trip (t=2τ) depending on the sheath grounding. The amplitude of the receiving-end current of Case S_s is much higher than that of Case S_o at the beginning (Fig. A.3 (c)).

A.2 Theoretical Calculation

A.2.1 Travelling wave calculation

The travelling waves of the voltage and current up to one round time (2τ) are analytically calculated in this section. The transient voltage and current characteristics are obtained from a circuit shown in Fig. 4.

$$V_1 = E_{f1} + E_{b1} \qquad V_2 = E_{f2} + E_{b2} = E_{f1}e^{-\gamma l} + E_{b1}e^{\gamma l}$$

$$I_1 = Y_0\left(E_{f1} - E_{b1}\right) \quad I_2 = Y_0\left(E_{f2} - E_{b2}\right) = Y_0\left(E_{f1}e^{-\gamma l} - E_{b1}e^{\gamma l}\right)$$

Fig. A.4. Bergeron model to calculate the travelling wave.

The relationship between the forward and the backward waves at the receiving end is defined as:

$$E_b = \theta E_f \tag{A.1}$$

where θ is reflection coefficient.

The relationship between the voltage and the current at the receiving-end should follow the Ohm law:

$$V_2 = Z_t I_2 \tag{A.2}$$

From (A.2) and the travelling wave theory, the reflection coefficient can be obtained.

$$E_{b2} + E_{f2} = Z_t Y_0 \left(E_{f2} - E_{b2}\right)$$

$$E_{b2} + Z_t Y_0 E_{b2} = Z_t Y_0 E_{f2} - E_{f2}$$

$$\left(U + Z_t Y_0\right) E_{b2} = \left(Z_t Y_o - U\right) E_{f2}$$

$$E_{b2} = \left(Z_t Y_0 + U\right)^{-1} \left(Z_t Y_0 - U\right) E_{f2} \tag{A.3}$$

To take into account the induction between the core and the sheath of the coaxial cable, the impedances of the circuit should be expressed by 2-by-2 square matrices. The impedances connected to the cable at the receiving-end and sending-end are assumed to be Z_t and Z_p, respectively. The reflection coefficients at the sending-end and receiving-end θ_1 and θ_2 become matrices.

Z_t: impedance of cable at the receiving-end.

$$Z_t = \begin{bmatrix} R_{ct} & 0 \\ 0 & R_{st} \end{bmatrix}$$

where R_{ct} and R_{st} are core and sheath grounding impedance, respectively.

Z_o: characteristic impedance of any coaxial cable in a high frequency region.

$$Z_0 = \begin{bmatrix} Z_c + Z_s & Z_s \\ Z_s & Z_s \end{bmatrix}$$

where Z_c and Z_S are coaxial and earth-return mode surge impedance, respectively.

Y_o: characteristic admittance of any coaxial cable in a high frequency region.

$$Y_0 = \begin{bmatrix} \dfrac{1}{Z_c} & -\dfrac{1}{Z_c} \\ -\dfrac{1}{Z_c} & \dfrac{Z_c + Z_s}{Z_c Z_s} \end{bmatrix}$$

Hence (A.3) becomes:

$$[E_{b2}] = ([Z_t][Y_0] + [U])^{-1}([Z_t][Y_0] - [U])[E_{f2}] \quad \text{(A.4)}$$

where U: 2x2 identity matrix

The reflection coefficient at the receiving-end is obtained from (A.1).

$$[\theta_2] = ([Z_t][Y_0] + [U])^{-1}([Z_t][Y_0] - [U]) \quad \text{(A.5)}$$

In the same manner, the reflection coefficient at the sending-end (θ_1) is:

$$[\theta_1] = ([Z_p][Y_0] + [U])^{-1}([Z_p][Y_0] - [U]) \quad \text{(A.6)}$$

The sending-end impedance is expressed by (A.7) because the PG consists of a coaxial cable.

$$Z_p = \begin{bmatrix} Z_c' + Z_s' & Z_s' \\ Z_s' & Z_s' \end{bmatrix} \quad \text{(A.7)}$$

where Z_c' (=26.75 Ω) is expressed by the characteristic impedance of the RG55-U cable installed in the PG (53.5 Ω) and a termination resistor (53.5 Ω) which is connected in parallel; Z_S' is the impedance of the sheath. The sending-end reflection coefficient (θ_1) has the following value if the sheath is short-circuited at the sending-end:

$$\theta_1 = \begin{bmatrix} -0.303 & -0.697 \\ 0 & -1 \end{bmatrix}, Z_p = \begin{bmatrix} 26.75 & 0 \\ 0 & 0 \end{bmatrix}\Omega \quad \text{(A.8)}$$

The reflection coefficient at the receiving-end (θ_2) is expressed by the following equations according to the receiving-end conditions:

Case C_o-S_o: The core and the sheath are open-circuited.

$$\theta_2 = \begin{bmatrix} 1 & 0 \\ 0 & 1 \end{bmatrix}, Z_t = \begin{bmatrix} \infty & 0 \\ 0 & \infty \end{bmatrix}\Omega \quad \text{(A.9)}$$

Case C_o-S_s: The core is open-circuited while the sheath is short-circuited.

$$\theta_2 = \begin{bmatrix} 1 & -2 \\ 0 & -1 \end{bmatrix}, Z_t \begin{bmatrix} \infty & 0 \\ 0 & 0 \end{bmatrix}\Omega \quad \text{(A.10)}$$

Case C_s-S_s: The core and the sheath are short-circuited.

$$\theta_2 = \begin{bmatrix} -1 & 0 \\ 0 & -1 \end{bmatrix}, Z_t = \begin{bmatrix} 0 & 0 \\ 0 & 0 \end{bmatrix} \Omega \tag{A.11}$$

Case C_s-S_o: The core is short-circuited while the sheath is open-circuited.

$$\theta_2 = \begin{bmatrix} -1 & 0 \\ \dfrac{-2Z_s}{Z_c + Z_s} & 1 \end{bmatrix}, Z_t = \begin{bmatrix} 0 & 0 \\ 0 & \infty \end{bmatrix} \Omega \tag{A.12}$$

The travel of the travelling wave is illustrated in a lattice diagram shown in Fig. A.5 with the reflection coefficients θ_1 and θ_2, and the diagram determines the transient voltage and current waveform. The voltage and current at the sending-end are calculated assuming that the sheath at the sending-end is connected to the ground.

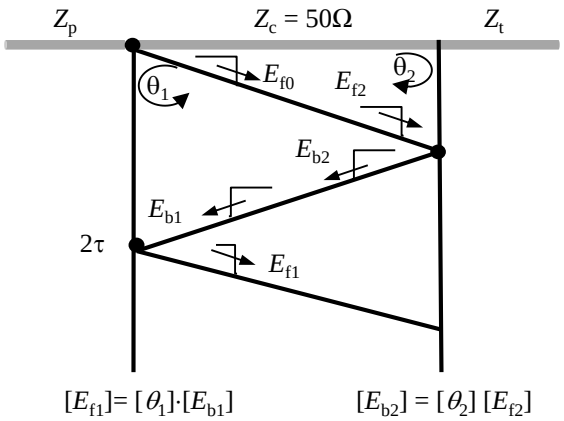

Fig. A.5. Calculation of transient voltage and current using lattice diagram.

The following is an example of the theoretical calculation. Case C_s-S_o will be calculated with the configuration of Case I. If Z_c = 50 Ω and Z_s = 207 Ω, the characteristic admittance of coaxial cable Y_0 and the reflection coefficient θ_2 become:

$$Y_o = \begin{bmatrix} 0.02 & -0.02 \\ -0.02 & 0.025 \end{bmatrix}, \quad \theta_2 = \begin{bmatrix} -1 & 0 \\ -1.61 & 1 \end{bmatrix}$$

At t = 0:

$$E_{f0} = E_{f1} = \begin{bmatrix} 66.7 \\ 0 \end{bmatrix}$$

$$V_1 = \begin{bmatrix} V_{c1} \\ V_{s1} \end{bmatrix} = E_{f0} + E_{b1} = \begin{bmatrix} 66.7 \\ 0 \end{bmatrix} + \begin{bmatrix} 0 \\ 0 \end{bmatrix} = \begin{bmatrix} 66.7 \\ 0 \end{bmatrix} \text{V}$$

$$I_1 = \begin{bmatrix} I_{c1} \\ I_{s1} \end{bmatrix} = Y_0 \left(E_{f1} - E_{b1} \right) = \begin{bmatrix} 1.33 \\ -1.33 \end{bmatrix} \text{A}$$

At t = τ (=2.6m/200m/μs=13 ns):

$$E_{f2} = E_{f1}(t - \tau)$$

$$E_{b2} = \theta_2 \cdot E_{f2} = \begin{bmatrix} -66.7 \\ -107.4 \end{bmatrix}$$

$$V_2 = \begin{bmatrix} V_{c2} \\ V_{s2} \end{bmatrix} = E_{f2} + E_{b2} = \begin{bmatrix} 0 \\ -107.4 \end{bmatrix} \text{V}$$

$$I_2 = \begin{bmatrix} I_{c1} \\ I_{s1} \end{bmatrix} = Y_0 \left(E_{f2} - E_{b2} \right) = \begin{bmatrix} 0.52 \\ 0 \end{bmatrix} \text{A}$$

At t = 2τ (=2(2.6m/200m/μs)=26 ns):

$$E_{b1} = E_{b2}(t - \tau)$$

$$E_{f1} = \theta_1 \cdot E_{b1} = \begin{bmatrix} 95.1 \\ 107.4 \end{bmatrix}$$

$$V_1 = \begin{bmatrix} V_{c1} \\ V_{s1} \end{bmatrix} = E_{f0} + E_{f1} + E_{b1} = \begin{bmatrix} 95.1 \\ 0 \end{bmatrix} \text{V}$$

$$I_1 = \begin{bmatrix} I_{c1} \\ I_{s1} \end{bmatrix} = Y_0 \left[\left(E_{f0} + E_{f1} \right) - E_{b1} \right] = \begin{bmatrix} 0.27 \\ 0.8 \end{bmatrix} \text{A}$$

The theoretical results were compared to the measured and simulated results from the similar case as shown in Fig. A.6. It shows that voltage and current in the core agree with the simulated and measured results.

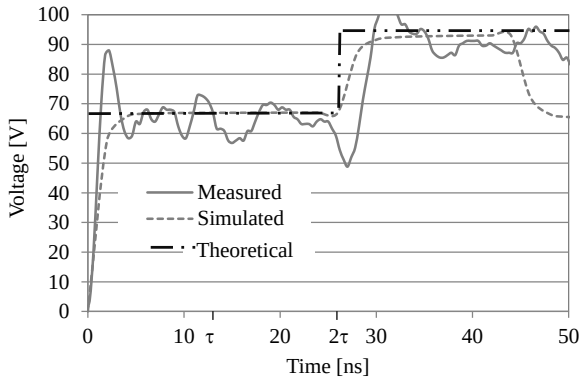

(a) Sending-end core voltage

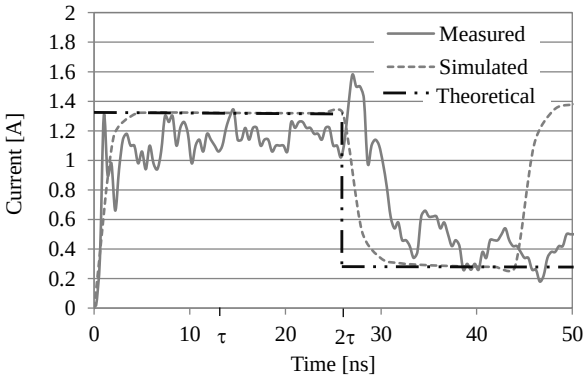

(b) Sending-end core current

Fig. A.6. Theoretical, measured and simulated results at sending-end in case Cs-So with configuration Case I.

If the receiving-end core is open circuited (Cases C_o-S_o, C_o-S_s) or both the core and sheath are short-circuited (Case C_s-S_s), the coaxial current of the cable is generated. The current flows into the core and returns from the sheath. From a practical point of view, the cable is terminated by a higher impedance than the characteristic impedance of the cable to inject a current similar to the voltage waveform. The receiving-end of the core of the current injection cable can be regarded as open-circuited.

If the core is short-circuited and the sheath is open-circuited at the receiving-end (Case C_s-S_o), an earth return current is also generated. A voltage on the receiving-end sheath also appears in the earth-return current. The earth-return current is generated due to the element $\theta_{2\text{-}21}$ of the reflection coefficient. The transient characteristic of the current injection cable

terminated by a resistor of small resistance can be roughly explained by the result of case C_s (the core is short-circuited).

A.2.2 Surge impedance

Surge impedance or characteristic impedance is one of properties of a distributed parameter circuit such as cable. It is defined as a ratio between a voltage and a current of a travelling wave propagating along a line. The estimated surge impedance of the current injection cable can be obtained from a measured and a simulated result using (A.13) [4]:

$$Z_0 = V_p / I(t_p) \tag{A.13}$$

where Z_0 is the estimated surge impedance, V_p is the peak voltage, $I(t_p)$ is the current at the time of the peak voltage and t_p is the time to peak voltage, which is less than the round-trip time (2τ) of a travelling wave.

Table A.1 shows the calculated results of the surge impedance Z_0 based on the measured and simulated results. The difference between the measured- and simulated-surge impedance is less than 6 %.

Table A.1. Surge impedance of the current injection cable.

Case		Z_0 [Ω]		Difference (%)
		Measurement	Simulation	
I	C_o-S_o	54.5	51.5	5.7
	C_s-S_o	54.2	51.5	5.1
II	C_o-S_o	54.9	51.9	5.6
III	C_o-S_o	55	52.4	4.8
	C_s-S_o	53.4	52.4	1.9

A.2.3 Sheath surge impedance

The theoretical sheath surge impedance is defined by (A.14).

$$Z_s = 60 ln(2h/r_s) \tag{A.14}$$

Where h and r_s are height and outer radius of the metallic sheath (1.85 mm), respectively.

The sheath surge impedance is determined by the height of the current injection cable. When the cable is placed on the floor (h≈5mm), the measured and theoretical sheath surge impedance are 130 Ω and 100 Ω, respectively.

As aforementioned, in case the sending end sheath is open-circuited (C_s-S_o), the earth return current is generated due to the element $\theta_{2\text{-}21}$ of the reflection coefficient. The theoretical calculation in the previous section clearly shows the receiving-end sheath voltage V_{s2} is generated due to this element. The element $\theta_{2\text{-}21}$ is a function of sheath surge impedance and coaxial surge impedance. Therefore, in case the sending-end sheath is open-circuited, the sheath surge impedance should not be ignored.

The analytical calculation shows if the receiving-end core is open-circuited or both the core and sheath are short-circuited, the reflection can be explained only by the coaxial mode. If the core is short-circuited and the sheath is open-circuited at the receiving-end, an earth return current is also generated. A voltage on the sheath appears in the earth return mode. The current generation can be explained by the reflection coefficient at the receiving end. The measured results of the surge impedance agree with the simulated ones.

The accuracy of the Semlyen line model of EMTP was confirmed by comparing with the measured results. The line model is suitable for a numerical simulation including a current injection cable.

A.3 References

[1] D. Permata, Y. Ikeda, and N. Nagaoka: “Effect of current injection cable on lightning surge measurement for scaled circuit,” *The Science and Engineering Review of Doshisha University*, vol. 55, no. 4, pp.61-67, Jan. 2015.

[2] N. Nagaoka, “Cable transient,” Proc. Int. Workshop Advanced Technologies Power System Simulations, Bangkok, 2011, pp.116-134.

[3] D. V. Dommelen and H. W. Dommel, *ATP Rule Book*, LEC., Belgium, 1987, p. 614-630.

[4] P. Yuttagowith, A. Ametani, N. Nagaoka, and Y. Baba, “ Influence of a measuring system to a transient voltage on a vertical conductor,” *IEEJ Trans. Electrical and Electronic Engineering*, vol.5, pp.221-228, 2010.